To the Graduate Council

I am submitting herewith a thesis written by Jonathan R. Vincent entitled "Instabilities of a Rich Premixed-Flame" I have examined the final copy of this thesis for form and content and recommend that it be accepted in partial fulfillment of the requirements for the degree of Master of Science, with a major in Mechanical Engineering

Dr Ke Nguyen, Major Professor

We have read this thesis
and recommend its acceptance

Dr Stuart Daw, Committee Member

Dr Jeff Hodgson, Committee Member

Dr J R Parsons, Committee Member

Accepted for the Council.

Dean of the Graduate School

Instabilities of a Rich Premixed-Flame

A Thesis
Presented for the
Master of Science
Degree
The University of Tennessee, Knoxville

Jonathan Robert Vincent

December 2000

Acknowledgements

I would first like to thank Dr Ke Nguyen for his excellent guidance, support, honesty, and patience in dealing with me as I obtained my Masters degree He has taught me many valuable things that I need to work at and improve in so that I will not be fired when I get a real job I would also like to thank the members of my committee, Dr. Stuart Daw, Dr Jeff Hodgson, and Dr J R Parsons for their patience in dealing with the many delays and postponements of this thesis I would like to especially thank Dr Dean Edwards and Dr Charles Finney for the giving of their time in helping me with this thesis and all of the background work that went into it None of the data analysis would have been possible or even conceivable without Charles and none of the initial setup of the burner apparatus and plumbing without Dean I would like to thank fellow Masters student Tiang-Yong Teh for going through many of the same experiences and problems that I went through and for helping me through them I would like to thank Mr Dennis Higdon for his help with many of the technical things involved in this thesis and for the people down in the shop for the fabrication and construction of the burner apparatus, control panel, etc I would also like to thank all of the other friends that I have made here over the years during graduate school who have given me something to do besides this thesis I would especially like to thank my parents for giving me the much-needed support and love that I have needed while working on this thesis and also in life And most of all I would like to thank my Lord and Savior Jesus Christ for making me a new man during the completion of this thesis, for imparting any redeeming qualities that I appear to have, and for providing a sense of purpose in this world

Abstract

The instabilities of rich premixed-flames in a low-NO_x burner operated with overfire air were experimentally investigated Specifically, the effects of equivalence ratio and gas volumetric flowrate on the instabilities of the flame were examined The transition from stability to instability was explored and documented as burner parameters were varied The feasibility of using both linear and nonlinear time-series analysis techniques of pressure and light measurements to predict instabilities was also studied A frequency generator was also used to further study the effects that very small changes in equivalence ratio have on flame stability.

Using overfire air the flame had a propensity to anchor at locations other than at the burner leading to periodic behavior Analysis of the pressure and light signals demonstrated that instabilities of the flame could be observed by using both linear and nonlinear analysis techniques It was found that linear techniques are adequate at characterizing the flame behavior due to the periodic nature of its instabilities The equivalence ratio of the premixed gases was found to have a more pronounced effect on flame stability than the gas flowrate

It is recommended that further investigations be conducted using a better-suited pressure transducer in order to get more accurate data The effect of varying the length of the glass tube above the burner on flame stability should also be studied

Table of Contents

Table of Contents (continued)

List of Tables

List of Figures

List of Figures (continued)

List of Figures (continued)

Figure	Title	Page

Appendix Figures

List of Figures (continued)

Chapter 1

Introduction

In the current regulatory climate, low-NO_x burners are needed to minimize the production of nitrogen oxides in emissions from fossil fuel combustion Nitrogen dioxide (NO_2) is classified as a criteria pollutant under the U S Clean Air Act of 1990 and is considered a major environmental concern NO_x emissions are one of the leading air pollutants because of their contribution to smog formation, acid rain, and ozone depletion in the upper atmosphere [1]* About 55 percent of NO_x emissions in the U S are emitted from stationary sources, such as utility boilers, industrial boilers, gas turbines, and stationary engines, of which almost 75 percent are from fossil fuels Motor vehicles and aircraft contribute the remaining 45 percent of NO_x emissions [2, 3] The work reported herein deals only with stationary sources of combustion

In stationary source combustion, approximately 95 percent of the NO_x formed is nitric oxide (NO), which can oxidize in the atmosphere to form nitrogen dioxide The formation of NO_x during combustion of fossil fuels occurs by three mechanisms oxidation of atmospheric nitrogen present in the combustion air at elevated temperatures (thermal NO_x), high speed reactions at the flame front (prompt NO_x), and oxidation of nitrogen contained in the fuel (fuel NO_x) [1] Fuel NO_x is more dependent on fuel nitrogen content, fuel properties, and the stoichiometric conditions present at combustion

---

* Numbers in [ ] refer to entries in bibliography

than on temperature Thermal NO_x is the dominant formation mechanism during combustion of gas or low nitrogen fuel oils Prompt and fuel NO_x are not discussed in detail since this work deals primarily with thermal NO_x formation

Thermal NO_x formation consists of two important reactions

$$N_2 + O \Leftrightarrow NO + N \quad (1\text{-}1)$$

$$N + O_2 \Leftrightarrow NO + O \quad (1\text{-}2)$$

Reaction 1-1 is highly temperature dependent and provides the atomic nitrogen (N) necessary for Reaction 1-2 Both reactions are equally important in the amounts of NO formed The NO formed is essentially fixed in the oxidizing environment downstream from the actual combustion (due to excess air for combustion) because the reverse reactions are not favored by the presence of molecular oxygen Thermal NO_x formation is minimized by reducing combustion temperatures and minimizing the oxygen concentration in the combustion gas Formation of thermal NO_x is not significant when temperatures in the regions of the combustion chamber are less than 1,200 °C (2,200 °F) [2, 4]

1.1 Methods of NO_x Reduction

Three general methods of NO_x reduction are

- Reduction **before** combustion by reducing potential for formation (pre-combustion)
- Reduction **during** combustion by modification of the combustion process itself
- Reduction **after** combustion by some means of flue gas treatment (post-combustion)

Pre-combustion techniques for reducing NO_x involve switching to fuels with a lower nitrogen content or a lower flame temperature The choice of the fuel is usually governed by economic factors that surpass the economics of NO_x control Because nitrogen in solid and liquid fuels is chemically bound to organic chemical constituents, it is not efficiently removed Another way of reducing NO_x is to switch oxidizers Using pure oxygen instead of air can minimize NO_x by drastically reducing N_2 in the system [1] However, this method is typically not economical

NO_x reduction during combustion, or combustion modification, is currently the principal NO_x reduction method for moderate control These techniques suppress thermal or fuel NO_x by modifying the conditions of combustion, specifically, stoichiometry, temperature, and residence time This can be accomplished through modification of the burner or externally through modification of the air or fuel flow to the combustion chamber Research in these areas is being performed primarily by burner and boiler manufacturers, the Environmental Protection Agency (EPA), the Electric Power Research Institute (EPRI), and the Gas Research Institute (GRI) [2] This method will be discussed in more detail later

Post-combustion techniques of reducing NO_x involve treatment of the flue gas and are classified as dry or wet processes These processes can also be simultaneously used to remove sulfur dioxide (primarily from coal-fired boilers) NO_x is removed from the exhaust gases after forming in the combustion chamber. Dry flue gas treatment systems usually consist of either reduction of NO_x to nitrogen by reducing agents or adsorption onto solids These can be noncatalytic or catalytic. In selective noncatalytic reduction (SNCR), ammonia (NH_3) or urea is injected into the flue gas to reduce NO_x to N_2 and water Selective catalytic reduction (SCR) involves injecting ammonia into the flue gas in the presence of a catalyst The catalyst advances reactions that convert NO_x to N_2 and water at higher removal efficiencies and lower flue gas temperatures than required for SNCR Adsorption processes add expense due to the solid waste generated Wet flue gas treatment systems offer only one real advantage over dry systems, the simultaneous removal of sulfur oxides Wet systems are attractive for applications requiring strict control of both pollutants NO_x reductions of over 60 percent have been achieved using SCR technologies [5] Application of flue gas technologies on coal-fired boilers has grown considerably over the past couple of years, while SNCR and SCR systems have been widely employed on gas- and oil-fired steam generating units for many years SCR technologies have been implemented on coal-fired steam generating units in Germany and Japan for over 15 years where NO_x emission limits are stricter than in the United States [1, 5, 6]

Typically, NO_x reduction from stationary sources is accomplished with the simplest and most cost-effective combustion modification that will achieve the necessary emission reduction The more stringent the NO_x emission limits, the more reduction is required, and hence, progressively more efficient (and more costly and difficult to implement) combustion modifications are thus needed to meet the requirements Post-combustion technologies are considered when the most efficient combustion modifications do not bring about the required reduction

1.2 Combustion Modification Technologies

The majority of NO_x control technologies for combustion sources involve modifying the parameters of combustion All are aimed at achieving one or more of the following goals reducing the available oxygen at critical stages of combustion, lowering the peak flame temperature, and reducing the residence time during which oxidation of nitrogen takes place [2] The technologies discussed in the following sections are applicable to both retrofit and new combustion sources

1.2.1 Low Excess Air

The simplest NO_x reduction technology to implement on a retrofit basis is operating burners with low excess air It requires no capital equipment and combustion chamber modifications are normally unnecessary The NO_x reductions achievable are modest and may not be sufficient to comply with prevailing or anticipated future NO_x emission regulations The amount of control is limited by the onset of unacceptable (reduced efficiency and safety concerns) carbon monoxide (CO) emissions [7] Low excess air technology is applicable to coal, oil, and gas firing in boilers of all sizes The low excess air method accomplishes NO_x reduction of both thermal and fuel NO_x Reduced availability of oxygen suppresses the formation of NO from nitrogen in the fuel and in the combustion air

1.2.2 Temperature Reduction Technologies

Several NO_x reduction technologies employ some method of reducing peak flame temperature to reduce thermal NO_x production Four types are discussed here· reducing combustion aır preheat, water injection, exhaust gas recirculation, and fluidized bed combustion All are generally applicable to oil- and gas-fired boilers and engines, except for fluidized bed combustion These technologies are not effective for sources firing coal or hıgh nitrogen oil because thermal NO_x formation is usually the less important mechanism in such unıts

In many combustıon devices, the combustion air is preheated by the hot exhaust gases to improve thermal efficiency Reducing the amount of air preheat reduces combustion temperatures and, as a result, NO_x formation In utility and large industrial boilers, economizers can be used to recover some of the thermal efficiency that is sacrificed in reducing the combustıon air preheat The loss of thermal efficiency can represent a severe economic penalty, and consequently these methods of NO_x reduction are considered only for interim control [2, 7]

Injecting water reduces flame temperatures because combustion energy is used to vaporize and superheat the water to combustion temperatures Water injection technology involves a slight modıfication to allow water to be injected into the combustion air stream Nozzles are normally mounted in the windbox in a manner that allows vaporization of the water before it enters the combustion chamber The vaporization removes some of the heat from the combustion chamber and in turn lowers the peak flame temperature The vaporization of the water should occur before the combustion air reaches the combustion chamber to avoid corrosion in this area Water injection, like the reduction of combustion air preheat, has a significant energy penalty and should be used as an interim measure for utility boilers [1, 7]

Exhaust gas recirculation, or flue gas recirculation, is similar to that of water injection in that both act as dilutents Its greatest applicability is with stationary engines and turbines, but it is also applicable on a new or retrofit basis for boilers, process heaters, and engines Part of the exhaust or flue gas is recycled into the inlet combustion air flow This dilution lowers the peak flame temperature, reducing thermal NO_x formation in the process The local oxygen level in the flame is also reduced, limiting NO_x formation as well The effectiveness of flue-gas recirculation depends on both the quantity and temperature of the recirculated gas This technique is not applicable for coal-fired boilers because the greater portion of NO_x emissions is from fuel NO_x in coal combustion NO_x reductions from approximately 50 to 85 percent are possible with flue-gas recirculation in gas-fired boilers [1, 2, 7]

Fluidized bed combustion facilities also operate at low combustion temperatures (primarily for peak sulfur capture) and thus produce low amounts of NO_x They are also fuel efficient and environmentally friendly There are three main types of fluidized beds bubbling fluidized beds (BFB), circulating fluidized beds (CFB) and pressurized circulating fluidized beds (PCFB) Bubbling fluidized bed units are very efficient when firing fuels with low heating values and high moisture ash content Circulating fluidized bed technology is useful for clean combustion of waste coals, petroleum coke, and even shredded automobile tires Pressurized fluidized bed technology is relatively new and can operate with very high efficiencies. PFBs have the potential to reduce the cost of energy and further cut the emission of acid rain gases (NO_x and SO_x) in utility and industrial applications [9]

1.2.3 Low-NO_x Burners

Low-NO_x burners delay the mixing of fuel and air within the immediate flame envelope to create lower combustion temperatures and to create chemical reduction zones within the flame to control and reduce thermal NO_x Low-NO_x burners delay mixing to reduce oxygen availability and extend flame length Burners designed for low-NO_x emissions employ fuel or air staging Fuel staging creates a sequential lean-rich combustion process while air staging creates a rich-lean process These burners are applicable on a new or retrofit basis and can be used for utility, large industrial, and small packaged boilers Low-NO_x burner development has been primarily performed by boiler and burner vendors This type of burner has been and continues to be developed for coal-, oil-, and gas-fired boilers [4]

In fuel-staged burners, all of the air required for combustion is introduced into the primary combustion zone The fuel is staged so that the amount of fuel that the primary zone receives is less than stoichiometric Primary combustion consists of fuel-lean conditions and therefore NO_x formation is inhibited by the lower flame temperature brought about by the excess air The remaining fuel is injected into the flame through a peripheral pattern of high-velocity nozzles. Rapid mixing is achieved by the entraining action of the injected fuel, which is similar to exhaust gas recirculation NO_x formation is reduced by a lower flame temperature in the secondary zone and by the decreased availability of oxygen in the staged zone [1, 2]

Air-staged burners employ staged air **within** the burner itself to effect NO_x reductions The detailed design of the burner is responsible for the staged combustion This type of burner utilizes primary and secondary air for combustion in such a way that conditions in the primary flame zone are fuel-rich The remaining air (tertiary or staged air) is injected outside of the combustion zone Staged-air combustion encourages the formation of N_2 rather than NO_x Primary air (70-90 percent) is mixed with the fuel producing a relatively low temperature, oxygen deficient, fuel-rich zone, and therefore moderate amounts of fuel NO_x are formed [10] The relatively low-temperature secondary-stage limits the production of thermal NO_x because of its low peak flame temperature The improved flame structure produced also reduces the amount of oxygen available in the hottest part of the flame, thus improving burner efficiency Staged-air burners are equally applicable in new or retrofitted boilers Air staging is much easier to retrofit than fuel staging, and thus is much cheaper. NO_x reductions of 25 to 30 percent for oil and 35 to 40 percent for gas have been achieved [1, 11]

1.2.4 Staged Combustion

Staged combustion is a method of NO_x control that applies to the operation of existing burners in a multi-burner device that are modified to create a rich-lean staging of combustion This is achieved by three different methods The first, burners out of service, has upstream burners operate rich, while adjusting downstream burners to supply only air The second, biased firing, adjusts some burners to run rich and some to run lean The third type of staged combustion, overfire air, adjusts all burners to operate rich, with additional air supplied through downstream ports The methods most frequently employed for retrofit of large industrial and utility boilers are BOOS and biased firing Overfire air is applied most frequently for new units NO_x reductions attainable with these techniques range from 10 to 40 percent [7]

Burners out of service (BOOS) is generally applicable to wall-fired utility and large industrial boilers BOOS employs an upper row of burners as sources of secondary combustion air only, without introduction of fuel through these burners. Selected burners can also be removed from service other than the top row if the BOOS pattern is balanced The effect is to provide overfire air above the active burners that comprise the primary combustion zone This zone is maintained at fuel-rich conditions by introducing air to these burners at lower than stoichiometric rates The operation of the lower furnace zone with a substoichiometric amount of air (fuel-rich conditions) lowers the conversion of fuel nitrogen to nitrogen oxide The cooling and dilution of the combustion gas with the secondary air from the upper (out of service) burners reduces the peak flame temperature and thus minimizes the formation of NO_x by thermal processes NO_x reductions of 10 percent have been achieved [2, 8]

Biased firing is another retrofit technology that only applies to oil-fired and gas-fired utility and large industrial boilers It is as easy to implement as BOOS, with no new equipment necessary or any major boiler modifications needed The overall combustion chamber stoichiometry is kept constant while air and fuel flows to individual burners are varied Many combinations may yield the desired effect, so there is no generally accepted pattern to variation of the burner conditions. The objective is to create fuel-rich and fuel-lean regions in the combustion chamber with an effect similar to that of overfire air or BOOS The fuel-rich regions generate relatively low thermal and fuel NO_x NO_x emissions may be reduced by up to 30 percent using this technology [2, 8]

The third type of staged combustion discussed is overfire air, which is applicable to coal-, oil-, and gas-fired utility and large industrial boilers Using overfire air lowers the combustion temperatures which reduces the formation of thermal NO_x Overfire air requires modification of the combustion chamber, unlike BOOS and biased firing Air ports above most or all of the rows of burners must be added to provide the secondary combustion air above the burners Fuel-rich burners reduce fuel and thermal NO_x formation, and interstage cooling by boiler tubes located between the burners and overfire air ports reduces peak flame temperatures, thus also restricting thermal NO_x formation [4] A low-NO_x burner that can be operated with both primary and secondary air is used in this investigation Without using any secondary air and operating the burner fuel-rich, the overfire air condition is simulated by introducing excess air supplied downstream from the burner

1.3 Objectives of Investigation

In this investigation, experimental studies are conducted on a low-NO_x burner with methane (CH_4) as the fuel Low-NO_x burners are much better at reducing emissions than conventional burners, but industries and utilities are finding it more and more difficult to maintain optimal fuel efficiency while meeting emission limits The difficulty arises from the fact that staged combustion is inherently unstable As the reduction of NO_x is attempted by increasing staging, a point is reached where the flame temperature is so low that carbon monoxide (CO) and unburned fuel emissions rise sharply and/or the burner flames out (extinguishes) The behavior of a flame near the flameout point is extremely nonlinear and consequently extremely sensitive to small changes in burner operation These changes include fuel-air mixing patterns and the steadiness and temperature of the fuel and air feeds Low-NO_x burners pulsate due to this instability producing spikes of NO_x, CO and unburned fuel Operators tend to limit the level of staging significantly below the point of optimal NO_x reduction to avoid flameout and CO spikes [12] Existing burner monitoring systems do not permit very fine control of burners near the flameout point because they are too slow to track the developing instabilities

The low-NO_x burner used in this investigation is modified into a simulated overfire air burner by increasing the air and fuel flowrates and using no secondary air The burner is operated fuel-rich with the overfire air supplied downstream of the burner Many of the problems associated with low-NO_x burners are also found using overfire air Of special significance with this configuration is the fact that the flame begins to have two states of equilibrium and at certain conditions jumps between the two Since the primary flame zone is fuel-rich, the flame has a propensity to anchor at a location where oxygen is more prevalent This leads to extreme instabilities in the flame, especially around the rich flammability limit of methane The primary focus of this investigation is centered on this area of burner operation An ideal laminar-flow burner is used to remove some of the complexity associated with turbulent mixing The general trends found using laminar flow should be similar to those found in real-world burners

The purpose of this study is to improve burner performance and control by providing a high-speed method to accurately monitor the flame dynamics This is attempted using pressure and light signals from burner-mounted sensors to characterize the small-timescale dynamic flame stability The signals measured are caused by large-scale fluctuations in the combustion rate associated with extinction/ignition events in the flame These fluctuations are commonly the result of the flame-flicker pattern that can be observed visually Both linear and nonlinear tools are used for signal analysis

The three main objectives of this investigation are

- to evaluate the effects of equivalence ratio (Φ) and bulk gas velocity (or volumetric flowrate) on the flame instabilities of a rich premixed CH_4-air burner,
- to determine the flame instabilities by using linear and nonlinear time-series analysis techniques, and
- to determine the mechanism of flame propagation

The exploration of the transition from a stable to an unstable flame is accomplished by varying the equivalence ratio of the fuel-air mixture through control of the fuel and air flowrates A frequency generator is also used to further study the effects of very small changes in the equivalence ratio on a flame by periodically injecting small amounts of air into the primary combustion zone Pressure and light signals are obtained and compared using linear and nonlinear time-series analysis techniques The visual observations of the flame are used to categorize the flame and to complement the results obtained from the time-series analysis techniques The flame is manually recorded in the notebook log and videotaped for a more thorough analysis An explanation of the reasons for the propagation of the flame is given and verified by the frequency generator experiments No attempt to control the flame is undertaken in this investigation

The overall design of the low-NO_x burner test rig and the testing procedures used in this work are presented in Chapter 2 The linear and nonlinear data analysis techniques used are described in Chapter 3 Chapter 4 presents the experimental results and discussion Finally, Chapter 5 gives the conclusions gained from this research effort and presents recommendations for future studies

Chapter 2

Experimental Apparatus and Procedure

This chapter describes the experimental apparatus and procedure used throughout this study An overview of the experimental apparatus is outlined in Section 2 1 The burner assembly is described in detail in Section 2 1 1, the plumbing system is detailed in Section 2 1 2, and the data acquisition system is described in Section 2 1 3 The experimental procedure complete with detailed instructions for running the burner is presented in Section 2 2 The start-up procedure is described in Section 2 2 1 and the types of experimental tests run are described in Section 2 2 2

2.1 Experimental Apparatus

2.1.1 Burner Assembly

A schematic of the experimental apparatus is shown in Figure 1 The burner apparatus consists of three main parts, a centrally-located burner, an outer cylinder for staged air, and a glass tube The centrally-located cylindrical burner is made of stainless steel and is approximately 200 mm long with an outside diameter of 33 mm and a wall thickness of 3 mm. The cylindrical burner assembly is fabricated in-house with the exception of the air manifold, which comes from a Fisher Scientific Blast Burner (Model 03-910-5) The top of the burner is recessed 10 mm to accommodate a 29 mm diameter cellular-structure flame holder that is used to anchor the flame The air manifold is

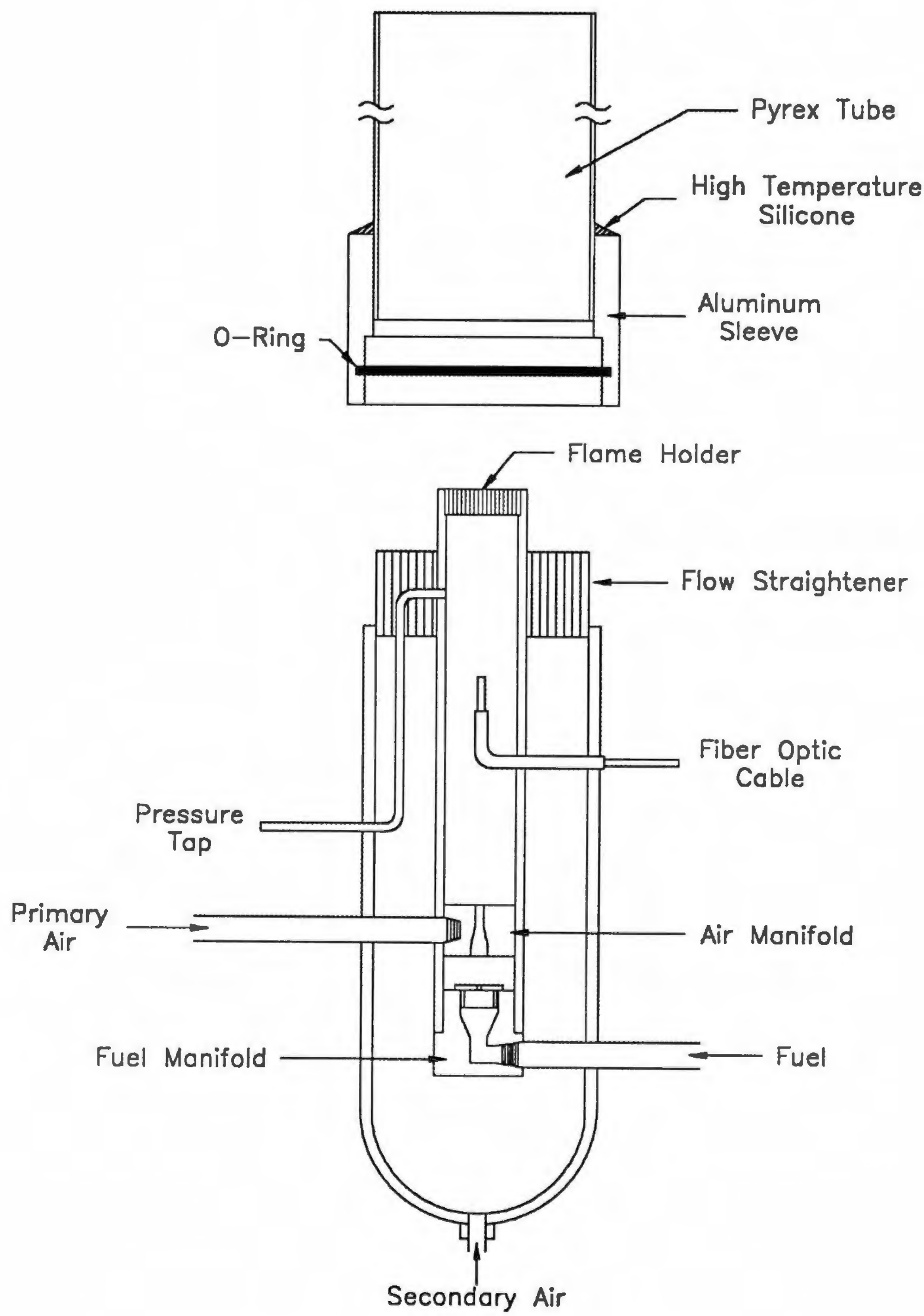

Figure 1: Schematic of the Burner Apparatus

located 38 mm from the bottom of the burner and is used to inject the primary air into the burner The air is injected into the burner through eight 1-mm holes spaced evenly around a central nozzle 3 mm in diameter through which a fuel jet issues from the fuel manifold As a result, the fuel and primary air are allowed to mix adequately to create a premixed flame The fuel manifold is machined from a solid piece of stainless steel and is welded to the bottom of the burner An orifice of 1 5-mm diameter is screwed to the top of the fuel manifold through which the fuel is injected A schematic of the fuel manifold is shown in Figure 2

A Cuda flexible fiber optic cable enclosed in stainless steel sheathing is used to measure the light emitted by the premixed-flame The tip of the fiber optic cable is placed approximately 75 mm beneath the flame holder looking upward along the axial centerline Thus, the flame is measured globally because the cable is not focused on any particular region in the flame As a result, the measured intensity is much higher when the flame is located very close to the burner A silicon photodiode detector, powered by a regulated power supply (Wall Industries, Inc.), is placed at the end of the fiber optic cable to measure the flame intensity

A pressure tap is placed approximately 175 mm above the bottom of the burner The pressure tap consists of a 3 mm stainless steel tube that is welded into a similar size hole drilled in the burner Plastic tubing is connected to the metal tube outside of the burner assembly and is connected to a Baratron rapid response differential pressure transducer (Model 223BD) that measures the low differential pressures generated by the gas flow through the burner before the flame The input range of the transducer is 0 to 10 Torr producing an electrical output voltage of 0 to 1 VDC The transducer operates on a

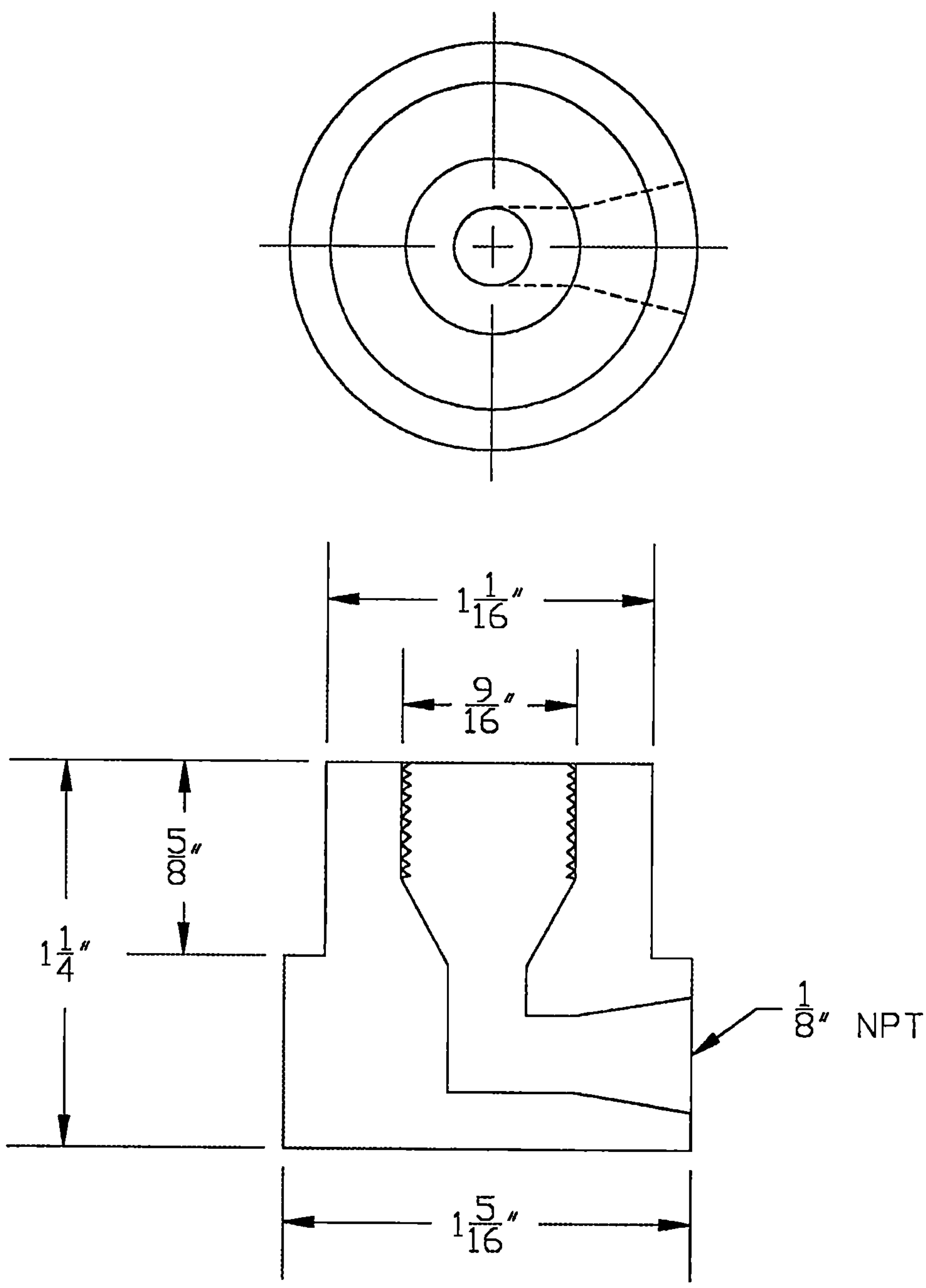

Figure 2: Schematic of the Fuel Manifold

variable capacitance technique The capacitance change produced by the differential pressure generates an AC voltage that the transducer's signal conditioner converts into a DC voltage output that is linear with pressure The power supply used to power the photo-diode detector is also used to power the pressure transducer

A stainless-steel bottle cylinder (Whitey, Model 304L-HDF4-1000) 276-mm long, with an outside diameter of 90 mm, and a wall thickness of 5 mm is used to create an annulus for the secondary (or staged) air One end of the cylinder is cut off to produce a length of 229 mm as measured from the base The secondary air is supplied from the bottom of the cylinder A cylinder is selected to produce smooth airflow with low vorticity The entire burner assembly is placed inside of the cylinder, with the top of the burner protruding approximately 50 mm above the top of the cylinder An aluminum honeycomb flow straightener placed around the burner inside of the cylinder has an inside diameter of approximately 33 mm, an outside diameter of 80 mm, and a height of 32 mm The honeycomb cells have a diameter of about 3 mm The flow straightener is used to provide one-dimensional axial flow

To provide an undisturbed envelope for the flame and to reduce the effects of the surrounding air, a glass shield is placed on top of the burner The glass shield consists of a Pyrex glass tube (height of 267 mm, width of 83 mm, and thickness of 2 mm) and an aluminum sleeve An O-ring with a diameter of 95 mm is used to seal the assembly to ensure no air leakage The glass shield is sealed with high temperature silicone to prevent cracking because of the difference in the thermal expansions of the glass tube and aluminum sleeve

A photograph of the experimental apparatus is shown in Figure 3

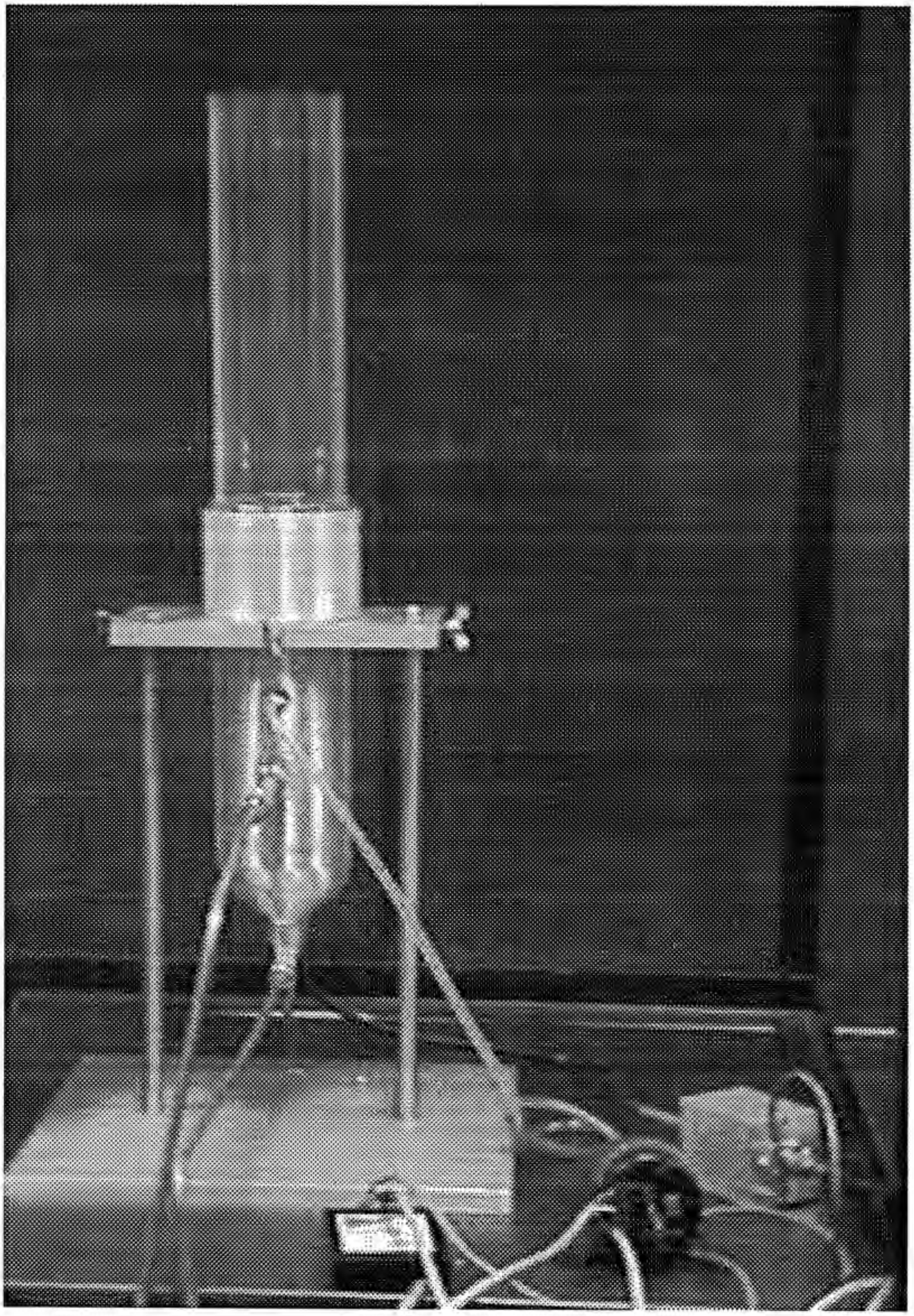

Figure 3: Photograph of the Experimental Apparatus

2.1.2 Plumbing System

The plumbing system (shown in Figure 4) consists of piping to supply the air (primary and secondary) and methane to the burner assembly. The primary and secondary air is supplied by the same house air. The inlet pressures of the primary and secondary airflows are measured using two identical pressure gauges (Robershaw Fulton Controls Company Acragage) with a range of 0 to 414 kPa (gage). The primary air volumetric flowrate is controlled using a needle valve rotameter (Sho-Rate Brooks, Model 1355-01F1AAA) with a range of 6 to 64 Lpm The secondary air has its own cut-off valve that can be used when only primary air is desired. The secondary air flowrate is controlled using a Dwyer needle valve rotameter with a range of 0 to 195 Lpm with the secondary air leaving the rotameter and entering into the bottom of the bottle cylinder It is important to note that secondary air is not used in this investigation.

Methane (CH_4) is supplied from a gas cylinder and the fuel pressure is measured using a Duragauge pressure gauge with a range of 0 to 414 kPa (gage) As a safety precaution the fuel has two cut-off valves. One is located close to the cylinder, while the other is a part of the control panel. The fuel flowrate is controlled using a needle valve rotameter (Sho-Rate Brooks, Model 1355EGL7CFG1A) with a range of 1 66 to 16.6 Lpm A photograph of the control panel is shown in Figure 5

For the flame stabilization study, an in-house constructed frequency generator is used to control a solenoid valve to inject air into the burner. A tee is placed in the primary air piping to allow the additional air to be introduced into the primary combustion zone. The rotameter used to control this airflow is identical to that used to control the fuel flowrate.

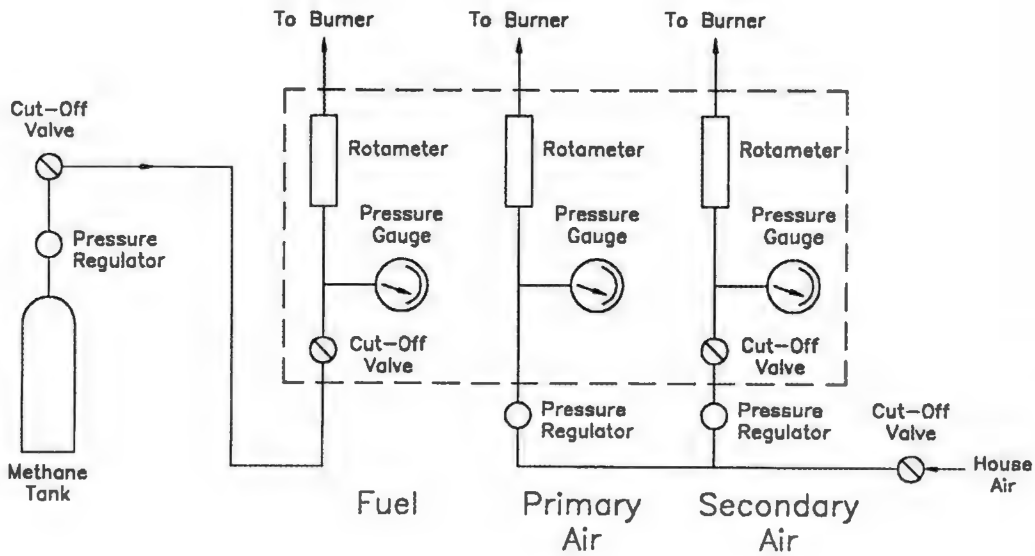

Figure 4: Schematic of the Plumbing System

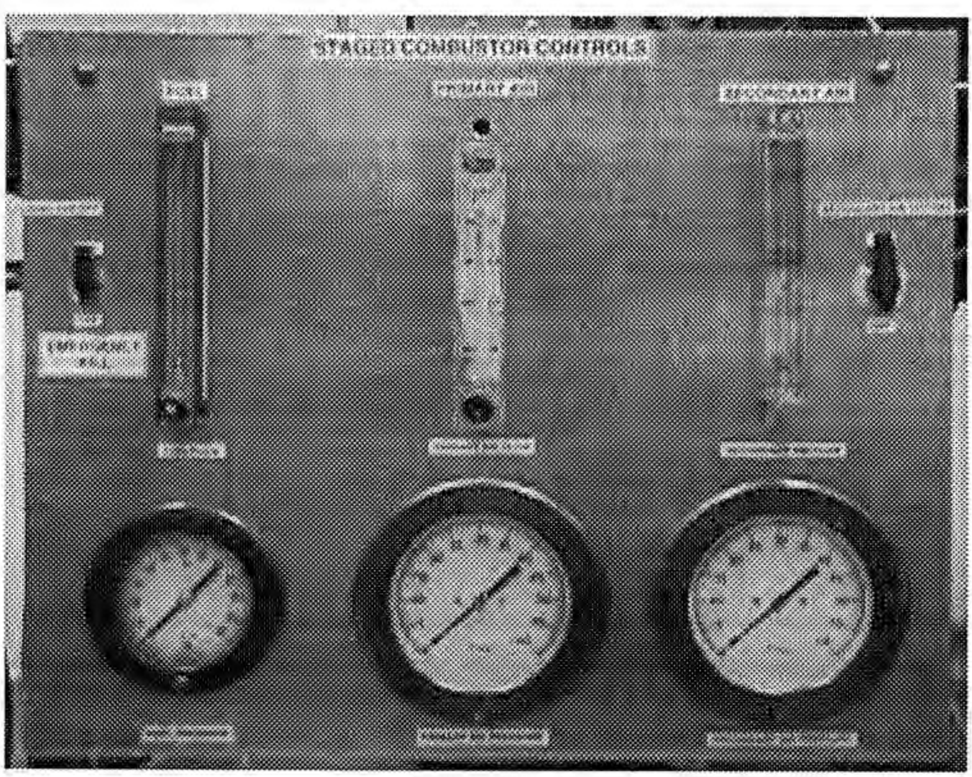

Figure 5: Photograph of the Control Panel

2.1.3 Data Acquisition System

Data collected from the experiments consist of light and pressure signals obtained from the burner flame. The signals from the silicon photodiode detector and from the pressure transducer are filtered before any data is acquired. The signals are filtered to remove 60 Hz powerline noise and DC offset using analog filters. The light and pressure signals are high-pass filtered at 0.1 Hz and low-pass filtered at 50 Hz using a Wavetek Dual Hi/Lo filter (Model 452) and a Rockland Dual Hi/Lo filter (Model 852), respectively. A 20-dB gain is used to amplify the low-pressure signal.

Light and pressure signals from the dual high/low pass filters are simultaneously recorded by a multichannel digital oscilloscope (Nicolet, Model 440). This allows the two signals to be compared to each other for differences and similarities. A sampling rate of 500 Hz is used over a two-minute time period to produce a total of 60,000 data points for both the light and pressure signals for a typical test run.

A photograph of the digital oscilloscope is shown in Figure 6.

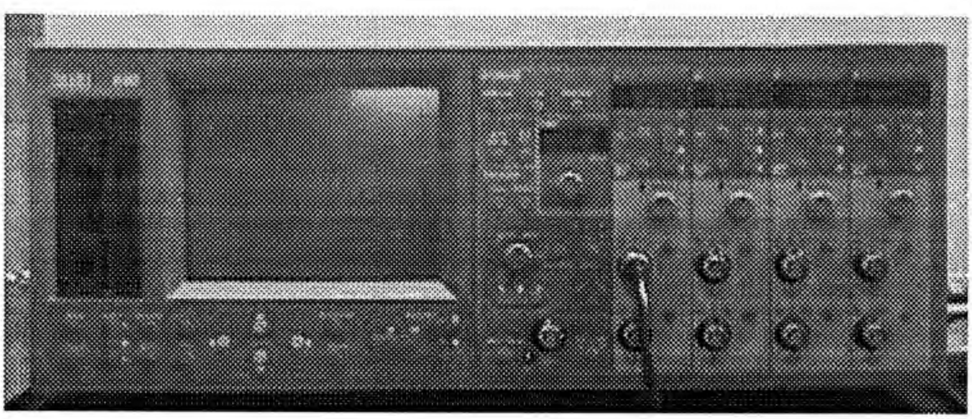

Figure 6: Photograph of the Nicolet Oscilloscope

2.2 Experimental Procedure

2.2.1 Start-up Procedure

At startup, the main cut-off valve for the house air is opened to start air flowing through the burner At the beginning of the experiment, the primary air pressure is regulated to 138 kPa (gage) The secondary air is not used and is shut off during start-up If needed, it can be turned on by opening the cut-off valve located on the control panel. The primary air flowrate is set to the desired value for each specific test After the desired air flow(s) is established, the first cut-off valve for the fuel is opened To light the burner, the second fuel cut-off valve located on the control panel is opened and the flame is ignited with a pilot flame For safety reasons, the fuel pressure is adjusted to its final setting only after the flame has been ignited This keeps methane from filling the room while the pressure is being set The fuel pressure is typically set to 138 kPa (gage), and the fuel flowrate is adjusted to the desired value After the flame has properly stabilized, light and pressure data signals are acquired After all desired tests have been run, the fuel is shut off at both cut-off valves The air is left on until the burner assembly has adequately cooled down (about ten minutes) and then shut off at the main cut off valve

2.2.2 Experimental Testing

The main objective of the experiments covered by this work is to investigate the instabilities of a premixed-flame as a function of equivalence ratio and volumetric flowrate Equivalence ratio is defined as the stoichiometric air-to-fuel ratio divided by the actual air-to-fuel ratio The experiments conducted in this study use overfire air in which excess air is supplied downstream from the burner. Special emphasis is placed on the rich conditions of the flame because these are the conditions most notably seen in the primary zone of overfire air burners No modifications to the burner assembly are necessary to conduct the experiments using the frequency generator The flame is observed during the experiments with a video camera This allows more indepth study of the flame shape and helps to explain the results A drawing of the flame is recorded in the data log for each run

Overfire air experiments are conducted to study the effects of bulk gas velocity (volumetric flowrate) on a rich premixed-flame This set of experiments is the main focus of this investigation, while the frequency generator experiments are conducted to support this area of study and provide comparative data The primary air flowrates are varied from 14 to 62 Lpm Each primary air flowrate constitutes one test The fuel flowrates are varied in each test from stoichiometric to very rich conditions with special emphasis added on areas of flame instability

A frequency generator is used to study the effects of very small changes in equivalence ratio on a flame The frequency generator is connected to a solenoid valve that injects small amounts of air into the primary combustion zone These tests are conducted at an equivalence ratio of 1 7, which is around the rich flammability limit of methane The fuel flowrate is maintained at 2 6 Lpm, the primary air flowrate is maintained at 19 Lpm, and the injected air flowrate is varied

Chapter 3

Data Analysis Methods

This chapter describes the basic concept and theoretical background for each of the different analysis techniques that are used to evaluate the linear and nonlinear structures in the pressure and light time-series measurements. In this study, linear and nonlinear time-series analysis of pressure and light measurements are used to characterize the instabilities of a premixed-flame as a function of equivalence ratio and bulk gas velocity (volumetric flowrate) Linear analysis techniques include the Fourier power spectrum, the autocorrelation function, and the crosscorrelation function Kolmogorov entropy is a nonlinear analysis technique The moving average filter used to pre-process the pressure and light time-series is described in Section 3 1 The Fourier power spectrum is detailed in Section 3 2, time-delay embedding in Section 3 3, the autocorrelation function in Section 3 4, the crosscorrelation function in Section 3 5, and Kolmogorov entropy is detailed in Section 3 6

3.1 Moving Average Filter

A finite-length, moving average filter is used to pre-process both the pressure and light time-series The moving average filter is used to eliminate (filter) the noise contained in the raw unfiltered time-series In the case of pressure, the noise is associated with the low, insufficient resolution of the pressure transducer The light signal is filtered using the same window size as the pressure signal for consistency and comparison The window size is selected by determining the size that provides the best correlation between the pressure and light signals

The window consists of the sum of the number of records, or data points, before each record, the record itself, and the number of records after each record For simplicity, the number of records before and after each record is chosen to be identical For example, for a window size of 5 $MA_j = 1/5[V_{j-2} + V_{j-1} + V_j + V_{j+1} + V_{j+2}]$, where V is the data value, MA is the moving average at temporal index, and j is the index point The moving average values for the first and last two records are not calculated and thus only the filtered time-series are used for further analysis [13]

3.2 Fourier Power Spectrum

Power spectra of time-series measurements are determined using FFT (Fast Fourier Transform) This is a common linear analytical technique that represents the frequencies present in a signal and their relative strength, or power The real component of the Fourier transform is squared to obtain the power at each frequency An input block size of 2^n measurements is used, where n is usually between 10 and 12 Power spectral densities (PSDs) from typically 10 to 15 consecutive, nonoverlapping blocks are averaged to form the overall PSD composite. For a pure, single-frequency signal, the power is concentrated in a single peak. Near the onset of chaos, there is a widening of the spectral peaks, as power is distributed among a range of frequencies [13]

During stable flame behavior, little is obtained from the power spectra of the time-series due to the flame's chaotic behavior As the flame begins to become ordered, a single- predominant frequency signal is easily seen The pressure and light time-series signals are compared to each other and should exhibit similar power spectra

3.3 Time-Delay Embedding

A system's complete dynamical state can be reconstructed from a single time-series measurement through time-delay embedding Embedding converts a scalar time-series to a vector space For a time-series given by

$$\vec{x} = \left\{x_1, x_2, x_3, \ldots, x_N\right\}^{\mathrm{T}} , \tag{3-1}$$

time-delay vectors are formed by

$$\vec{\xi}_i = \left\{x_i, x_{i+\tau_E}, x_{i+2\tau_E}, \ldots, x_{i+(m-1)\tau_E}\right\} , \tag{3-2}$$

where i is the vector index, τ_E is the embedding lag, and m is the embedding dimension The quantity $\vec{\xi}_i$ is now a vector in m-dimensional space This analytical procedure allows more advanced techniques to be used such as the autocorrelation function, crosscorrelation function, and Kolmogorov entropy These three analysis techniques are described in detail below [13, 14]

3.4 Autocorrelation Function

The evaluation of the autocorrelation of a temporal sequence is used to measure/quantify serial coupling between elements in a time-series. The best estimate of the autocorrelation coefficient is defined as

$$r_k = \frac{c_k}{c_o}, \tag{3-3}$$

for

$$c_k = \frac{1}{N-k} \sum_{1 \le i \le N-k} (x_i - \bar{x})(x_{i+k} - \bar{x}) , \tag{3-4}$$

where k is the lag or number of events in time, c_k is the correlation coefficient at lag k, c_o is the variance in x, $\bar{x}$ is the set mean, and N is the number of elements in the set The first autocorrelation coefficient is one by definition, as the correlation coefficient at lag zero (c_o) is the data variance For higher-order coefficients, non-zero values indicate the degree of coupling in time For a zero-mean, random process, all finite-lag coefficients tend to zero The first zero crossing, or minimum in the absence of a zero crossing, of the autocorrelation function is taken as the *decorrelation time*, or the number of timesteps on average between totally decoupled events Peaks beyond the initial dip in the autocorrelation function denote periodicities or strong coupling and are defined as *correlation times* The dominant timescales as indicated by the autocorrelation function are important indicators of the expected time window for accurate predictions [13]

For very stable flames, little is obtained from the autocorrelation function As the flame becomes periodic, very distinct peaks are seen This occurs when the flame begins to anchor somewhere else other than at the burner and alternate between the two The pressure and light time-series are compared to each other to determine any correlations

3.5 Crosscorrelation Function

The crosscorrelation function determines the correlation between two simultaneously measured time-series Crosscorrelation measures the amount of predictability of the test (light) signal as a function of time based on the reference (pressure) signal Crosscorrelation is defined as

$$r_{xy}(\tau) = \frac{1}{N-\tau+1}\left[\frac{\sum_{i=1}^{N-\tau} x(i)y(i+\tau)}{\sigma_x \sigma_y}\right], \qquad (3\text{-}5)$$

where τ is the lag time, i is the correlation length, and N is the length of the time-series [13]

When the flame is stable, both the pressure and light signals are very complex due to the flame's chaotic behavior As a result, the correlation between the two signals is very low When the flame becomes periodic, when jumping occurs, strong correlation is seen between the pressure and light signals The crosscorrelation shows strong very periodic behavior that dies out over time

3.6 Kolmogorov Entropy

Kolmogorov entropy can be considered as a measure of the amount of information loss in a signal or as a measure of predictability in a signal The Kolmogorov entropy is zero for a periodic or cyclic signal, infinite for a perfectly random signal, and finite for a deterministically chaotic signal The maximum-likelihood estimator of the Kolmogorov entropy is based on the calculation of the average time for initially close trajectory segments to diverge beyond a specified tolerance, or *cutoff length* Candidate pairs of points are randomly sampled from the time-series, and the trajectory segments are tested pointwise using the maximum norm to find divergence beyond the cutoff length Candidate pairs that do not diverge beyond the test *segment length* are classified as *qualifying pairs*, and each qualifying pair is tracked until divergence beyond the cutoff length occurs The maximum-likelihood estimate of Kolmogorov entropy is

$$\hat{K}_{ML} = -\frac{1}{\tau_S}\log\left[1-\frac{1}{\overline{b}}\right], \tag{3-10}$$

for

$$\overline{b} = \frac{1}{M}\sum_{1\le i\le M} b_i , \tag{3-11}$$

where τ_s is the timestep size, b is the divergence time in timesteps, and M is the number of qualifying pairs [13, 16] The segment length is specified according to a dominant time scale of the data, conveniently defined as the average time between upward crossings of the data mean, and the cutoff length is specified with respect to a characteristic length scale, such as the average absolute deviation about the mean [13]

The normalization of entropy is accomplished by comparing the entropy value against an *ultimate entropy* The ultimate entropy is the entropy of a random signal with the same probability distribution as the original signal and it accounts for the probability that a certain fraction of point pairs will not diverge purely by chance The ultimate entropy is defined as

$$\hat{K}_{ult} = -\log C'_{l_c}, \tag{3-12}$$

where C is a one-dimensional correlation integral given as

$$C_{l_c} = \frac{1}{M}\sum_{i \neq j} \Theta\left(l_c - \left\|\vec{x}_i - \vec{x}_j\right\|\right) \tag{3-13}$$

In equation 3-13, Θ is the Heaviside function defined as

$$\Theta\,(\mathrm{a}-\mathrm{b}) = \begin{Bmatrix} 1 & \mathrm{a} > \mathrm{b} \\ 0 & \mathrm{a} \leq \mathrm{b} \end{Bmatrix}, \tag{3-14}$$

l_c is the cutoff length, $\vec{x}_i$ and $\vec{x}_j$ are embedded vectors, and M is the number of pairs in the initial random sample [13] The ultimate entropy provides a practical limit of infinite entropy and serves as a basis to measure the *normalized entropy* defined as

$$\langle \hat{K}_I \rangle = \frac{\hat{K}_{ML}}{\hat{K}_{ult}} \tag{3-15}$$

The entropy values are plotted as a function of equivalence ratio for both the pressure and light signals For a perfectly periodic signal the expected Kolmogorov entropy is zero When the flame begins to jump, the signals become periodic, and the entropy is very small For positionally stable flames, the entropy value increases considerably

Chapter 4

Experimental Results and Discussion

This chapter consists of a presentation and discussion of results obtained from the study of the instabilities associated with a rich premixed-flame Section 4 1 discusses the results from the overfire air experiments Section 4 2 discusses the results obtained using the frequency generator An uncertainty analysis is given in the Appendix Due to the large amount of data taken it would be impractical to show the entire collection Instead, only typical observations of all data are presented

4.1 Overfire Air

Using high air and fuel flowrates in the low-NO_x burner modifies it into an overfire air burner The overfire air is supplied from outside the burner apparatus above the glass shield from the surrounding air The overfire air configuration occurs only when the burner is operated in the fuel-rich condition Without secondary air and at these high air flowrates, the flame is extremely unstable and tends to blowout when operated in the fuel-lean condition Around the rich flammability limit of methane, occurring around an equivalence ratio (Φ) of 1 65, the flame becomes unstable at the burner and begins to alternate between the burner and the top of the glass shield where more oxygen is prevalent This continues until the flame becomes extremely fuel-rich, and at which point anchors exclusively at the top of the glass shield, creating a diffusion flame

4.1.1 General Observations

In order to adequately categorize the instabilities associated with using overfire air, the entire range of flame phenomena is broken up into eight main characteristics, or flame events Each of these different flame events and the equivalence ratios at which it occurs is given in Table 1 The highlighted segments correspond to the best representative of each flame event and will be used for each analysis technique when describing that particular event, unless otherwise noted A sketch of each flame event can be seen in Figure 7 Each condition is described in detail below

The first flame event, FE-1, encountered is when the flame is anchored solely at the burner, as seen in Figure 7a This occurs around stoichiometric conditions, equivalence ratios ranging from 0 97 to 1 35, for the entire range of air flowrates tested The primary flame appears blue-violet in color and is very cellular The blue-violet color is due mostly to large concentrations of CH radicals [17] A very faint red-violet conical glow is seen outside of the inner cellular flame The red-violet color is due to the burned gases that consist of radiation from CO_2 and water vapor [17] This flame is considered stable

The second flame event, FE-2, shown in Figure 7b, is similar to the first except that now a second faint blue flame is seen at the top of the glass shield The blue color is due to the radiation of CH The inner flame also begins to become slightly unstable The second flame event is observed to be strongly dependent on the air flowrate As seen in Table 1, the equivalence ratios for airflows above 33 Lpm are appreciably lower than those for lower airflows This effect is due to the higher flow velocities produced by the higher air flowrates, producing less stable flames

Table 1: Equivalence Ratio at Which Each Flame Event Occurs for Various Volumetric Flowrates of Air

	Equivalence Ratio (Φ) for each Volumetric Flowrate of Air (Lpm)					
Flame Event	**14.2**	**18.9**	**33.0**	**42.5**	**51.9**	**61.4**
FE-1	0 99	1 35	0.97	1 05	1 11	1 04
FE-2	1.49	1 69	1 35	1 32	1 29	-----
FE-3	1.65-1 68	1 73	-----	-----	-----	1 25
FE-4	1.82	1 86	-----	1 39	1 35	1 35
FE-5	-----	-----	1 55	-----	1 54	1.56
FE-6	-----	-----	1 74	1.58-1.81	1 60-1 72	1 77
FE-7	2 31	2 03	1 94	1.96	1 91	1 98
FE-8	-----	2 37	2.32	2 11	2 09	2 08

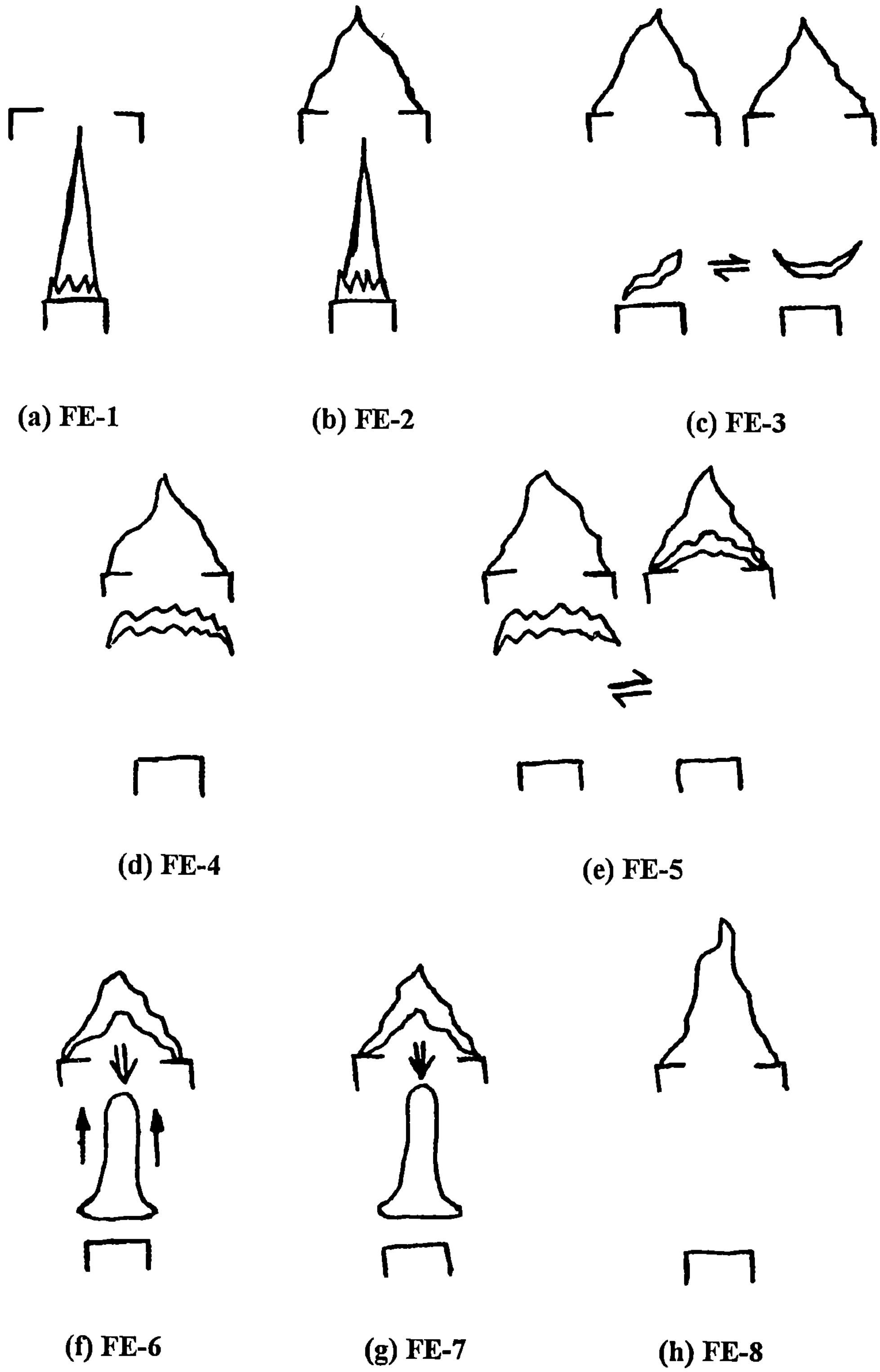

Figure 7: Sketch of Flame Events

Figure 7c shows the third flame event, FE-3, which depicts the onset of instability in regards to the flame anchoring at the burner. While the flame attached to the top of the glass shield remains the same, the inner flame at the burner becomes extremely unstable and begins to lift off of the burner, float in the tube, and return again to the burner This occurs repeatedly without any regularity, or periodicity The inner flame also becomes more blue-green, turquoise, in color This is due to the radiation from C_2 molecules, which means that the flame is becoming more fuel-rich [18] As the equivalence ratio approaches 1 65, i e , the rich flammability limit of methane in air, the flame instabilities occur The rich flammability limit is the point at which the richest concentrations will just self-support a flame The reason for the flame lifting off of the burner and returning is due to the small fluctuations in the gas flows This is proven by the supplemental tests conducted at an air volumetric flowrate of 18 9 Lpm using a frequency generator and will be discussed in detail below In Table 1 it is noticed that at an air volumetric flowrate of 61 4 Lpm the onset of flame instabilities occurs at a lower equivalence ratio only 1 25 This observation is discussed further in Section 4.1 2

In the fourth flame event, FE-4, the inner flame floats in the glass shield, or tube, with the outer flame still attached at the top and is shown in Figure 7d The floating flame is slightly greener than the previously unstable flame, while the flame attached at the top of the glass shield becomes blue-violet The outer flame is also much brighter than in previous cases The inner flame becomes positionally stable, floating in the tube because the burning velocity of the flame front, the laminar-flame speed, is equal in magnitude and opposite in direction to the flow of the premixed gases [19, 20] In flame event four at the higher gas flowrates, the unburned gas velocities become larger than the flame speeds much sooner than those at the lower gas flowrates As a result, the flame becomes unstable at much lower equivalence ratios

The fifth flame event, FE-5, shown in Figure 7e, occurs when the flame jumps from floating in the tube to the top of the tube and back again The flame colors are similar to those in the previous condition The flame is no longer stable inside the glass tube and seeks a place where there is more oxygen The instabilities of FE-5 are similar to those for FE-3 except now the inner flame attaches to the top of the glass shield instead of the burner The flame becomes nearly periodic in its jumping back and forth.

In flame event six, FE-6, the flame propagates down from the top of the tube through the entire length of the glass shield and up again in a periodic manner (period of 5 seconds) This process is called bifurcation This jumping is represented in Figure 7f by the arrows drawn in both directions indicating that the flame propagates back and forth With the flame unable to be supported at the burner, it now anchors at the top of the glass shield where more oxygen is prevalent and becomes more of a diffused flame than a premixed one During the time that the flame is anchored at the top of the glass shield, oxidizer from ambient air slowly diffuses into the glass tube When the mixture inside the glass tube is within the flammability limit, the flame propagates down the length of the tube When all of the available oxidizer is consumed, the flame either dies out or propagates back up the tube This is similar to a condition called flashback that occurs when the flow velocity is gradually reduced to the point where it is smaller than the flame speed and the flame propagates down into the burner [19] It is also worth noting that the jumping of the flame is accompanied by a whooshing sound

The seventh flame event, FE-7, is similar to the sixth except the jumping occurs much less periodically. Instead of the inner flame propagating down through the tube and back again, it typically dies out, with only the outer flame attached at the top sustaining the flame The singular motion of the flame is shown in Figure 7g. As can be seen in Table 1, the equivalence ratios for all volumetric flowrates are approximately equal for this event as with the first two flame events

The final flame event, FE-8, shown in Figure 7h, is where the flame is anchored solely at the top of the glass shield and becomes a diffusion flame No propagation occurs when the equivalence ratio is over 2 00 (fuel-rich) As expected with a diffusion flame, yellow is the predominant color This is a result of the highly fuel-rich mixture in which carbon particles form producing an intense yellow radiation [17].

4.1.2 Time Series of Pressure and Light Signals

Data are obtained for this study by acquiring pressure and light signals every 2 ms, or at a sampling frequency of 500 Hz, for two minutes creating time series records of 60,000 points in length Before any data analysis is carried out, both the pressure and light time series are filtered using a finite-length moving average filter with a window size of 51 The window size consists of the sum of the number of records, or data points, before a given record (25), the record itself (1), and the number of records after the given record (25) A window size of 51, which captures everything below 10 Hz, is chosen because it provides the best visual similarity between the pressure and light signals. The pressure signal is filtered because the pressure transducer has insufficient resolution to adequately measure the flame and because of the amplified flow noise. The light signal is filtered to provide better comparison with the pressure Figures 8-10 show the unfiltered and filtered time series for a few representative pressure signals All further time series presented in this thesis are filtered using a moving average filter with a window size of 51 and have been normalized to have unit standard deviation for direct comparison of the pressure and light signals

The time series for the first two flame events are extremely similar with no distinguishing characteristics between them Figure 11 shows a representative time series for these two flame events Specifically, it is that of a flame with a volumetric flowrate of air (AV) of 33 0 Lpm and an equivalence ratio (Φ) of 0 97 As can be seen, the pressure and light signals appear to be correlated, and the signals appear to be rather complex The signals are complicated in flame events one and two because the cellular structure of the flame anchored at the top of the burner There is a lot of movement of the flamelets, which result in the rather complex signals

Flame event three shows the onset of instability. In Figure 12, the time series of the pressure and light signals of a flame with an AV of 14 2 Lpm and Φ of 1 65 are shown The onset of instability is not clearly seen in the time series, but compared to Figure 11, the signals are less complex While not periodic, the signals are not completely random either, as seen by the large peaks in both the pressure and light signals There is strong correlation between the pressure and light signals with the pressure signal slightly leading the light The large peaks occur when the flame returns to the burner after temporarily lifting off. The low amplitude parts of the signal correspond to the flame when it is floating in the tube

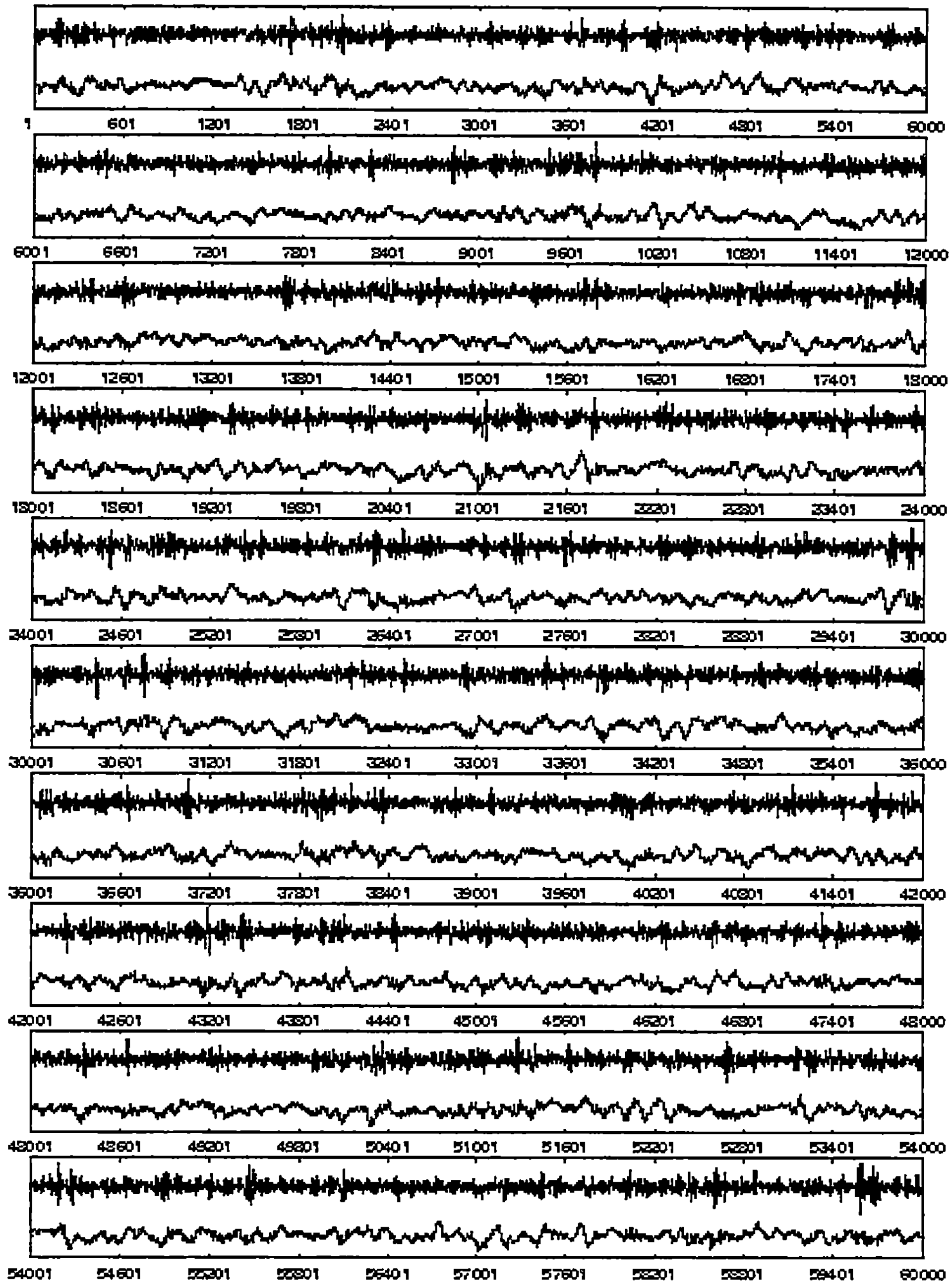

Figure 8: (a) Unfiltered (Top) and Filtered (Bottom) Pressure Signals

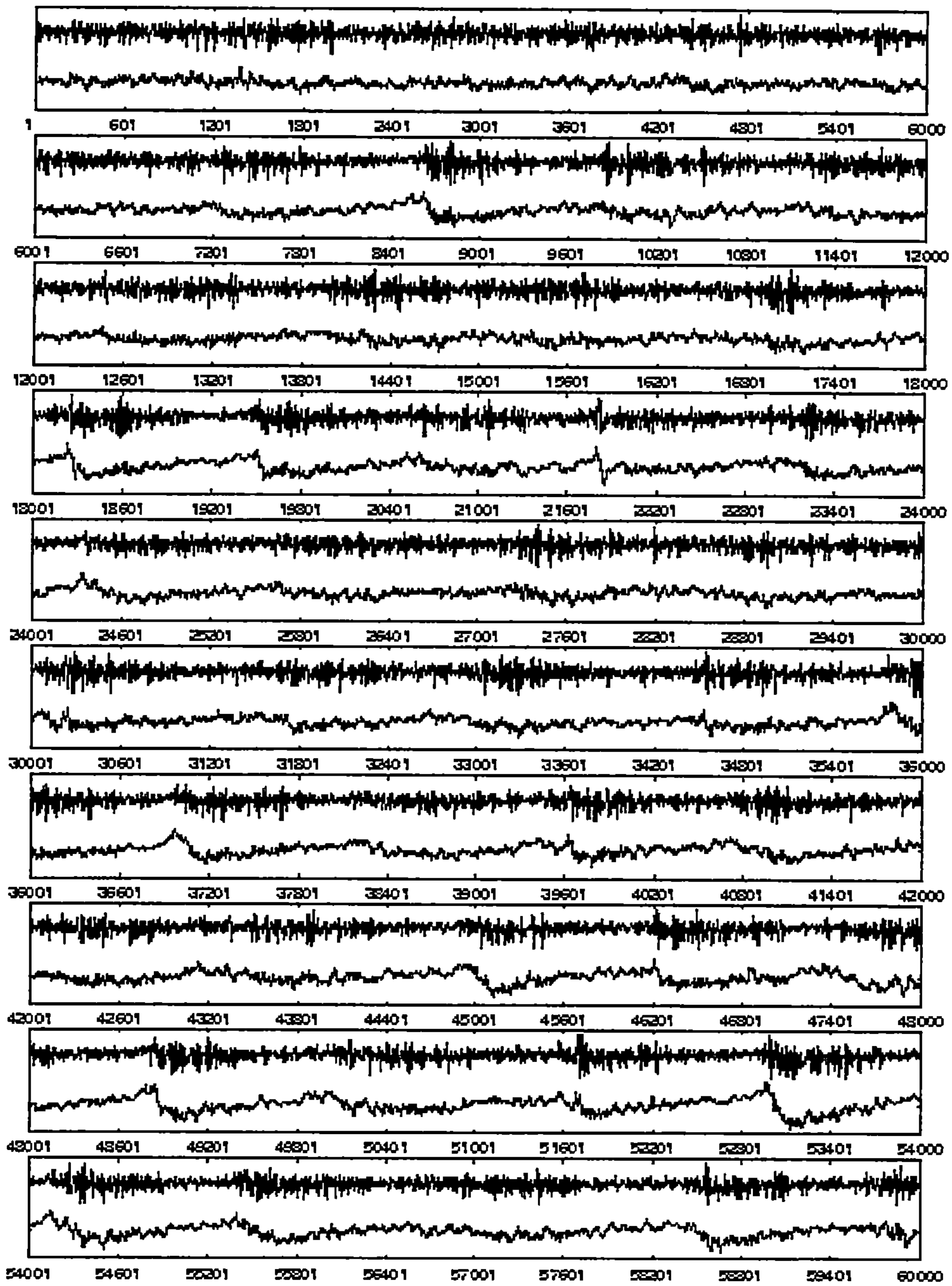

Figure 9: (b) Unfiltered (Top) and Filtered (Bottom) Pressure Signals

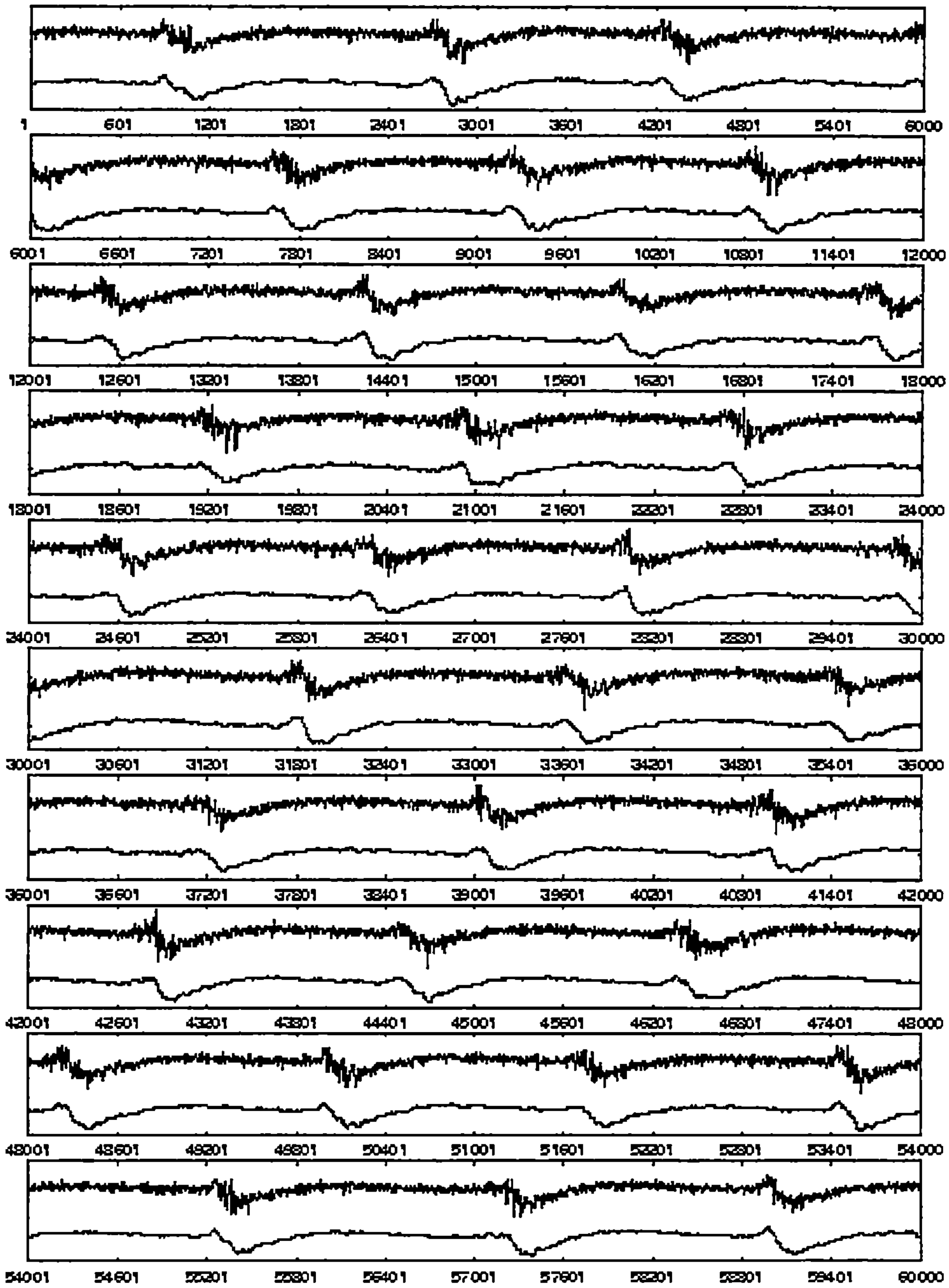

Figure 10: (c) Unfiltered (Top) and Filtered (Bottom) Pressure Signals

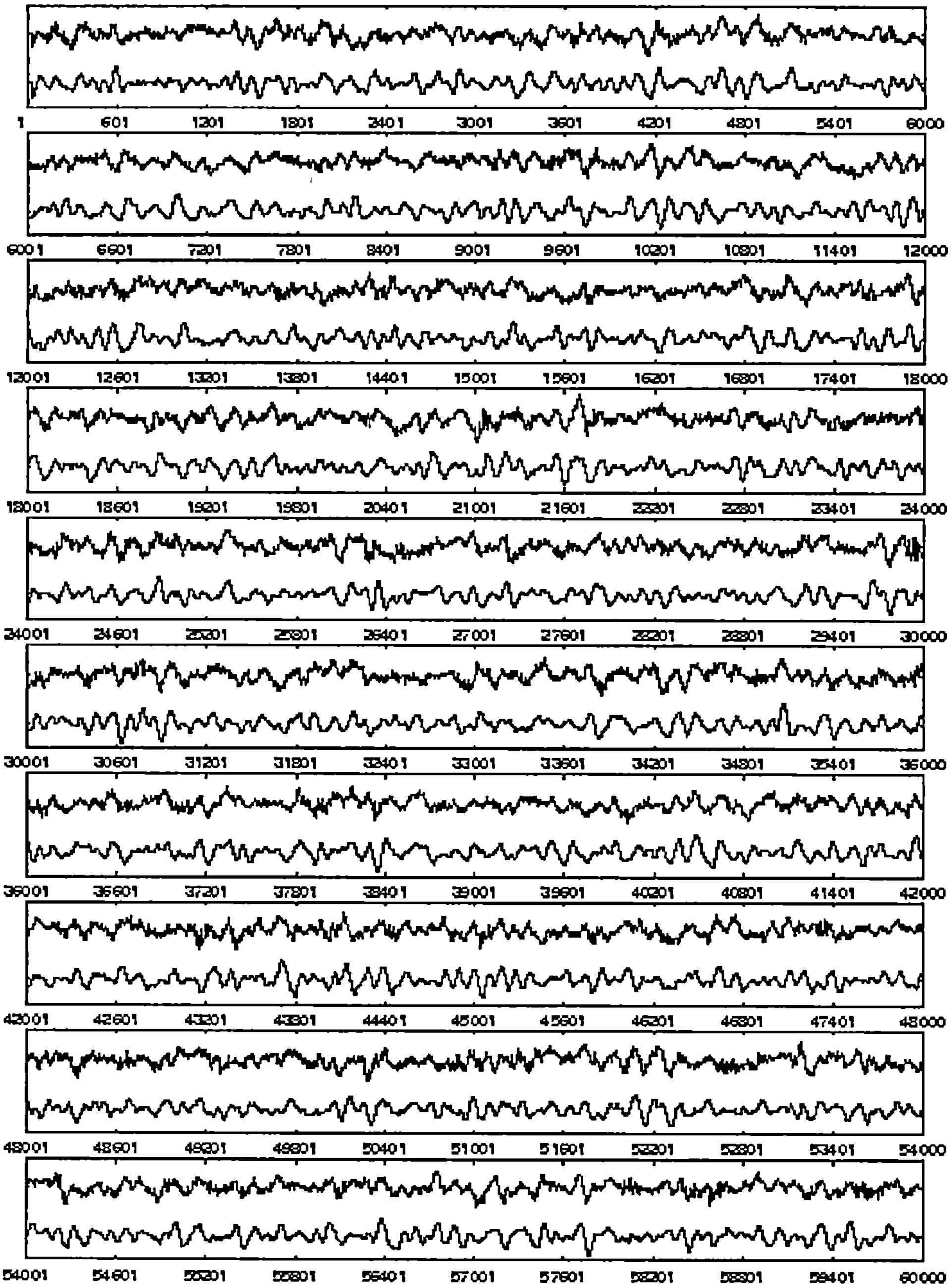

Figure 11: Pressure (Top) and Light (Bottom) Time Series

for FE-1 - AV = 33.0 Lpm and Φ = 0.97

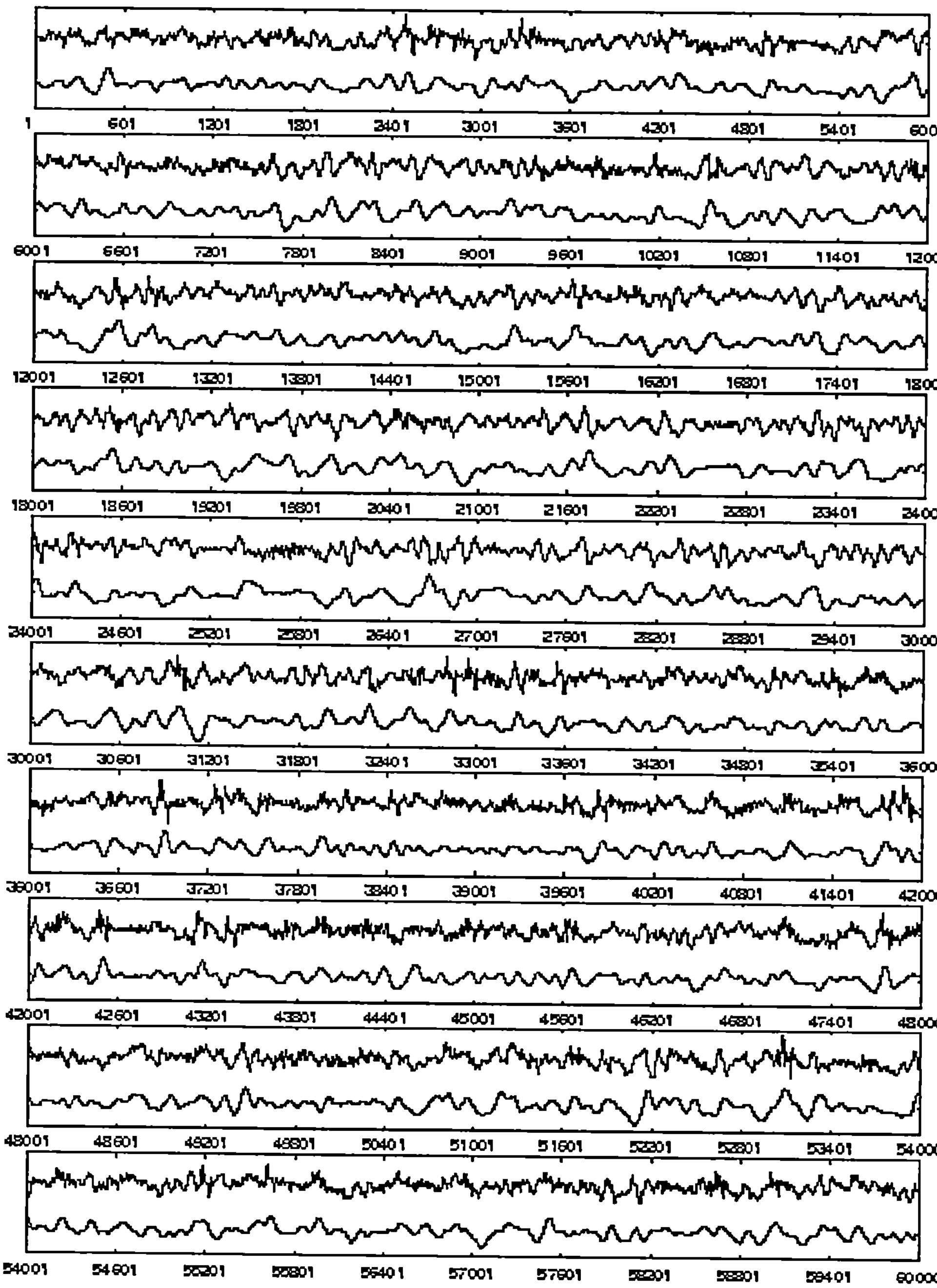

Figure 12: Pressure (Top) and Light (Bottom) Time Series

for FE-3 - AV = 14.2 Lpm and Φ = 1.65

Figure 13 shows a representative time series for flame event four, specifically that of a flame with an AV of 14 2 Lpm and Φ of 1 82 This flame event has the flame floating in the glass tube As a result of the flame being so far away from the burner, the magnitude of the light and pressure signals decreases considerably The pressure is measured from a pressure tap approximately 25 mm below the top of the burner The magnitude of the pressure signal will be at a maximum when the flame is anchored at the burner and as the flame moves further and further away, the magnitude of the signal decreases accordingly There is some correlation seen between the pressure and light

Figure 14 shows the time series for flame event five, FE-5, at an AV of 61 4 Lpm and Φ of 1 56 In this flame event the flame has become much more ordered and slightly periodic When the flame is floating in the tube, the amplitude of the pressure and light signals is very small When the flame approaches the burner, the amplitudes get much larger as expected The light signal has also started to slightly lag behind that of the pressure signal The reasons for this are discussed below

For flame event six, two representative time series are chosen to show two flames with two different jumping periods Figure 15 shows a flame at an AV of 42 5 Lpm and Φ of 1 58 This flame has a jumping period of about 1 6 seconds Figure 16 shows the time series of the pressure and light signals of a flame with the same air flowrate but at an equivalence ratio of 1 81 As the flame is made richer (larger Φ), the period is increased to approximately 3 seconds By making the flame just slightly more fuel-rich, the period becomes twice as large, indicative of period doubling This is expected because for the flame to propagate down the glass tube at a more rich condition, more oxygen is needed to induce the flame to jump, which accounts for the longer period As

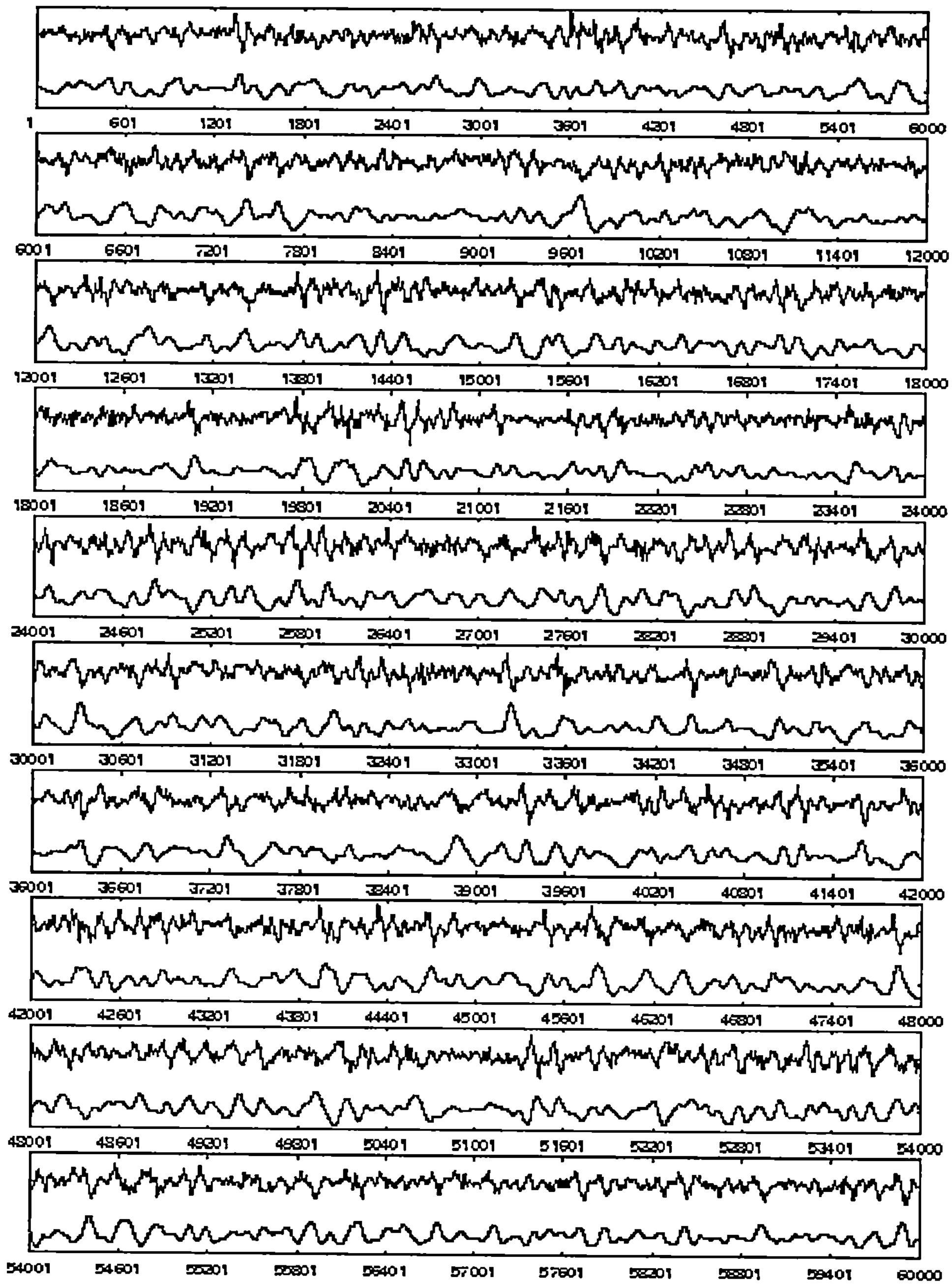

Figure 13: Pressure (Top) and Light (Bottom) Time Series

for FE-4 - AV = 14.2 Lpm and Φ = 1.82

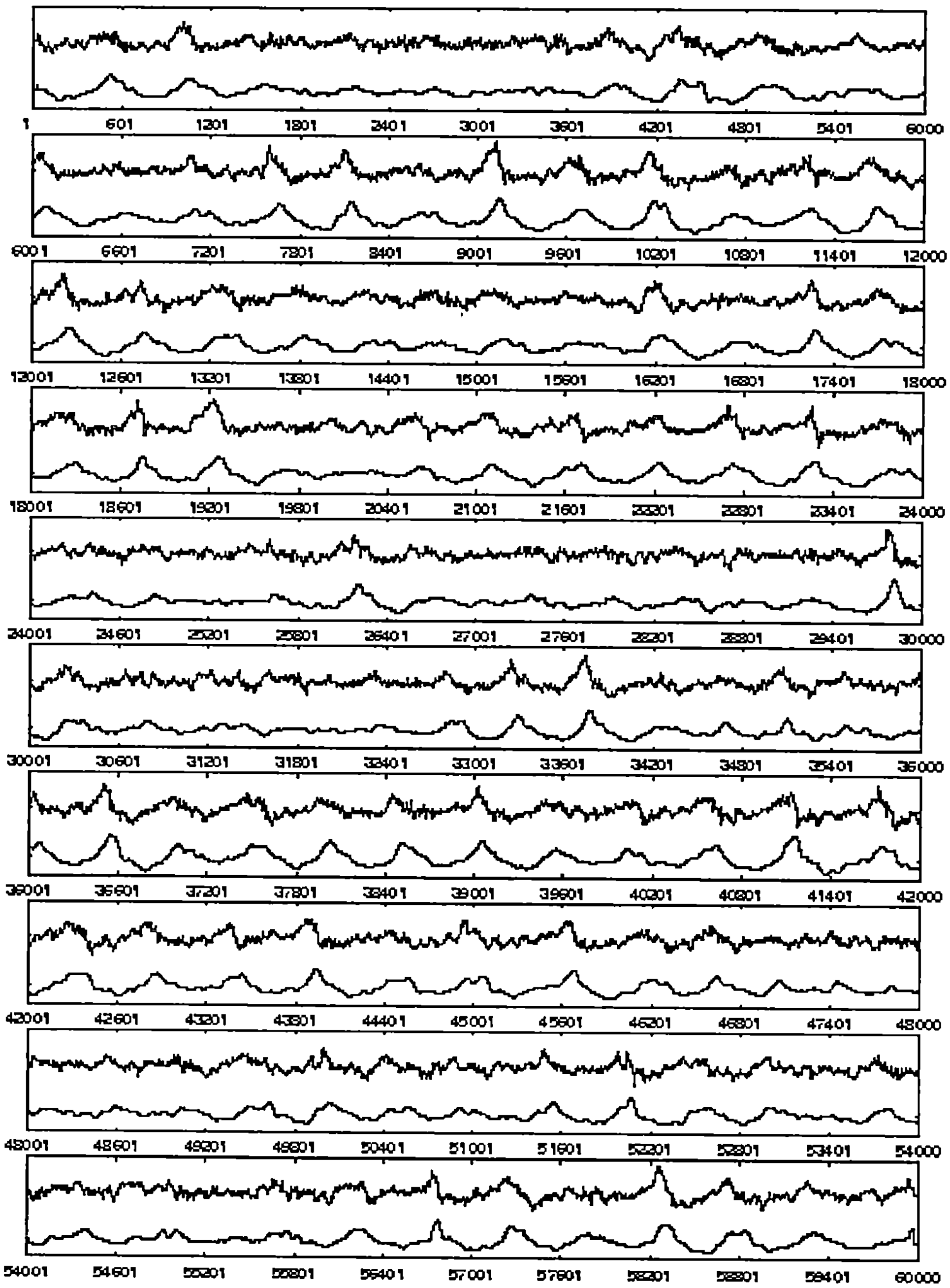

Figure 14: Pressure (Top) and Light (Bottom) Time Series

for FE-5 - AV = 61.4 Lpm and Φ = 1.56

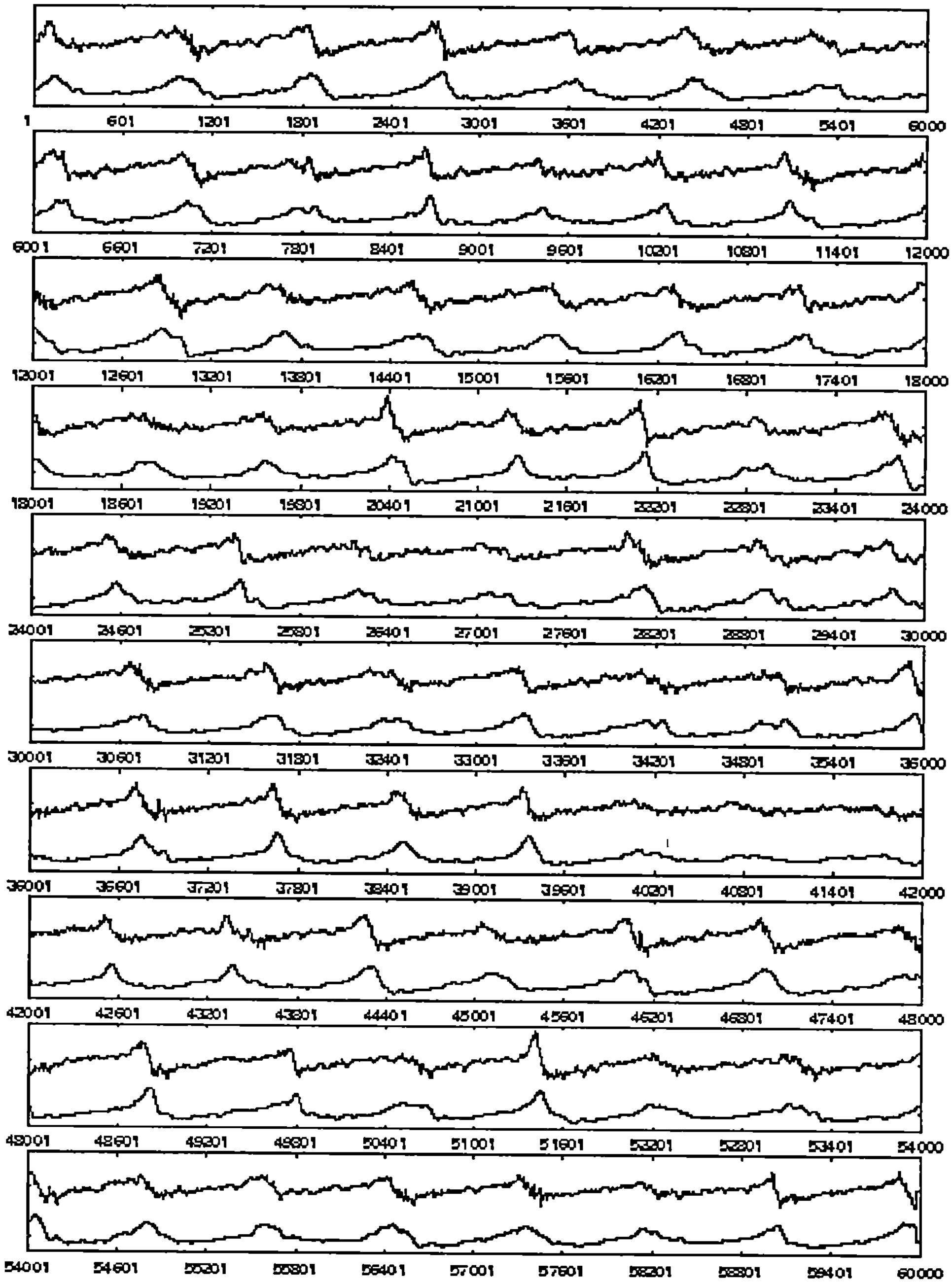

Figure 15: Pressure (Top) and Light (Bottom) Time Series

for FE-6 - AV = 42.5 Lpm and Φ = 1.58

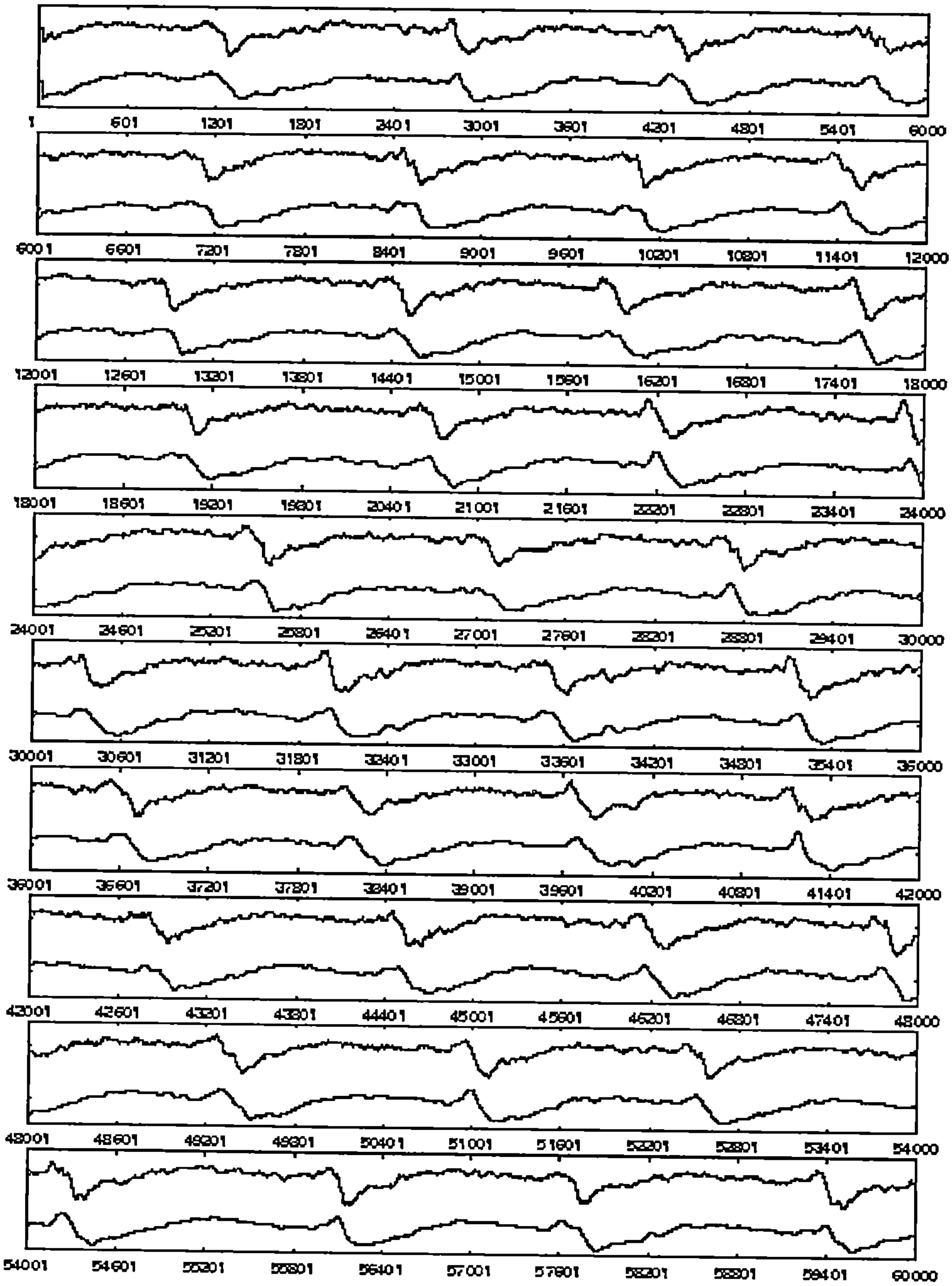

Figure 16: Pressure (Top) and Light (Bottom) Time Series

for FE-6 - AV = 42.5 Lpm and Φ = 1.81

before, the large magnitudes correspond to the flame when it is closest to the burner and the small magnitudes when the flame is furthest away at the top of the glass shield. The lag between the pressure and light signals is much more evident now than before The reason for the pressure leading the light is because pressure is the driving force It cannot be explained by any type of delay due to the speed of the light signal, since light travels much faster than pressure The pressure and light signal are at a maximum when the flame is closest to the burner The pressure signal slowly increases, and this is attributed to the build up of unused oxidizer inside of the glass tube When enough oxidizer is inside the tube to support the flame, the flame jumps, accounting for the peak in the light signal As the flame jumps, the oxygen is consumed, and the pressure signal drops Oxygen again builds up in the tube and the process starts all over again The burner assembly is tested for leakage to insure that the oxidizer is diffusing into the glass tube from above and not from below The mechanism of flame propagation is supported by performing an experiment in which air is injected into the burner using a solenoid valve

Flame event seven is similar to flame event six, except that now the jumping of the flame is not as periodic Figure 17 shows a flame with an AV of 42 5 Lpm and Φ of 1 96 The time series for this flame event show the sporadic jumping of the flame At this condition, the time series is similar to those of flame event six, FE-6

Figure 18 shows a representative time series for flame event eight, specifically that of a flame with an AV of 33 0 Lpm and Φ of 2 32 The flame is anchored solely at the top of the glass shield and the time series resemble those where the flame is either anchored at the burner or floating in the tube The reason for this is because in these positions, the

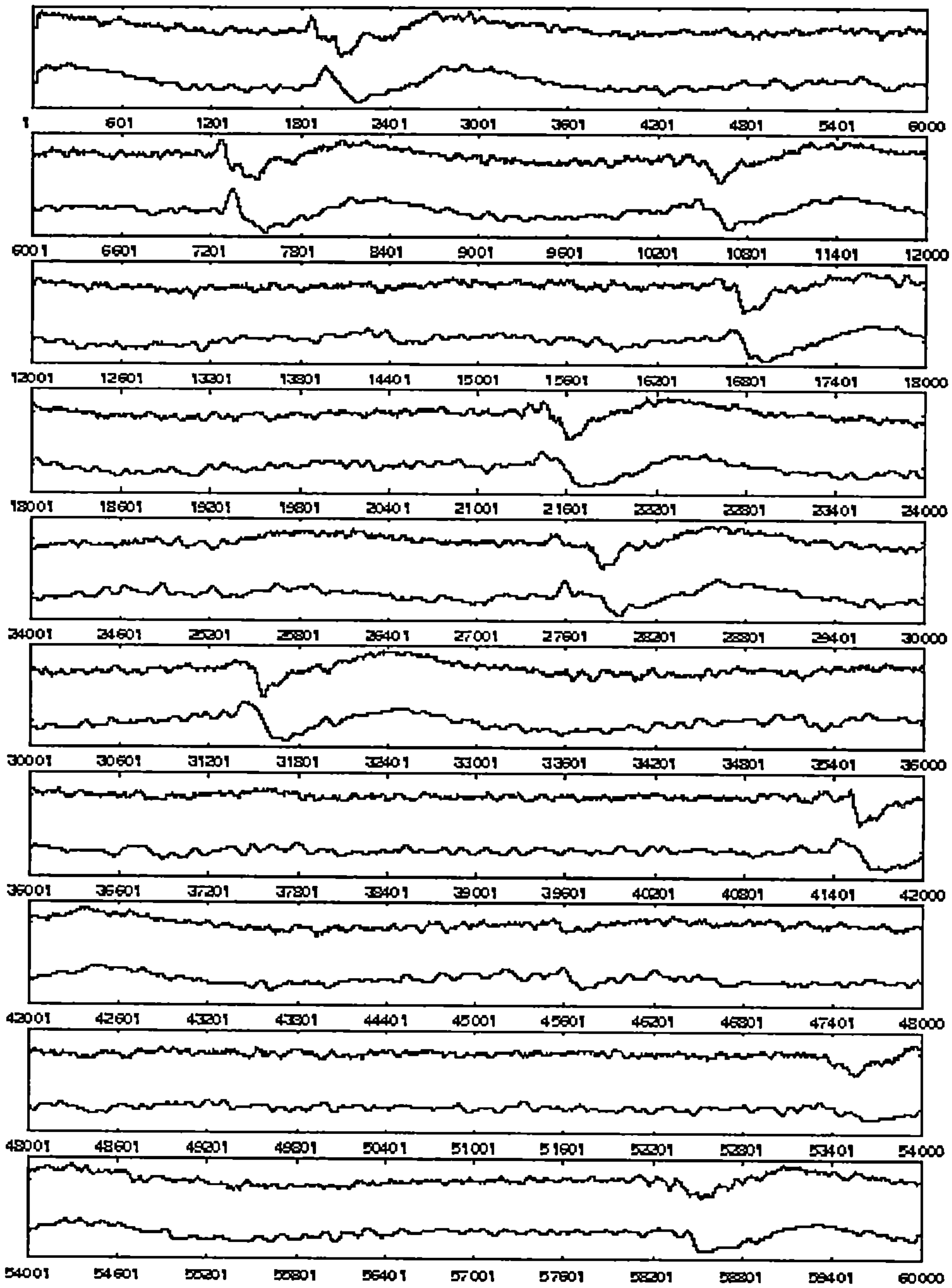

Figure 17: Pressure (Top) and Light (Bottom) Time Series

for FE-7 - AV = 42.5 Lpm and Φ = 1.96

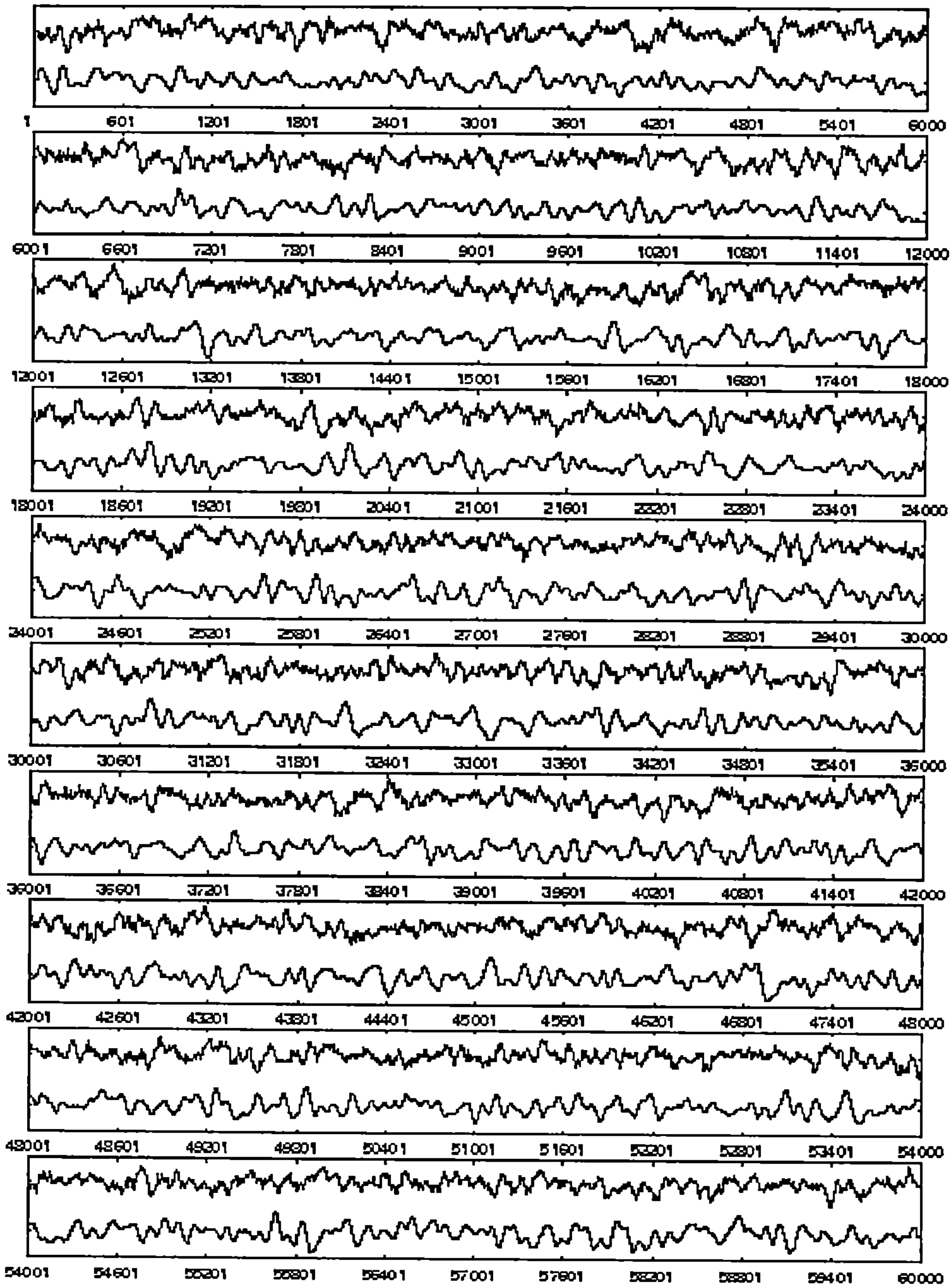

Figure 18: Pressure (Top) and Light (Bottom) Time Series

for FE-8 - AV = 33.0 Lpm and Φ = 2.32

flame is completely stable and only the chaotic characteristics of these flames are seen in the pressure and light signals

4.1.3 Fourier Power Spectrum

Representative Fourier power spectra for each of the eight flame events are shown in Figures 19-27 For both the pressure and light signals, power is plotted versus frequency The dominant frequencies in all power spectra are less than 10 Hz, with most less than 5 Hz Over 95 percent of the cumulative power for the light signals is less than 10 Hz, while 85 percent of the cumulative power for the pressure signals is less than 20 Hz The reason for this is that the signal-to-noise ratio of the light signal is much larger than that of the pressure signal, creating more dominant frequencies in the 0 to 10 Hz range Furthermore, the pressure transducer used does not have sufficient resolution to measure the pressure fluctuations of the flow Note that the amplitude and frequency scales in these figures are varied to show maximum detail

Figure 19 shows a representative power spectrum for flame event one, specifically that of a flame at an AV of 33 0 Lpm and Φ of 0.97 The pressure and light signals are more complex at this condition due to the movement of flamelets on the flame holder creating broadband power spectra This is seen in the wide range of frequencies for both the pressure and light signals The signals seem to correspond somewhat with the pressure signal having a greater frequency concentration below 2 Hz

Figure 20 shows a very strong correlation between the pressure and light signals for a flame with an AV of 14 2 Lpm and Φ of 1 49 Again, no single dominant frequency is

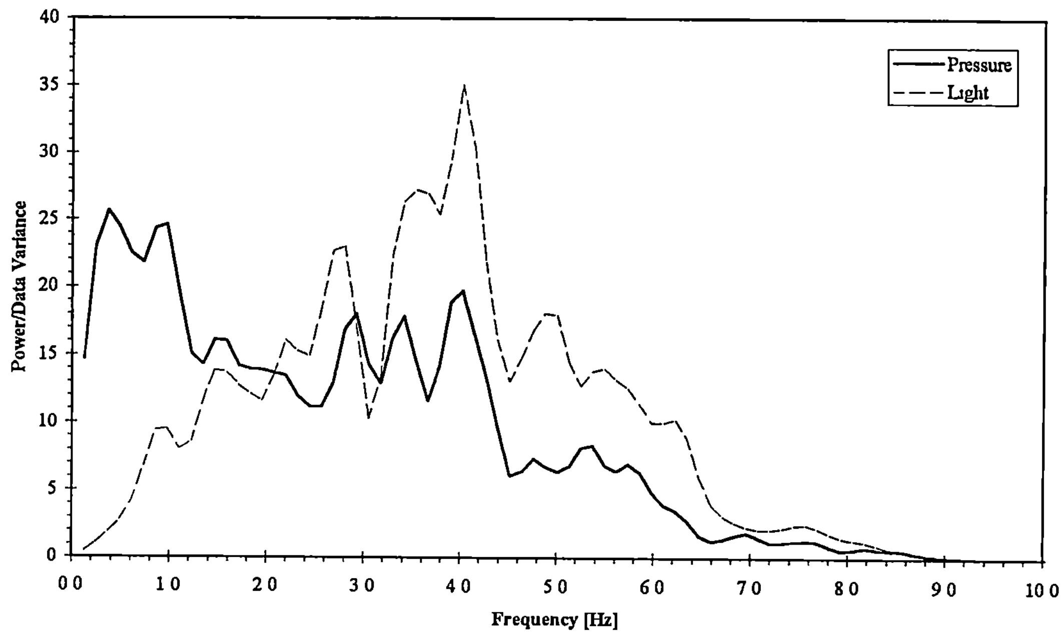

Figure 19: Fourier Power Spectra for FE-1 - AV = 33.0 Lpm and Φ = 0.97

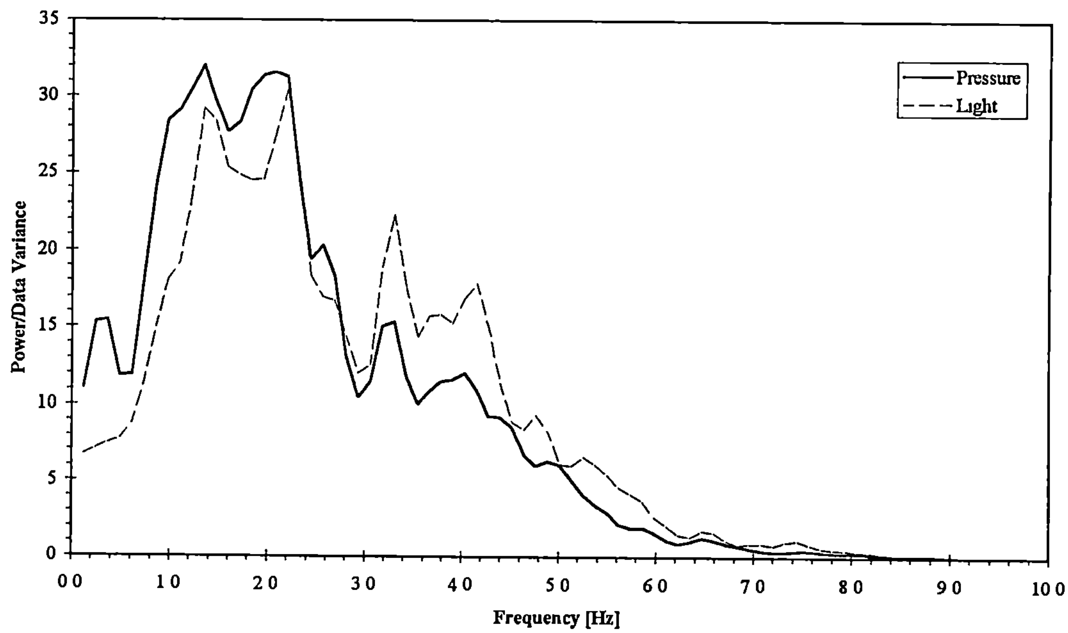

Figure 20: Fourier Power Spectra for FE-2 - AV = 14.2 Lpm and Φ = 1.49

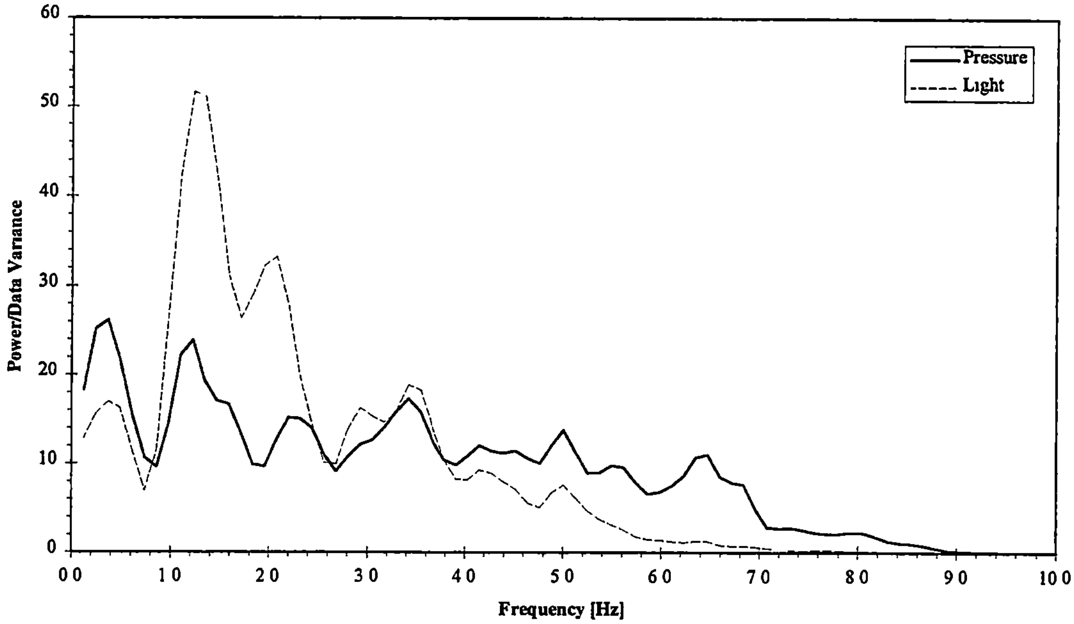

Figure 21: Fourier Power Spectra for FE-3 - AV = 14.2 Lpm and Φ = 1.65

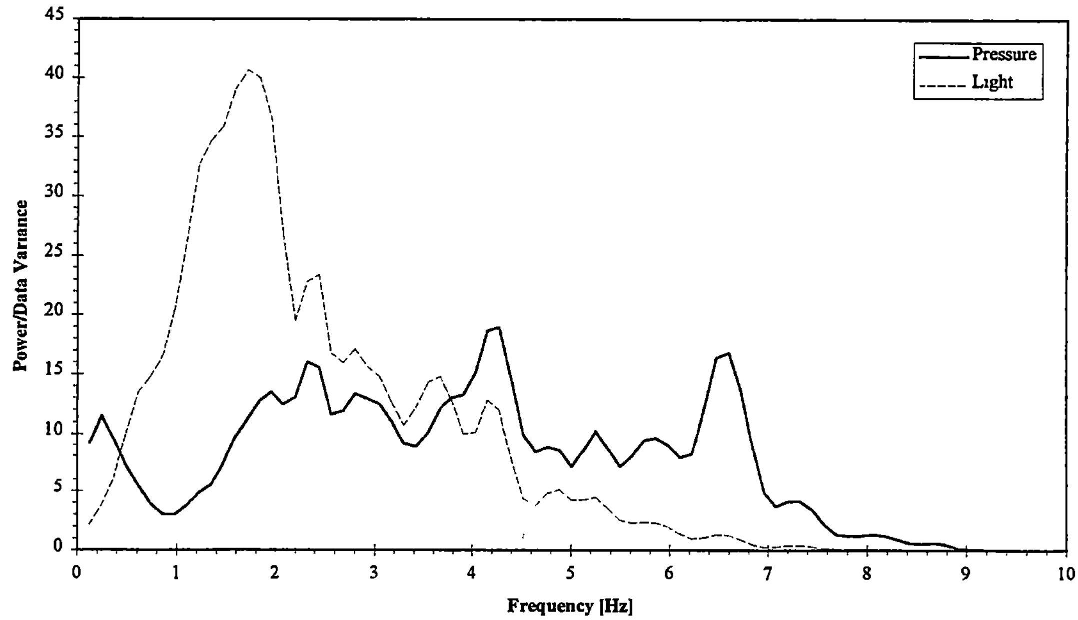

Figure 22: Fourier Power Spectra for FE-4 - AV = 14.2 Lpm and Φ = 1.82

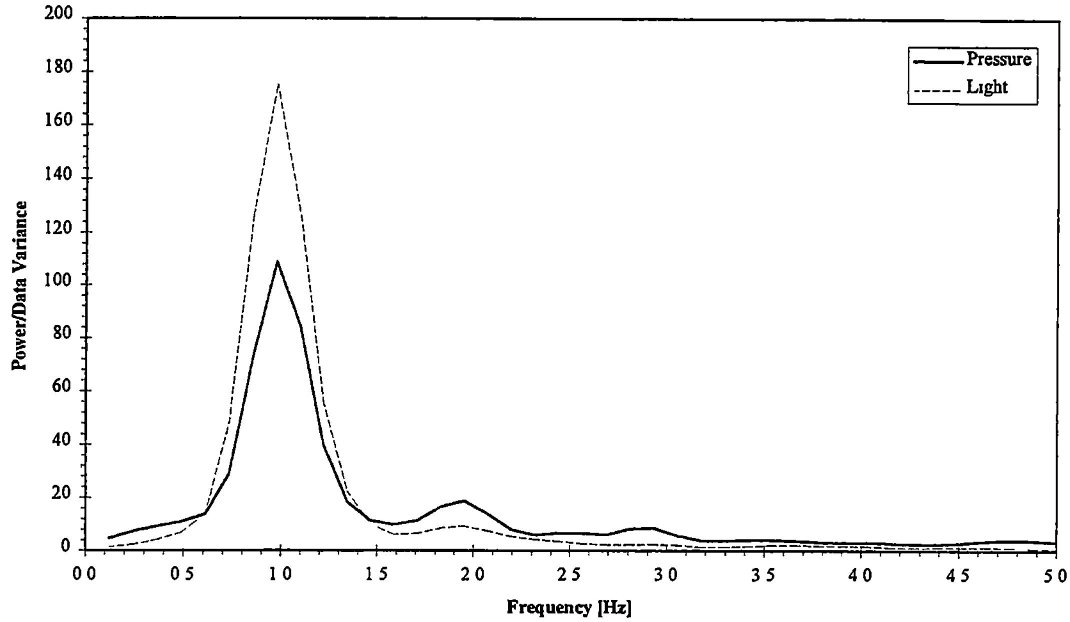

Figure 23: Fourier Power Spectra for FE-5 - AV = 61.4 Lpm and Φ = 1.56

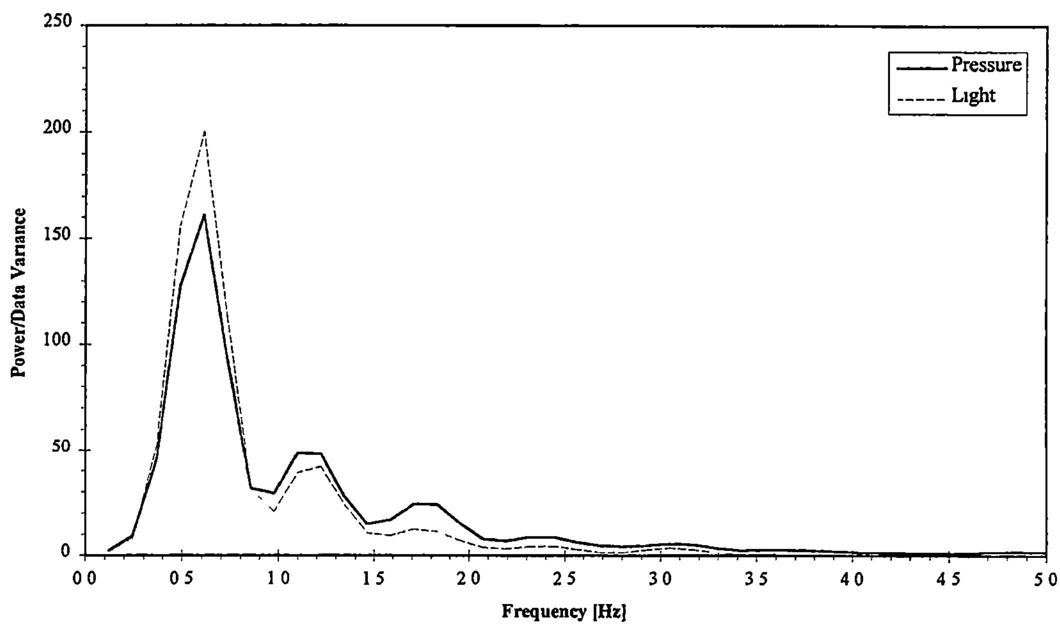

Figure 24: Fourier Power Spectra for FE-6 - AV = 42.5 Lpm and Φ = 1.58

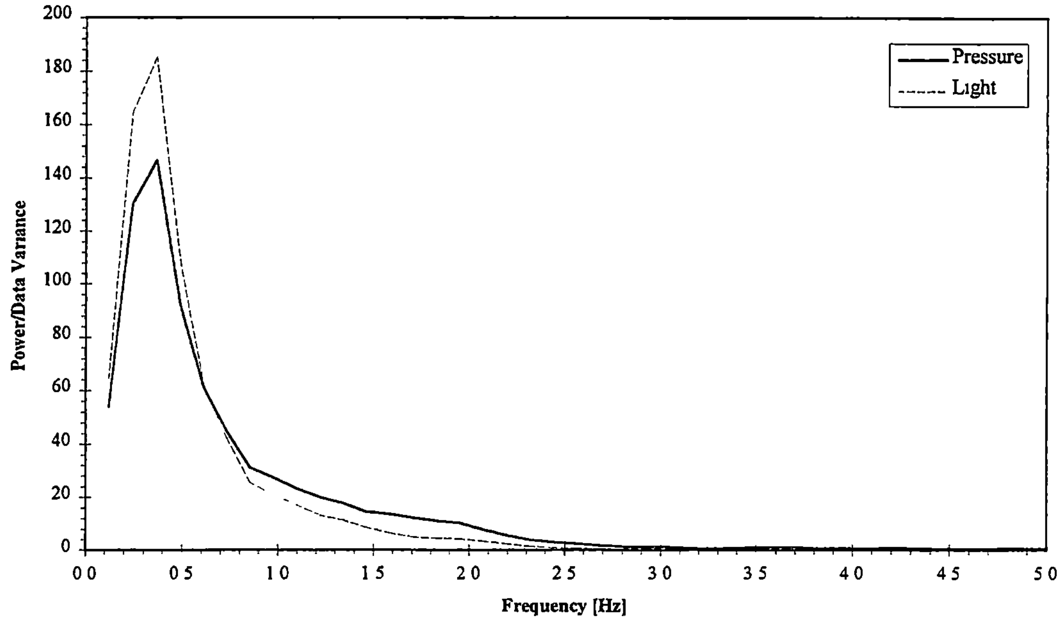

Figure 25: Fourier Power Spectra for FE-6 - AV = 42.5 Lpm and Φ = 1.81

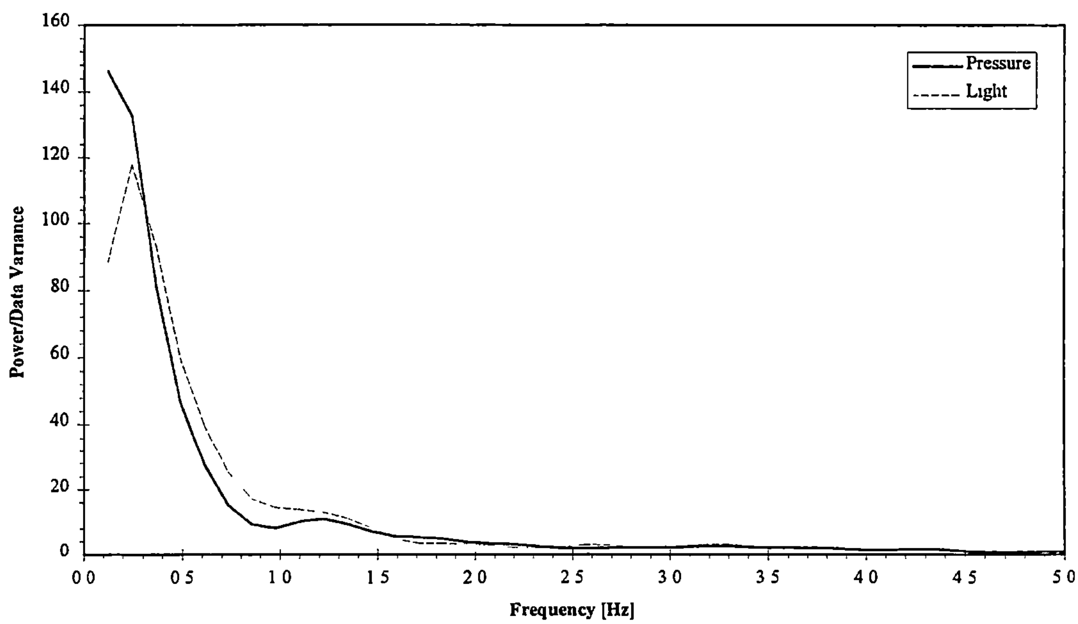

Figure 26: Fourier Power Spectra for FE-7 - AV = 42.5 Lpm and Φ = 1.96

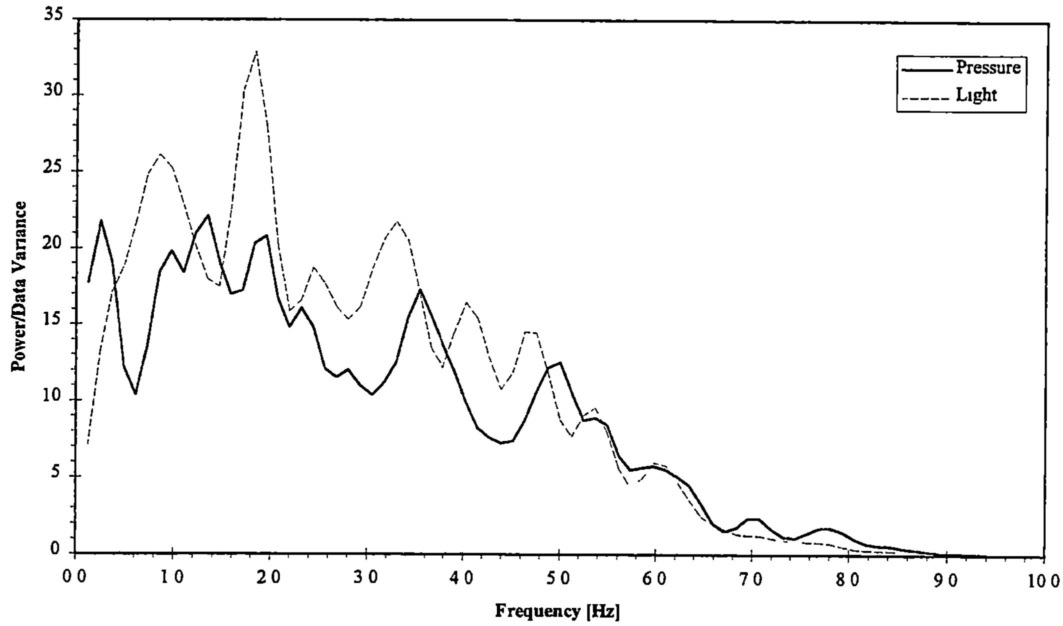

Figure 27: Fourier Power Spectra for FE-8 - AV = 33.0 Lpm and $\Phi = 2.32$

evident, but there is more concentration in the 1 to 2.5 Hz range. Again, the movement of the cellular flamelets on the flame holder grid creates broadband power spectra.

Figure 21 shows the power spectra for flame event three The flame with an AV of 14.2 Lpm and Φ of 1.65 has a dominant peak in the light signal at approximately 1.2 Hz. This represents the onset of instability of the flame, in which the inner flame begins to lift off Again, there is strong correlation between the pressure and light spectra.

The power spectra for flame event four are similar to that of flame event three (only a slight shift to higher frequencies for flame event four) even though the flames are completely different In flame event three the flame starts to lift off the burner, while in flame event four the flame is floating in the tube As shown in Figure 22, the flame with an AV of 14.2 Lpm and Φ of 1.82 has a dominant peak in the light signal at around 1 8 Hz, whereas the power spectrum of the pressure signal is broadband

In Figure 23, a large predominant narrowband frequency is seen at 1 Hz and harmonics at 2 and 3 Hz This corresponds to a flame with an AV of 61.4 Lpm and Φ of 1.56 Flame event five alternates from floating in the tube to the top of the tube This power spectrum is for the time series data shown in Figure 14. As expected with a relatively periodic flame, a single dominant frequency is visible in the spectra In addition, the magnitude of the dominant frequency is now more than three times larger than those of the previous power spectra.

In flame event six, FE-6, the flame propagates up and down through the glass shield very periodically. The power spectra given in Figures 24 and 25 correspond to the time series seen in Figures 15 and 16, respectively Figure 24 reveals a dominant frequency at 0.61 Hz that yields a period of 1.64 seconds. This corresponds to the predicted period of 1 6 seconds obtained from the time series Smaller harmonics at 1.2 and 1.8 Hz are also seen in the power spectrum. Figure 25 reveals a single dominant frequency at 0.37 Hz giving a period of 2.7 seconds, which corresponds to the predicted period of 3 seconds obtained from the time series. Also worth noting is that the power spectra for the pressure and light signals are almost identical except for slight differences in magnitude.

Figure 26 shows representative power spectra for flame event seven, specifically that of a flame with an AV of 42 5 Lpm and Φ of 1.96. A single dominant frequency of 0.24 Hz, yielding a period of 4.2 seconds, is seen for the light signal. The pressure signal also has a minor peak at this same frequency. Lower frequency data for the pressure signal is believed to be noise. The reasons for this dominant frequency are unclear because the time series, seen in Figure 17, do not seem to show a very periodic signal

The power spectrum shown in Figure 27 for flame event eight is very similar to that of Figure 20 belonging to flame event two The diffusion flame is anchored solely at the top of the glass shield. As with flame event two, no dominant frequencies are seen. This is now due to flame movement as a result of convection, as opposed to the movement of flamelets seen earlier.

4.1.4 Autocorrelation Function

The autocorrelation function denotes the periodicity of a time series The peaks beyond the initial dip in the autocorrelation functions of the time series are defined as correlation times, as described in Section 3.4. These correlation times are used to find the period or periods of the time series The autocorrelation function for both the pressure and light signals are shown on the same plot versus the lag (number of events in time).

Figure 28 shows a representative autocorrelation function for the first four flame events, specifically that of flame event two with an AV of 14.2 Lpm and Φ of 1 49. As seen, the pressure and light signals correlate remarkably well and there are no evident periods, as expected for relatively stable flames.

The autocorrelation function shown in Figure 29 for flame event five shows distinct frequencies of 1 Hz and its higher harmonics. This corresponds to those found from the power spectrum of the same time series. The strength of the autocorrelation function for each successive period is seen to grow exponentially weaker Again, the pressure and light signals correlate remarkably well, although the light signal is slightly more coherent.

Figures 30 and 31 show the autocorrelation function for flame event six at two different equivalence ratios for an AV of 42.5 Lpm, where the flame is jumping very periodically. Figure 30 (Φ = 1 58) reveals a period of approximately 1.7 seconds with its higher harmonics. This corresponds to the 1.64 seconds obtained from the power spectrum and the 1.6 seconds estimated from the time series Figure 31 for the slightly more fuel-rich flame (Φ = 1.81) reveals a period of approximately 3.2 seconds with its higher harmonics, which corresponds to the 2.7 seconds obtained from the power spectrum and the 3 seconds estimated from the time series. The autocorrelation functions for the pressure and light signals again correlate remarkably well in both figures. The strength of the autocorrelation function for each successive period decreases linearly

Flame event seven has the flame propagating through the tube rather randomly. Figure 32 shows the autocorrelation function for this flame event revealing a period of approximately 3.9 seconds for both the pressure and light signals. This corresponds to the period of 4.2 seconds obtained from the power spectrum of the same time series. The

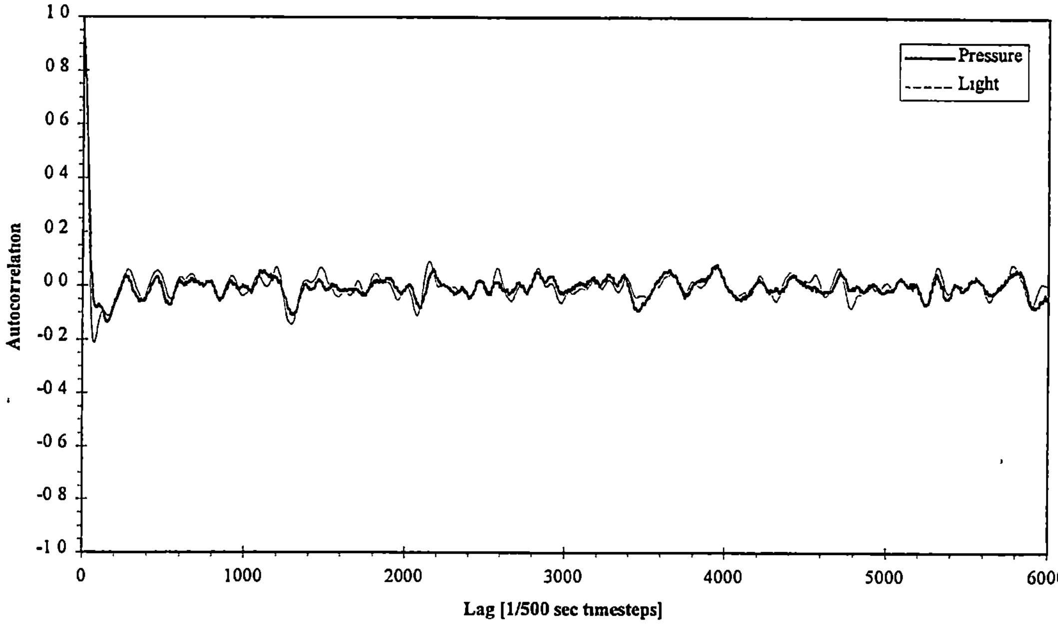

Figure 28: Autocorrelation Function for FE-2 - AV = 14.2 Lpm and Φ = 1.49

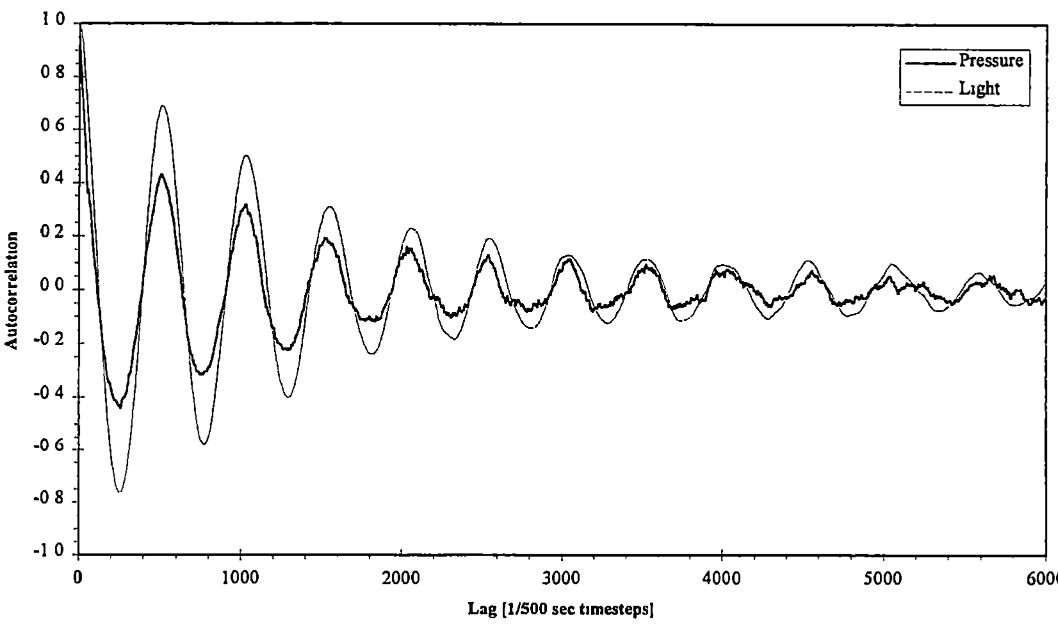

Figure 29: Autocorrelation Function for FE-5 - AV = 61.4 Lpm and Φ = 1.56

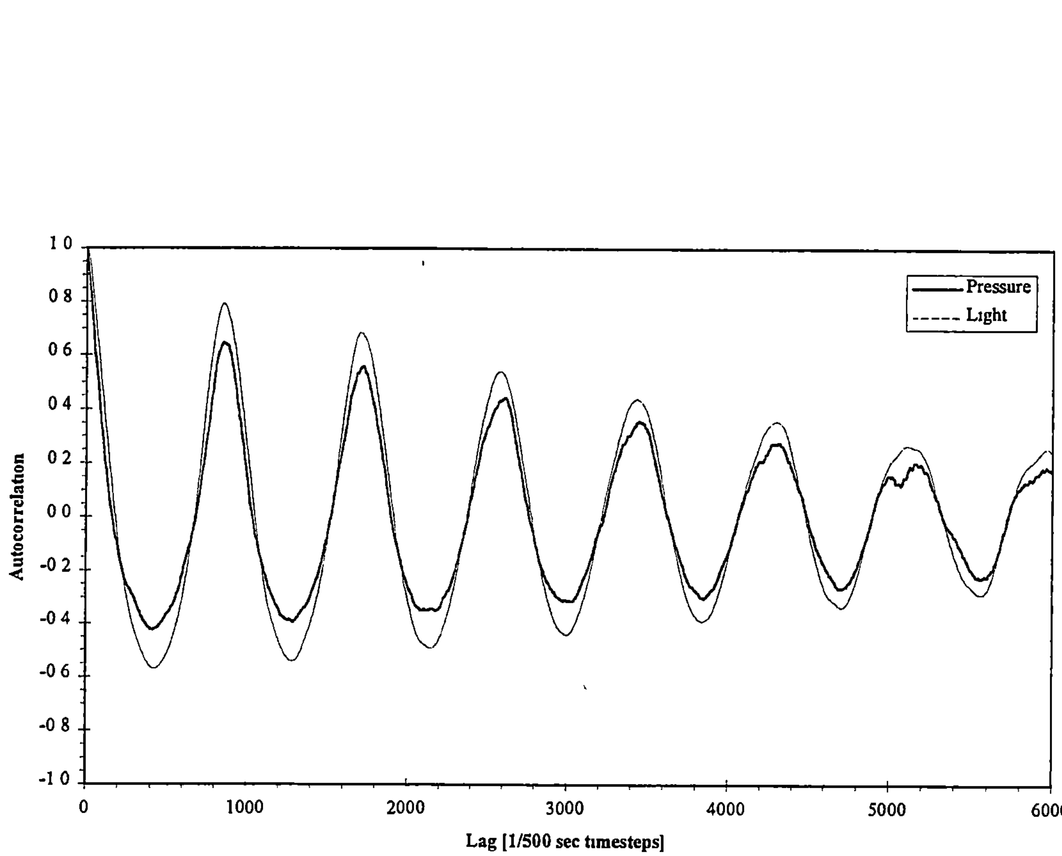

Figure 30: Autocorrelation Function for FE-6 - AV = 42.5 Lpm and Φ = 1.58

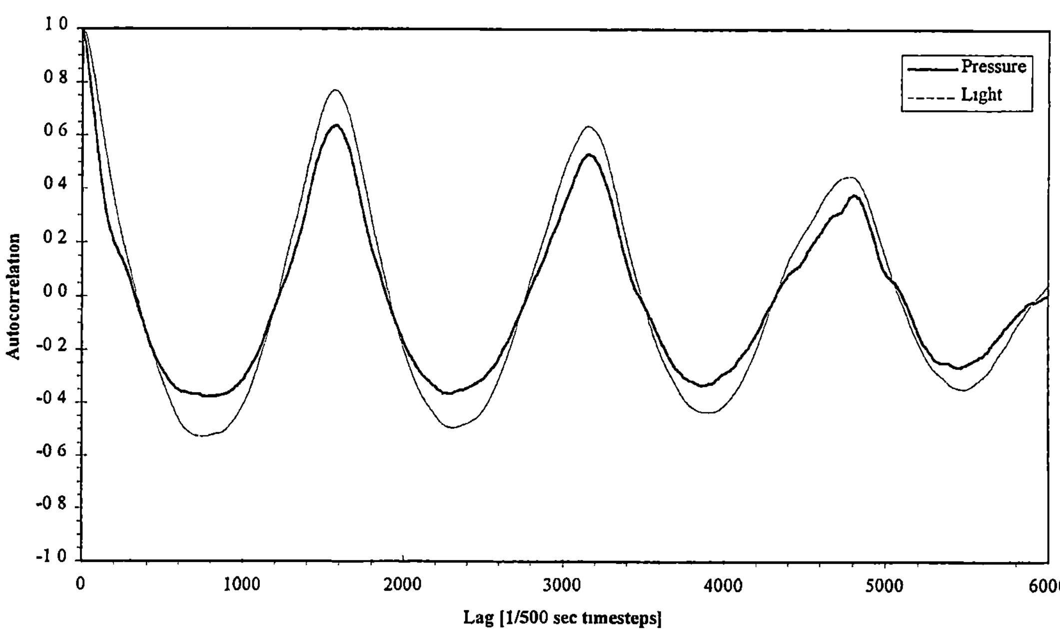

Figure 31: Autocorrelation Function for FE-6 - AV = 42.5 Lpm and Φ = 1.81

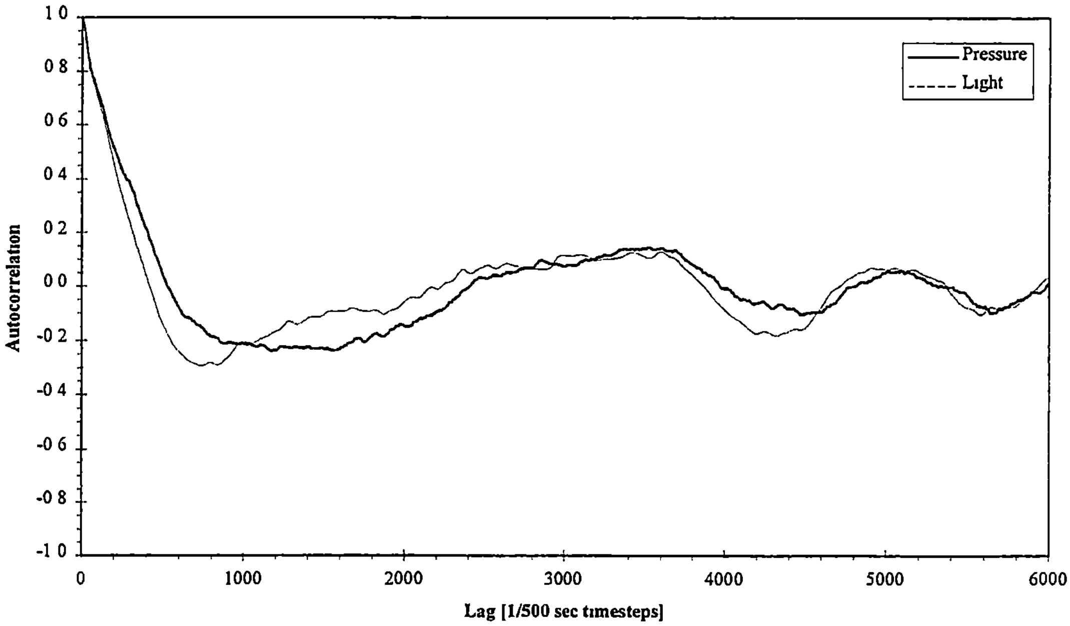

Figure 32: Autocorrelation Function for FE-7 - AV = 42.5 Lpm and Φ = 1.96

autocorrelation function for both signals is not very smooth and the periodicity of the signals is much less evident than for flame events five and six.

Figure 33 shows a representative autocorrelation function for flame event eight and is similar to that of the stable flames represented in Figure 28. The only difference is seen in the much less chaotic light signal, but no noticeable periods are discernable.

4.1.5 Crosscorrelation Function

The crosscorrelation function is used to quantify the correlation between the pressure and light signals. Crosscorrelation measures the amount of predictability of the test (light) signal as a function of time based on the reference (pressure) signal. The crosscorrelation is found for a lag of 500 data points in both the positive (correlation) and negative (anti-correlation) directions Correlation at a positive lag means that events seen in the light signal follow those in the pressure, and vice versa for correlation at negative lags.

Figure 34 shows the crosscorrelation for flame event two There is very strong correlation between the pressure and light signals, with no time lag. This shows that when the flame is anchored at the burner, the pressure and light measurements correlate very well. There is almost no correlation between the pressure and light signals after a lag of 50 in either the positive or negative direction indicating a very complex flame. The crosscorrelation for flame event one is not shown since it is relatively the same as for event two.

The crosscorrelation for flame event three shown in Figure 35 is similar to Figure 34 except that now there is less correlation between the signals and some anti-correlation is

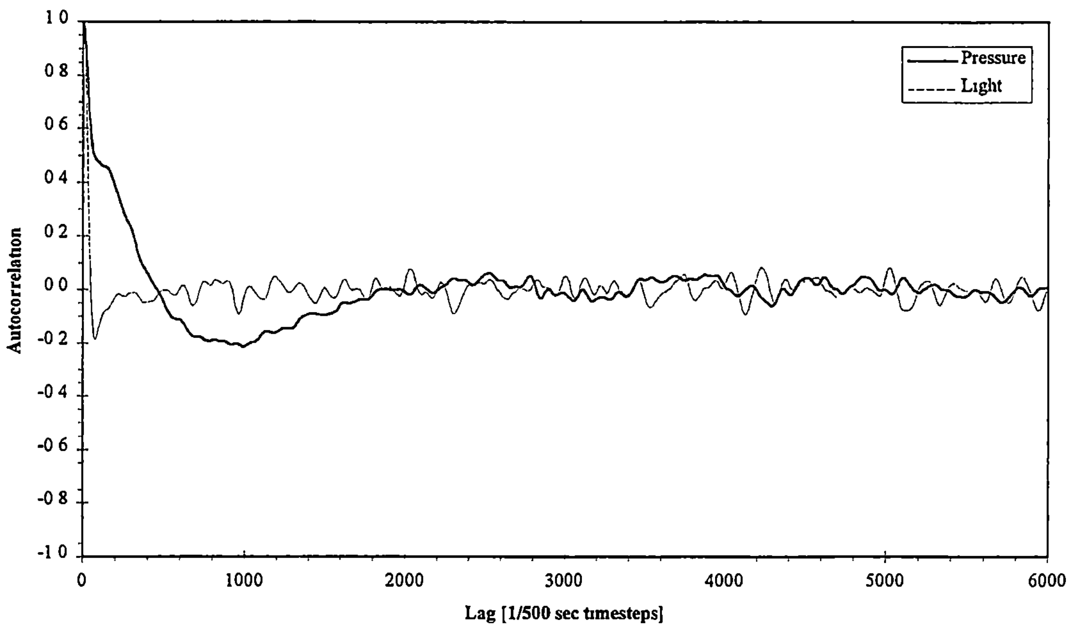

Figure 33: Autocorrelation Function for FE-8 - AV = 33.0 Lpm and Φ = 2.32

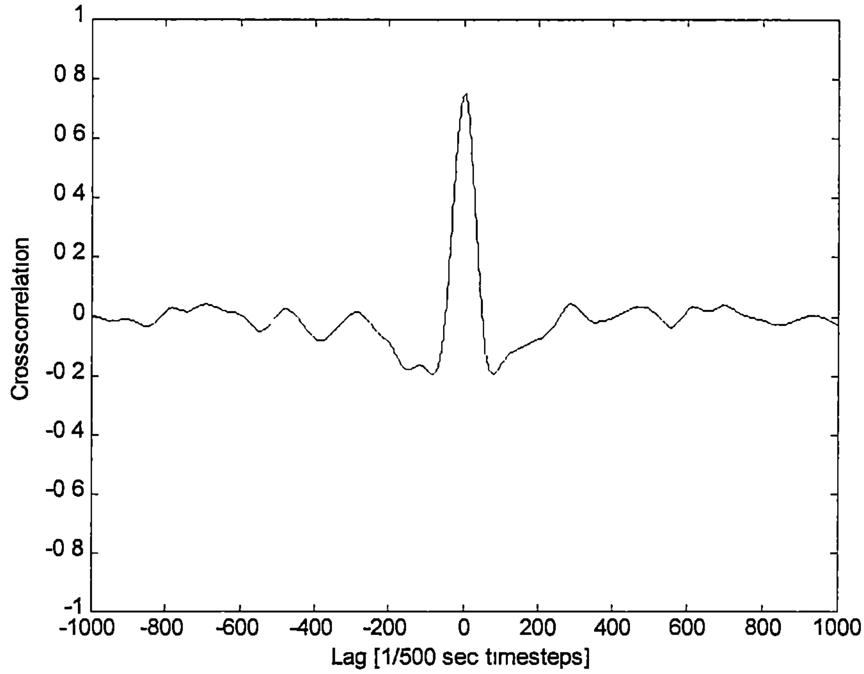

Figure 34: Crosscorrelation for FE-2 – AV = 14.2 Lpm and Φ = 1.49

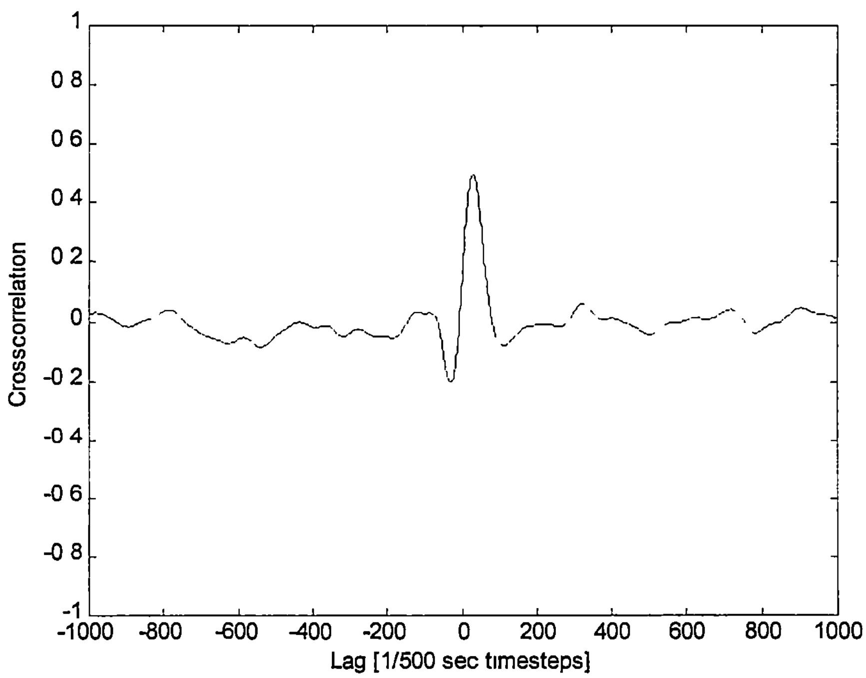

Figure 35: Crosscorrelation for FE-3 – AV = 14.2 Lpm and Φ = 1.65

now seen. The positive lag of the correlation and the negative lag of the anti-correlation are about the same. This seems to indicate the beginning of some periodicity in the behavior of the flame. As before, there is little correlation between the pressure and light signals beyond a lag of 50.

In Figure 36, the crosscorrelation for flame event four, the anti-correlation between the pressure and light signals is now larger than the correlation. As before, the positive lag of the correlation and the negative lag of the anti-correlation are about the same.

The crosscorrelation for flame event five is seen in Figure 37 and shows very strong correlation. The crosscorrelation is symmetrical with a definite time lag between the pressure and light signals The pressure signal is leading the light signal, as seen earlier in the time series of this flame event shown in Figure 14. Since the flame behavior is periodic, the crosscorrelation shows basically the same thing as seen in the autocorrelation except for the time lag between the signals The frequency of 1 Hz is again evident as seen previously. Strong correlation is seen at the frequency of the signals and anti-correlation is seen when the pressure and light signals are out of phase.

Figures 38 and 39 show the crosscorrelation for flame event six Figure 38 reveals a period of approximately 1.65 seconds, which agrees with that found earlier Figure 39 reveals a period of approximately 3.1 seconds, which again agrees with that found earlier. The pressure signal is seen to lead the light by about 50 data points in both figures.

The crosscorrelation for flame event seven is seen in Figure 40. It is similar to that seen in Figure 39, but is not as temporally symmetrical The plot yields a period of about 2.7 seconds, which by comparing this value to those found previously may not be reliable.

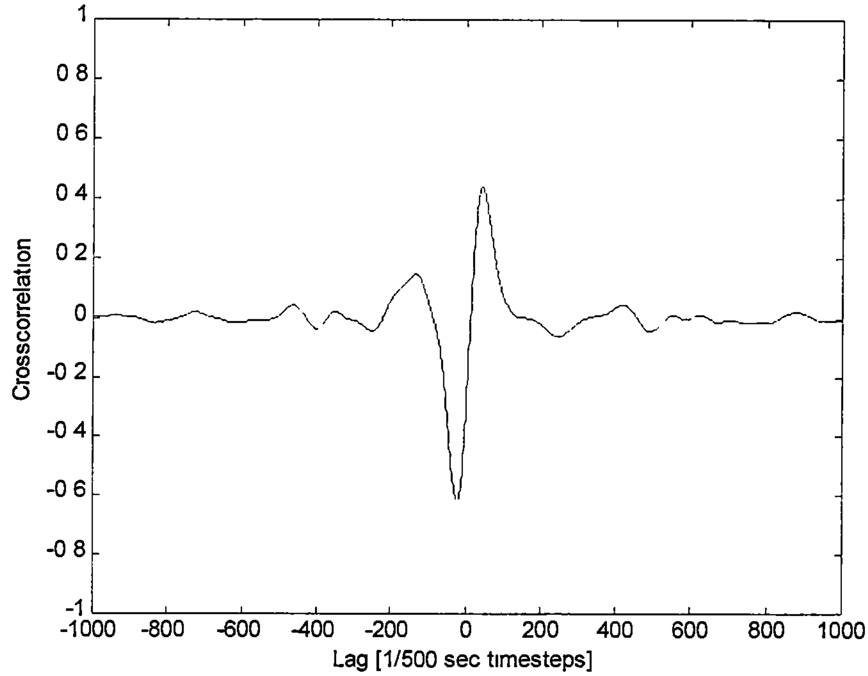

Figure 36: Crosscorrelation for FE-4 – AV = 14.2 Lpm and Φ = 1.82

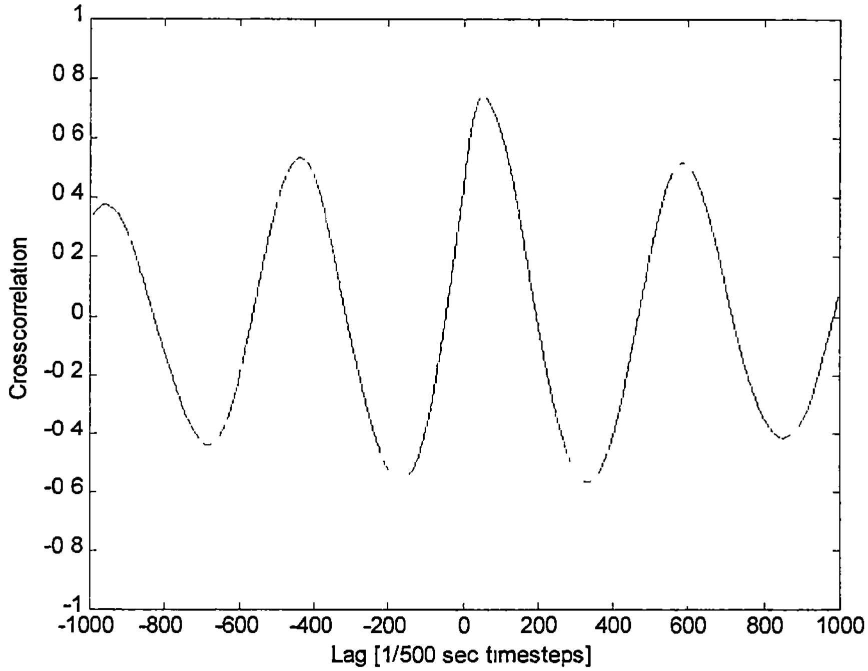

Figure 37: Crosscorrelation for FE-5 – AV = 61.4 Lpm and Φ = 1.56

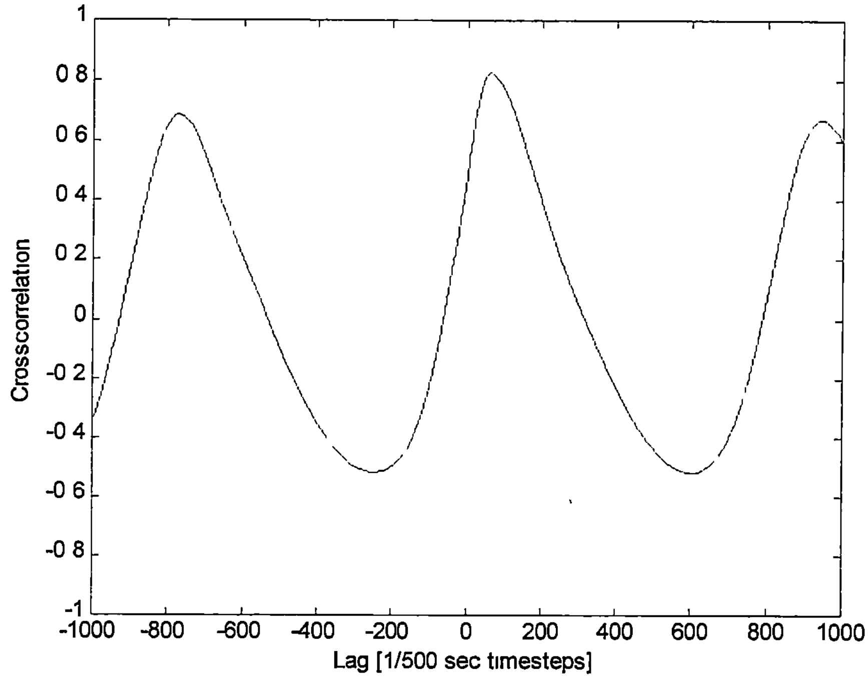

Figure 38: Crosscorrelation for FE-6 – AV = 42.5 Lpm and Φ = 1.58

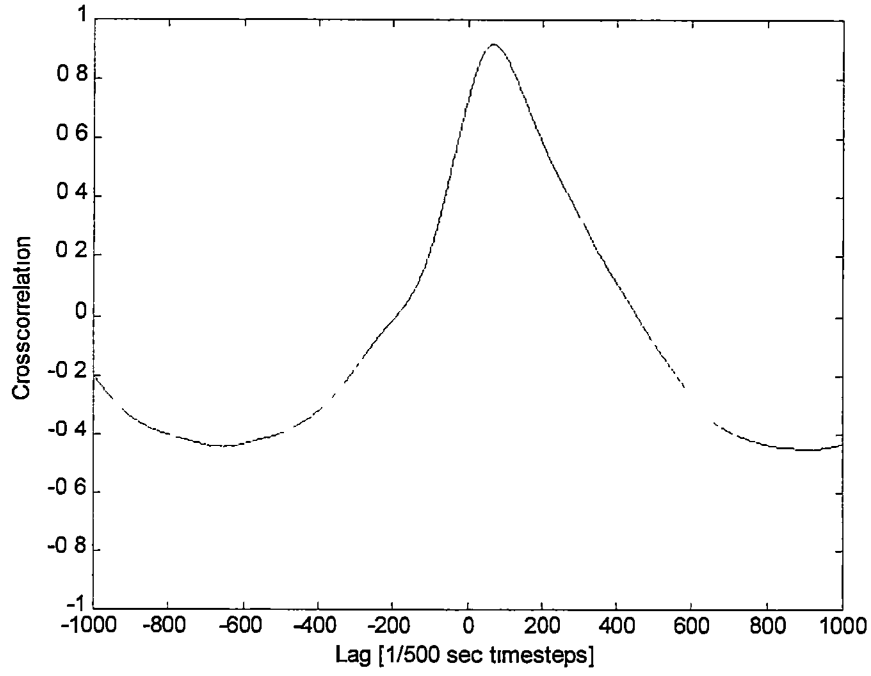

Figure 39: Crosscorrelation for FE-6 – AV = 42.5 Lpm and Φ = 1.81

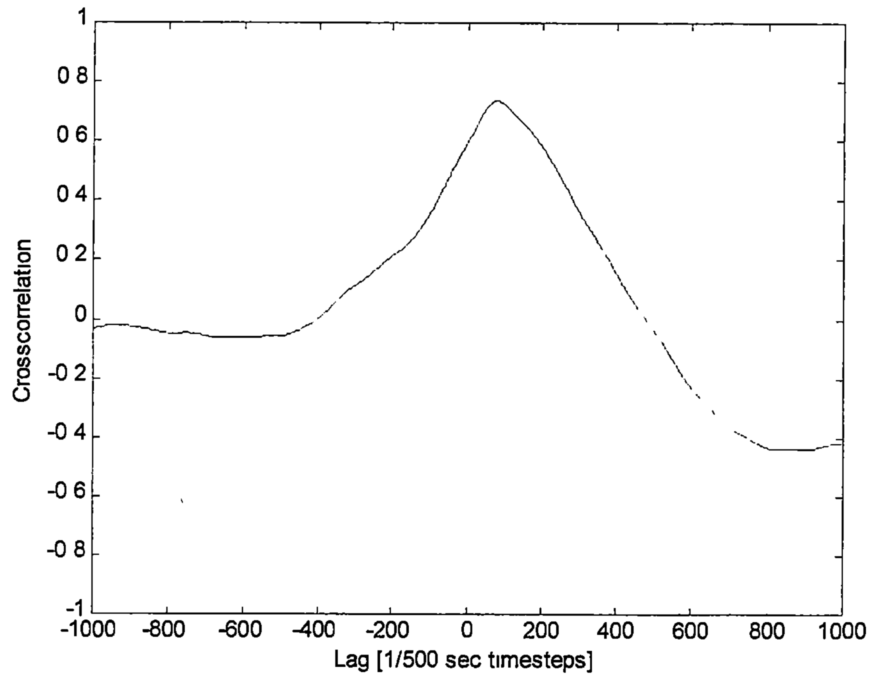

Figure 40: Crosscorrelation for FE-7 – AV = 42.5 Lpm and Φ = 1.96

Figure 41 shows a representative crosscorrelation function for flame event eight where the flame is anchored solely at the top of the glass tube There is very little correlation between the pressure and light signals. This is attributed to the fact that the flame is located far away from the pressure and light sensors.

4.1.6 Kolmogorov Entropy

Kolmogorov entropy provides a measure of signal predictability. For periodic or cyclic signals, the entropy is close to zero. For complex (chaotic) signals, a higher entropy value should be seen The Kolmogorov entropy of the pressure and the light for all air flowrates is plotted as a function of equivalence ratio as shown in Figures 42 –47

Figure 42 shows the Kolmogorov entropy for flames with an AV of 14.2 Lpm over a wide range of equivalence ratios The maximum entropy value of the pressure signal is found at a $\Phi = 1.82$. This corresponds to flame event four where the flame is floating in the tube. The entropy of the light is seen to decrease almost linearly from a peak value near stoichiometric conditions to a minimum at a $\Phi = 2\ 32$ (fuel-rich) This corresponds to flame event 7 where the flame jumps sporadically. This is also the minimum value for the pressure. This is expected since this is the only condition at this flowrate where the flame behaves periodically The characteristics seen at this flowrate will be much more evident at higher flowrates

The Kolmogorov entropy for flames with an AV of 18.9 Lpm is seen in Figure 43. The maximum value for the pressure signal is found at a $\Phi = 1.86$ which corresponds to flame event four. This is to be the flame event where the signal appears most complex,

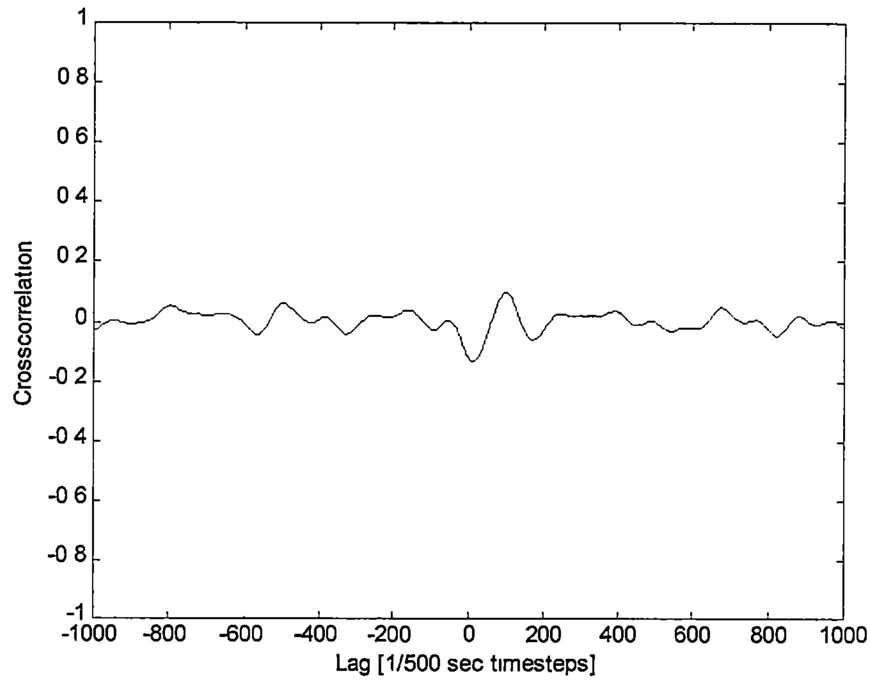

Figure 41: Crosscorrelation for FE-8 – AV = 33.0 Lpm and Φ = 2.32

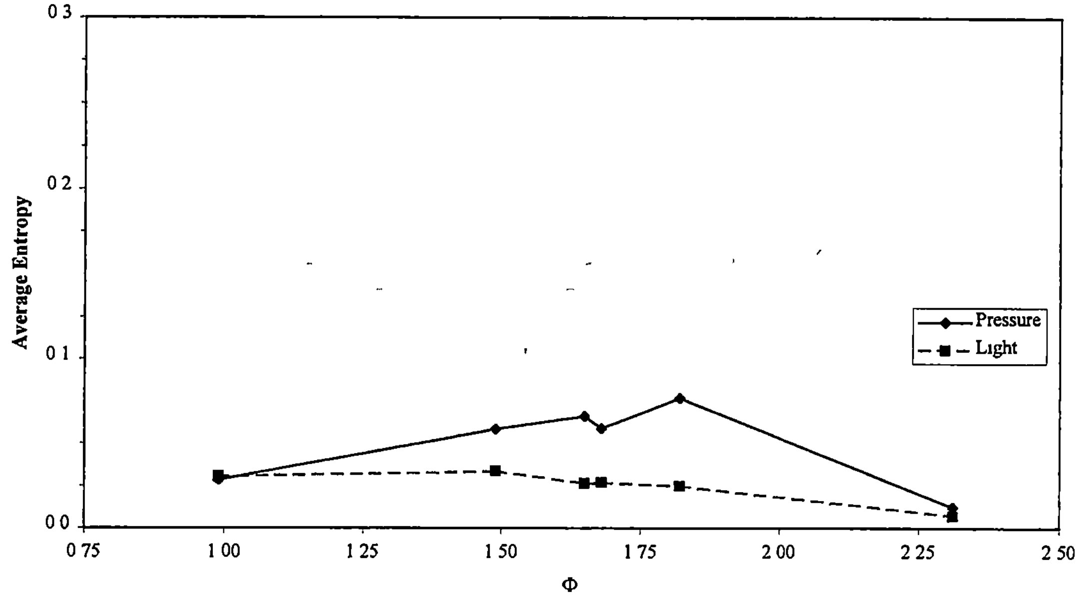

Figure 42: Kolmogorov Entropy for AV = 14.2 Lpm

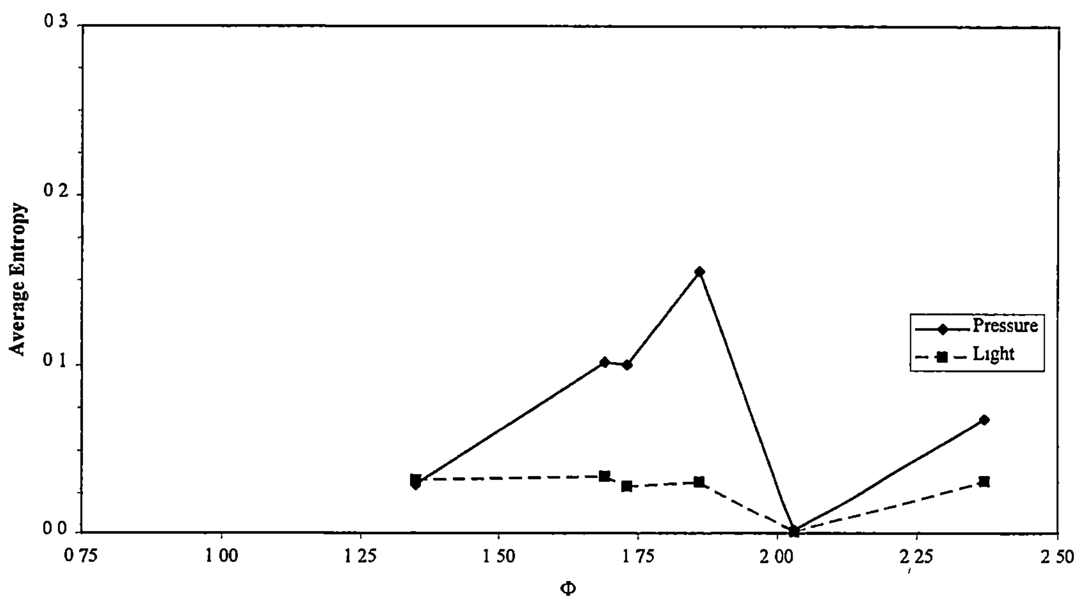

Figure 43: Kolmogorov Entropy for AV = 18.9 Lpm

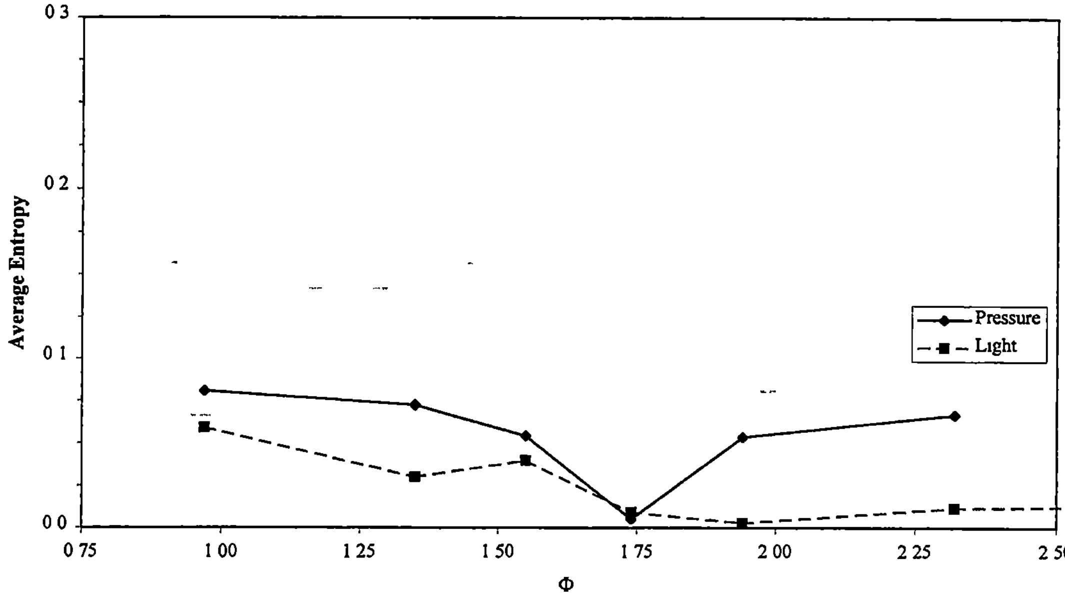

Figure 44: Kolmogorov Entropy for AV = 33.0 Lpm

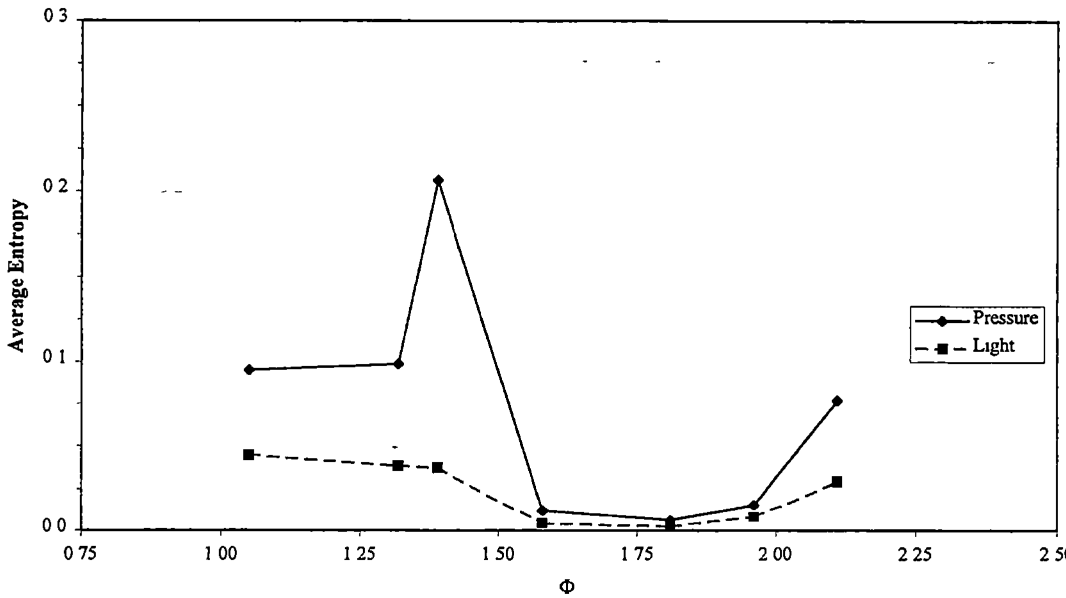

Figure 45: Kolmogorov Entropy for AV = 42.5 Lpm

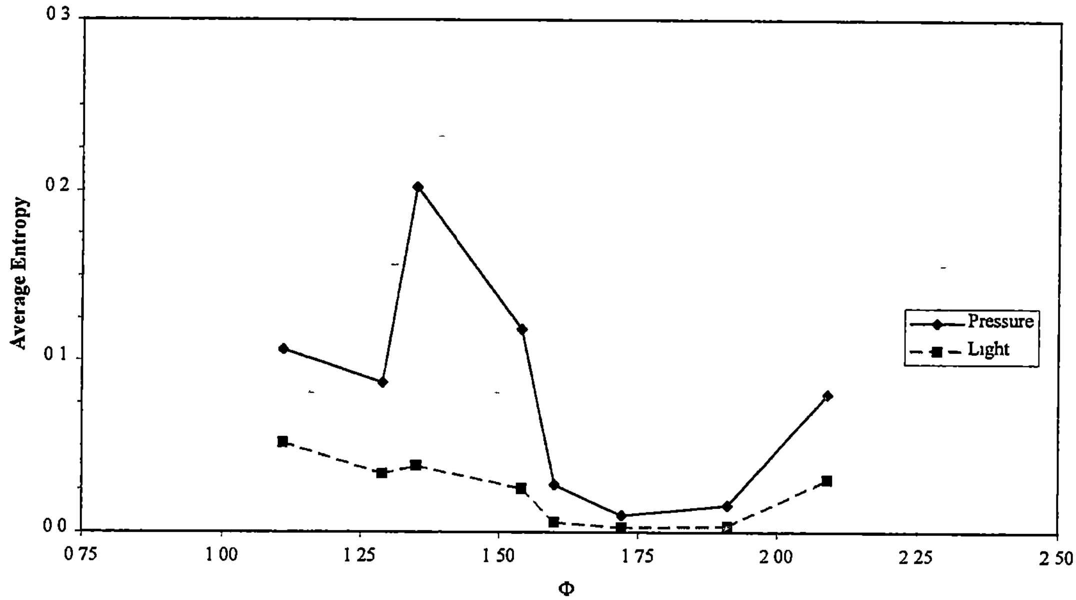

Figure 46: Kolmogorov Entropy for AV = 51.9 Lpm

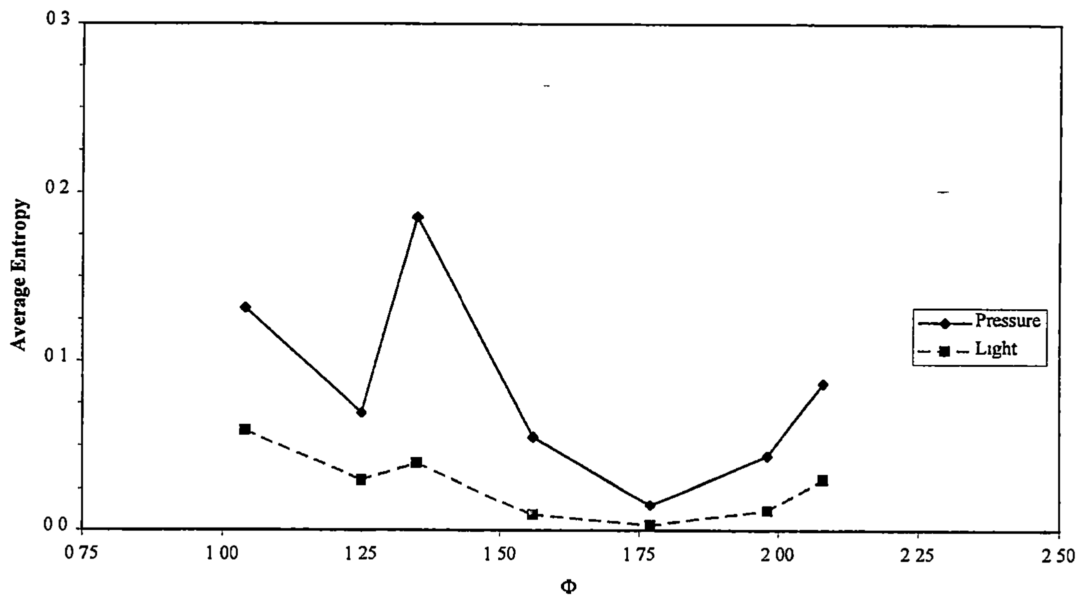

Figure 47: Kolmogorov Entropy for AV = 61.4 Lpm

especially for the pressure. The entropy values for the light are seen to be fairly constant up until a $\Phi = 1.86$, where the entropy drops at a $\Phi = 2.03$ and increases sharply to a $\Phi = 2.37$. The minimum entropy value corresponds to flame event seven, where the flame is jumping periodically producing an entropy value near zero. The last condition corresponds to flame event eight, where the flame is stationary at the top of the tube. These results compare very well with those found using linear analysis techniques. The pressure values are larger than those of the light because the pressure signals are more complex due to the inadequate resolution of the pressure transducer.

In Figure 44, the entropy values for flames with an AV of 33 0 Lpm are similar to those of Figure 42 in that they stay relatively constant except for the dip at a $\Phi = 1.74$ This corresponds to flame event six where the flame is jumping very periodically. The light signal is seen to further decrease to a minimum value at a $\Phi = 1.94$, corresponding to flame event seven. These results again compare well with those using the previous analysis techniques.

The Kolmogorov entropy for flames with air flowrates of 42.5 Lpm, 51.9 Lpm, and 61.4 are seen in Figures 45-47. All three follow the same trend with a maximum entropy value of both the pressure and light signals around a $\Phi = 1.35$, corresponding to flame event four At this point the entropy values sharply decrease to a minimum value around a $\Phi = 1\ 7$ and then increase to entropy levels around those found at stoichiometric conditions. The conditions at which the flame is positionally stable has much higher entropy values than those when the flame is behaving periodically where the entropy values are around zero. Kolmogorov entropy is a very useful analysis technique in characterizing the behavior of a flame, especially at high air flowrates

4.2 Flame Stabilization Study

A frequency generator is used to further study the effects of equivalence ratio on a rich premixed-flame. Keeping the gas and primary air flowrates constant, small amounts of air are injected into the primary combustion zone in an attempt to stabilize the unstable flame, i.e., to anchor the flame at the burner. The primary air flowrate is held constant at 18.9 Lpm, and the frequency of injection is 0.1 Hz. These tests are conducted around an equivalence ratio of 1.65, the rich-flammability limit of methane The flame is started in a condition similar to flame event four described in section 4 2.1 where the flame is floating in the tube. By increasing the amount of air injected into the burner, the flame becomes increasingly more stable. The flame becomes completely stable at the burner at an overall equivalence ratio of 1 57. These tests provide the necessary proof to support the reasons stated earlier for the mechanism of flame propagation up and down the glass tube A thorough explanation of the frequency generator data is not given due to its similarity to the previous data.

4.2.1 General Observations

In Table 2, the different amounts of air that are injected into the burner and the equivalence ratio of each flame are given The first test conducted has the flame floating in the tube with no air injected into the burner The second test injects 0.47 Lpm of air into the burner every 10 seconds, and the flame now starts to jump towards the burner when the air is injected The flame however is not anchored at the burner. When 1.6 Lpm of air is injected into the burner in test three, the flame begins to stay anchored at the burner for around three seconds. In experiment four, 2.4 Lpm of air into the burner resulting in an equivalence ratio of 1.57 at the time of injection. The flame is successfully stabilized at the burner with these parameters. When no air is injected, the equivalence ratio is 1.76, which is above the flammability limit of methane. By injecting 2.4 Lpm of air into the primary combustion zone at a frequency of 0.1 Hz, or every 10 seconds, the flame becomes completely stable at the burner. This shows the significance that small amounts of air have on a rich flame and as a result proves that flame propagation is not due to air and fuel flow fluctuations. This is proven by the fact that even very small disturbances in the air flowrate do have an effect on the stability of the flame. When no excess air is injected into the burner, the flame does not behave differently, showing that air and fuel flow fluctuations have almost no effect on the flame.

Table 2: Parameters of Frequency Generator Tests

Test	**Amount of Injected Air (Lpm)**	**Φ**
INJ-1	0.0	1 76
INJ-2	0 47	1 72
INJ-3	1.6	1.63
INJ-4	2.4	1 57

4.2.2 Time Series of Pressure and Light Signals

The time series for the frequency generator experiments are given in Figures 48-51. Figure 48 shows the time series for experiment one, where the flame is floating in the tube. The time series is similar to Figure 13, the representative time series for flame event four. Figure 49 shows the time series for the second experiment where air is first injected. Some periodicity is seen from the time series The time series in Figure 50 is that of experiment three, where 1.6 Lpm of air is injected into the burner. A period of approximately 3 seconds is obtained from the time series. The pressure and light signals correlate rather well except for the phase shift between them. Figure 51 shows the time series where the flame is anchored solely at the burner. Again a period of approximately 3 seconds is seen in the time series. The phase shift between the pressure and light signals is much less than in Figure 50.

4.2.3 Fourier Power Spectrum

Figures 52-55 show the Fourier power spectra for the frequency generator experiments Figure 52 shows the power spectrum where the flame is floating in the tube It is very similar to the same conditions found in flame event four seen in Figure 22. The dominant frequency is around 1 34 Hz. Figures 53, 54, and 55 all show a single dominant frequency of 0.37 Hz with each frequency more dominant than the previous. The frequency of 0 37 Hz gives a period of 2.7 seconds that corresponds very well to the approximate value of 3 seconds obtained from the time series These figures are similar to those of flame events six and seven in which the flame is jumping periodically.

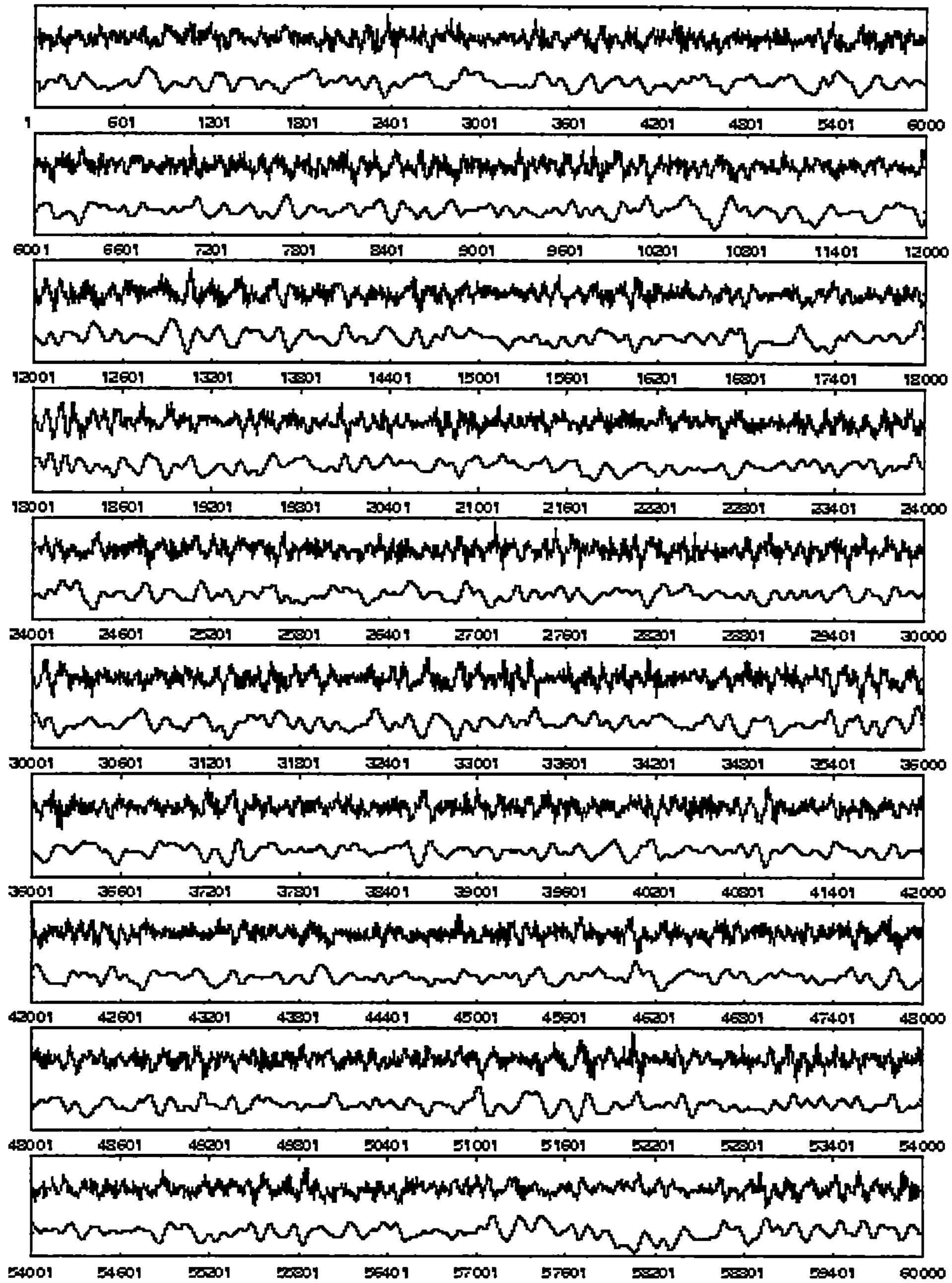

Figure 48: Pressure (Top) and Light (Bottom) Time-Series for INJ-1 – AV = 18.9 Lpm and Φ = 1.76

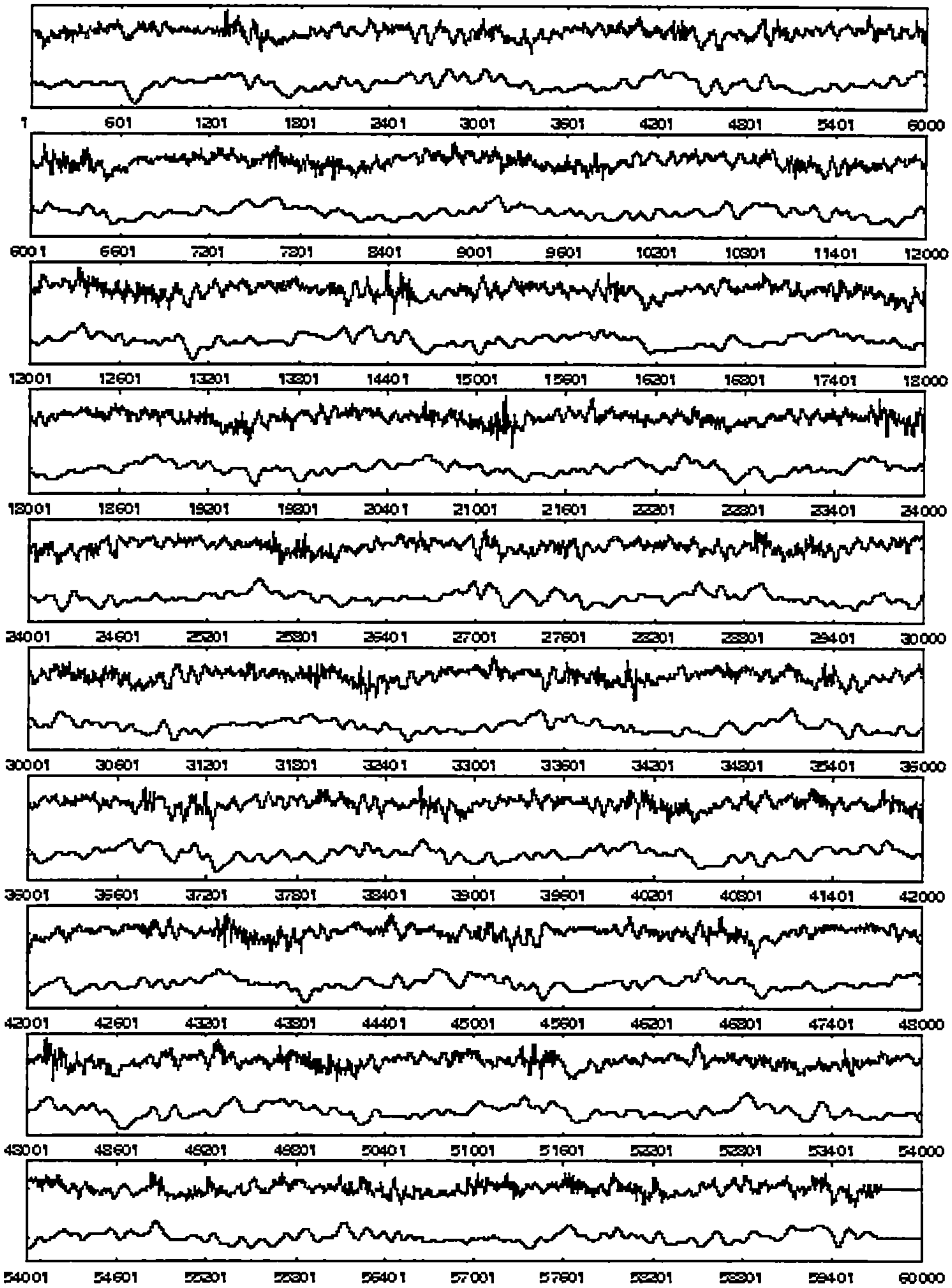

Figure 49: Pressure (Top) and Light (Bottom) Time Series

for INJ-2 – AV = 18.9 Lpm and Φ = 1.72

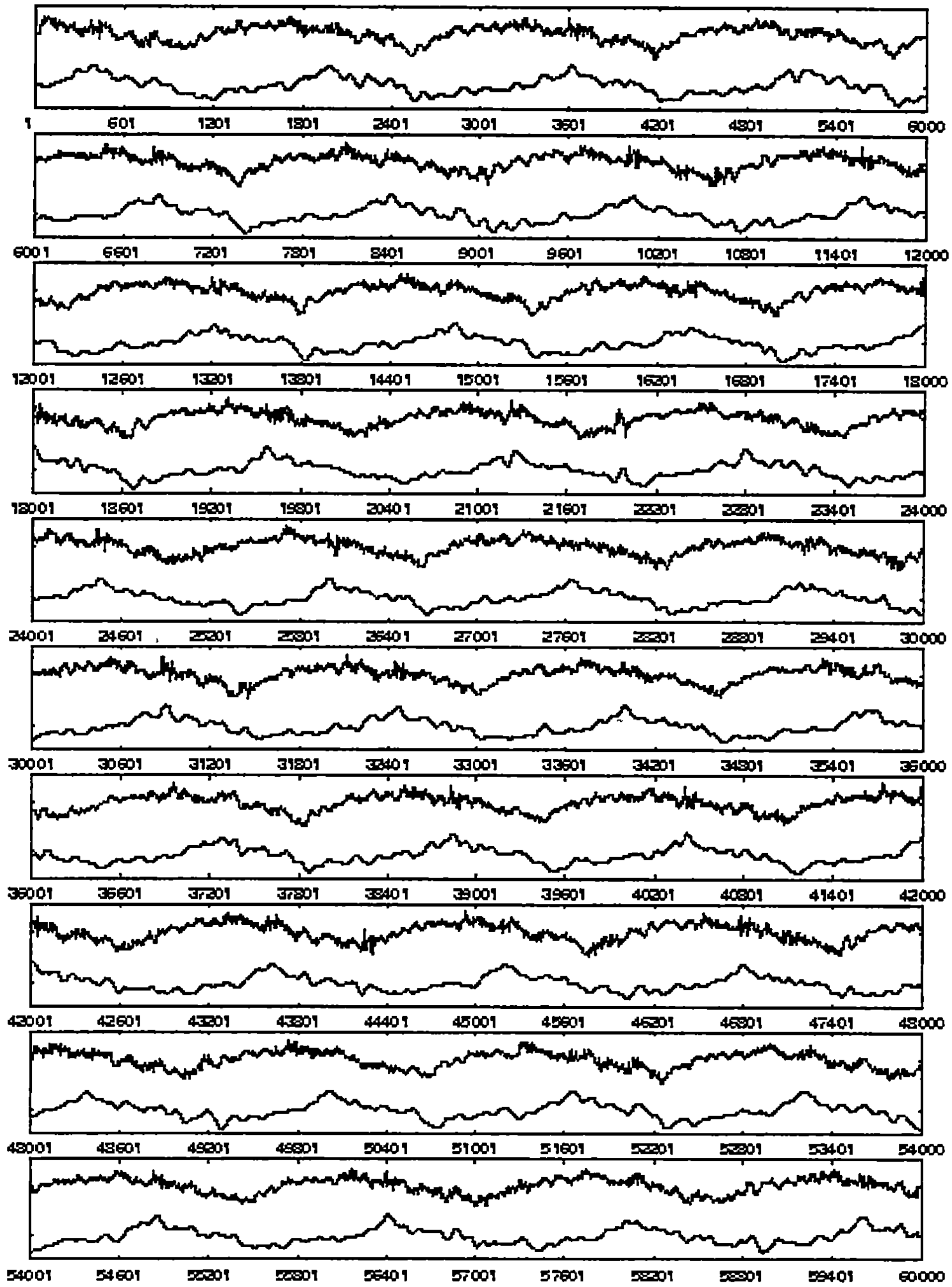

Figure 50: Pressure (Top) and Light (Bottom) Time Series

for INJ-3 – AV = 18.9 Lpm and Φ = 1.63

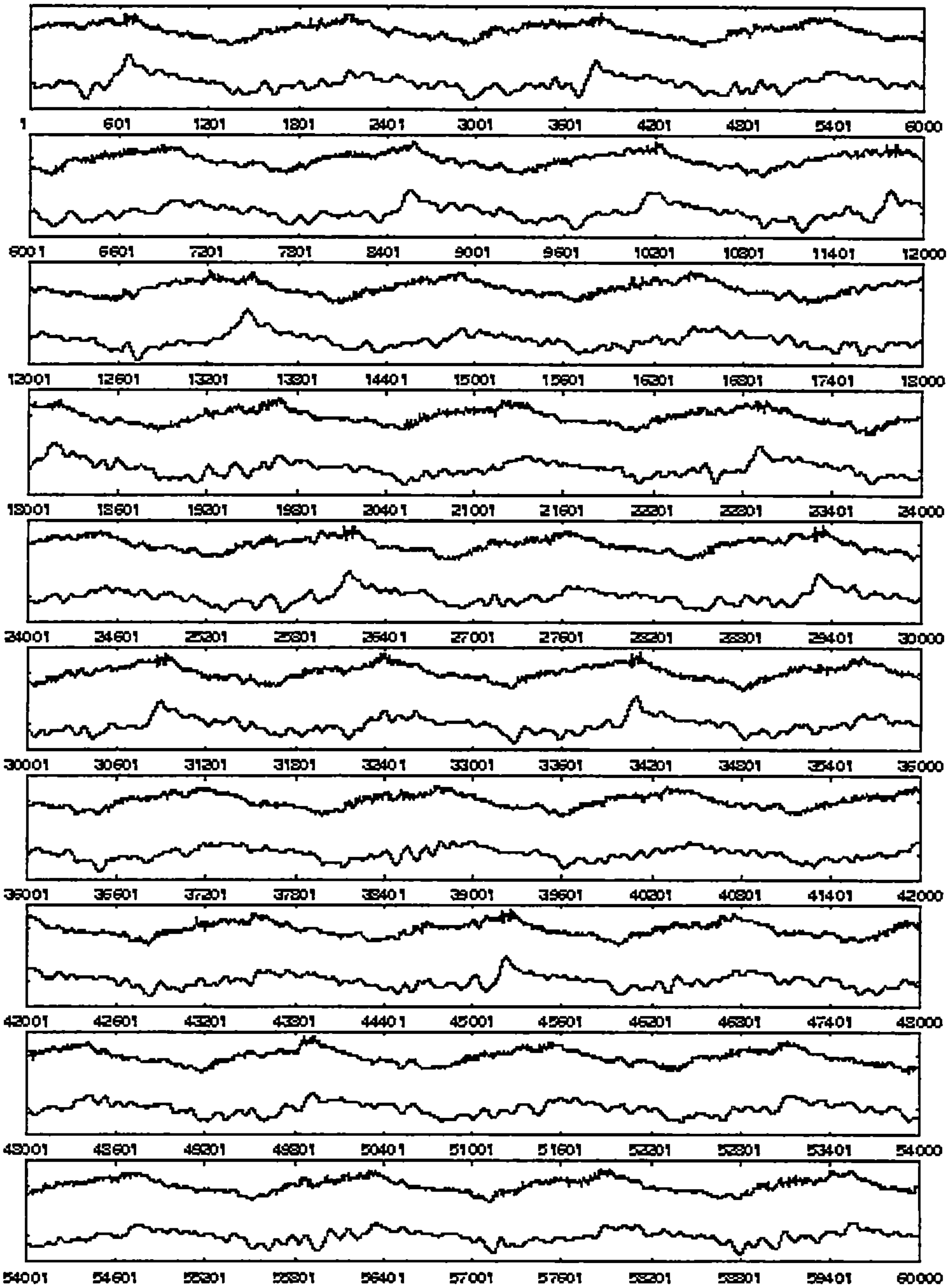

Figure 51: Pressure (Top) and Light (Bottom) Time Series

for INJ-4 – AV = 18.9 Lpm and Φ = 1.57

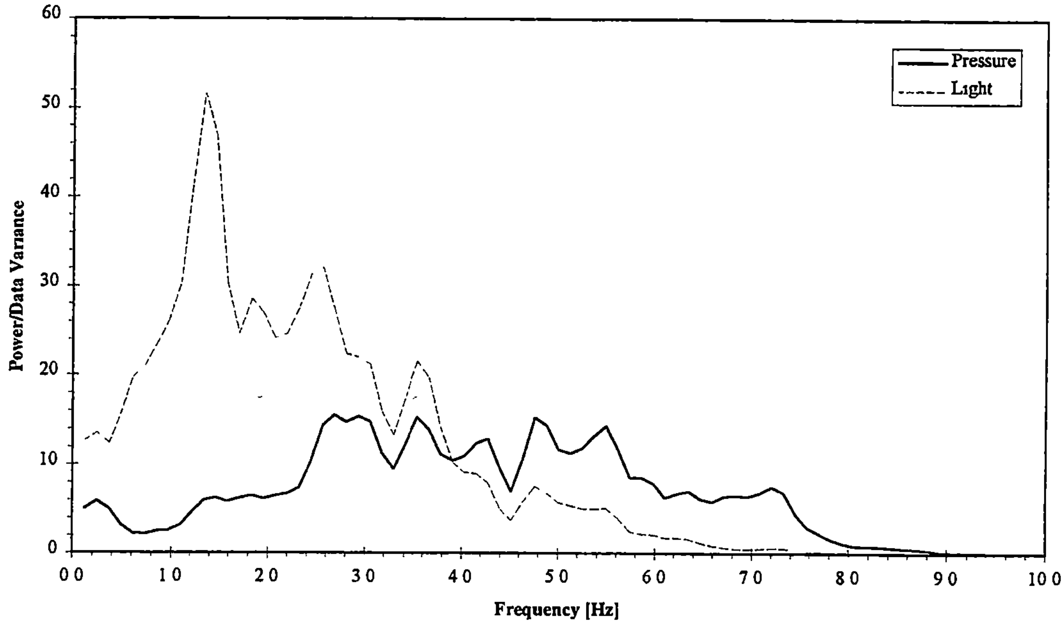

Figure 52: Fourier Power Spectra for INJ-1 – AV = 18.9 Lpm and Φ = 1.76

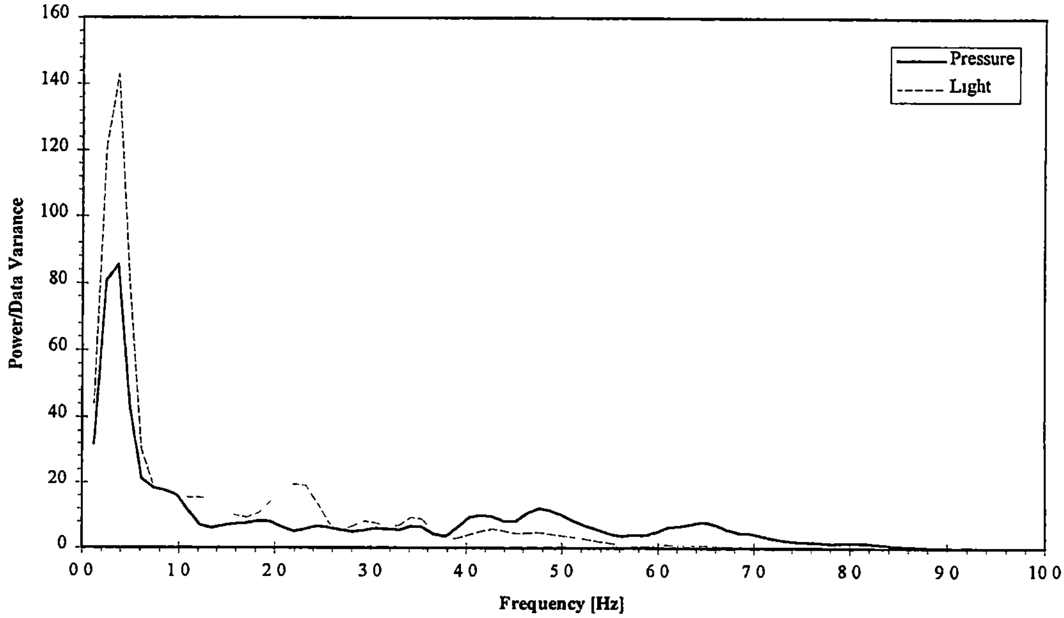

Figure 53: Fourier Power Spectra for INJ-2 – AV = 18.9 Lpm and Φ = 1.72

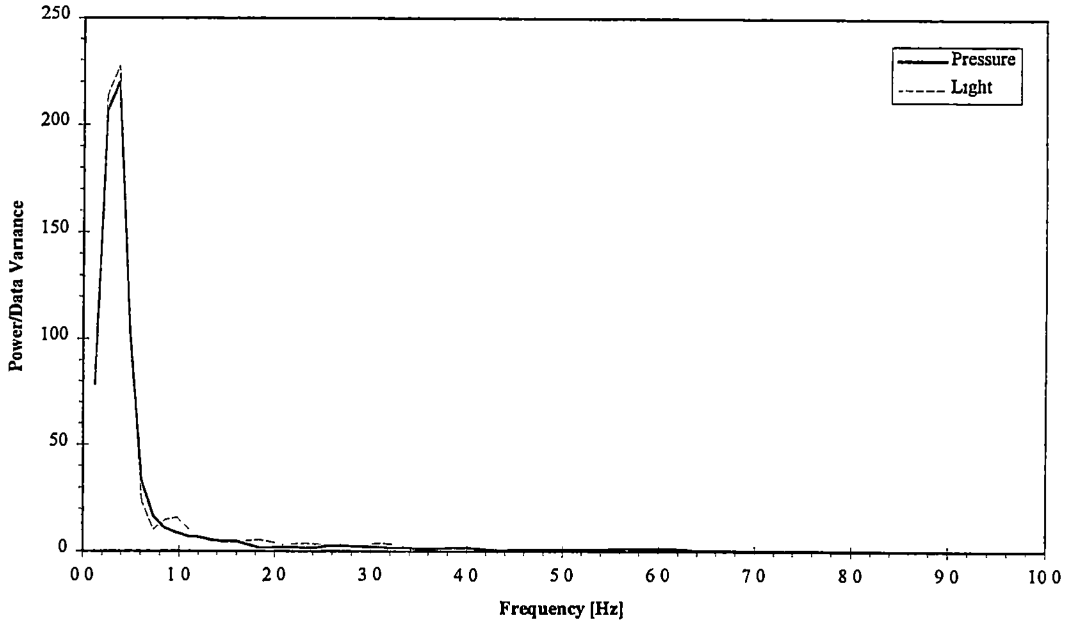

Figure 54: Fourier Power Spectra for INJ-3 – AV = 18.9 Lpm and Φ = 1.63

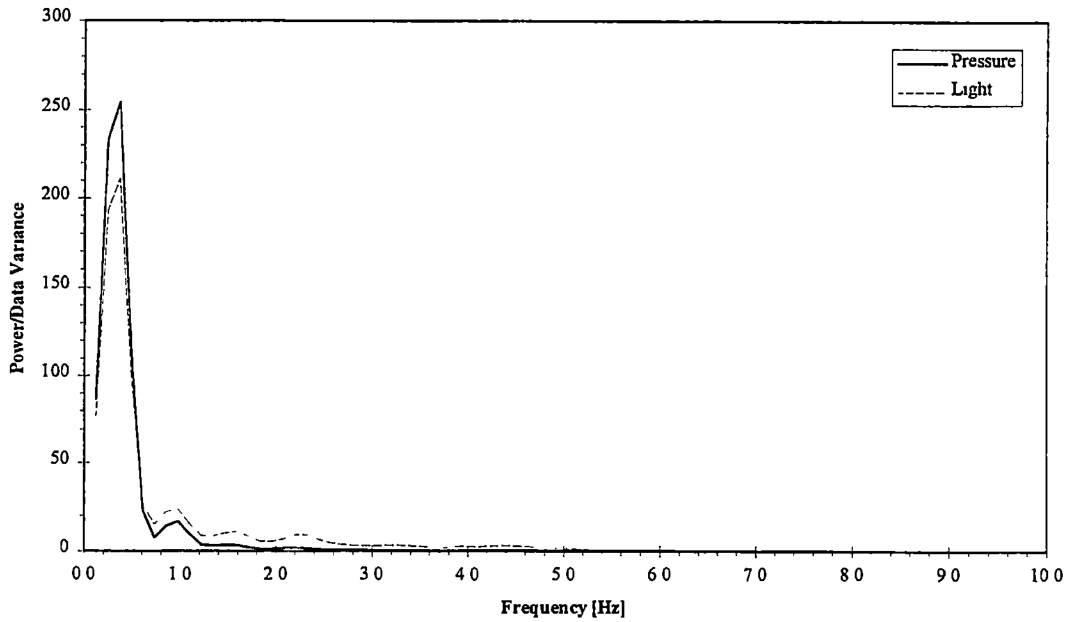

Figure 55: Fourier Power Spectra for INJ-4 – AV = 18.9 Lpm and Φ = 1.57

4.2.4 Autocorrelation Function

Figure 56 shows the autocorrelation function for the flame floating in the tube No evident periods are obtained, as the flame is stable. Figures 57, 58, and 59 all show the same period of 3.2 seconds. In Figure 57, the pressure signal is seen to be less periodic than the light This is due to the better data capture recorded by the light as compared to the pressure Figures 58 and 59 show extremely well correlated pressure and light signals. The periodicity of these signals cannot be due to the movement of the flame because in experiment four the flame is stable The periodicity must be related to the injection frequency.

4.2.5 Crosscorrelation Function

Figure 60 shows the crosscorrelation function of the flame floating in the tube without any injected air It is nearly identical to Figure 36, which is the condition where the flame is floating in the tube. There is very little lag in either direction. Figures 61, 62, and 63 show the same period of 3.2 seconds. In Figure 61 the effects of the air injection are seen in the sharp peaks in the middle of the otherwise smooth plot. The same thing is seen in Figures 62 and 63 but to a much less degree For test three, the pressure leads the light by a lag of 300, while for test four, the pressure leads the light by a lag of only 200 This is explained by the superior stability of test four and the much better correlation of the time series seen in Figure 51

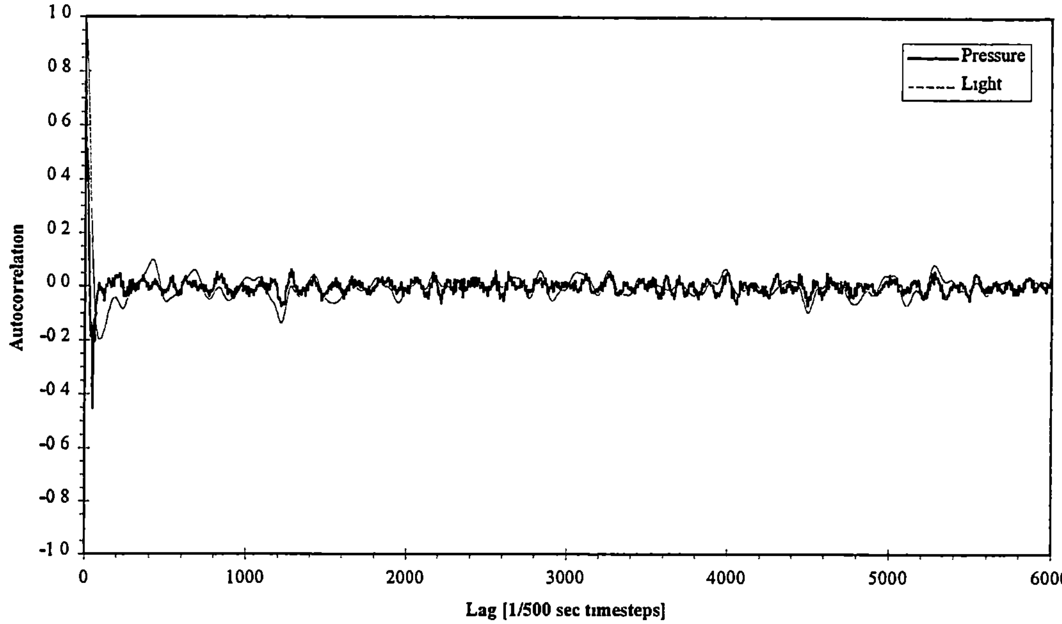

Figure 56: Autocorrelation Function for INJ-1 – AV = 18.9 Lpm and Φ = 1.76

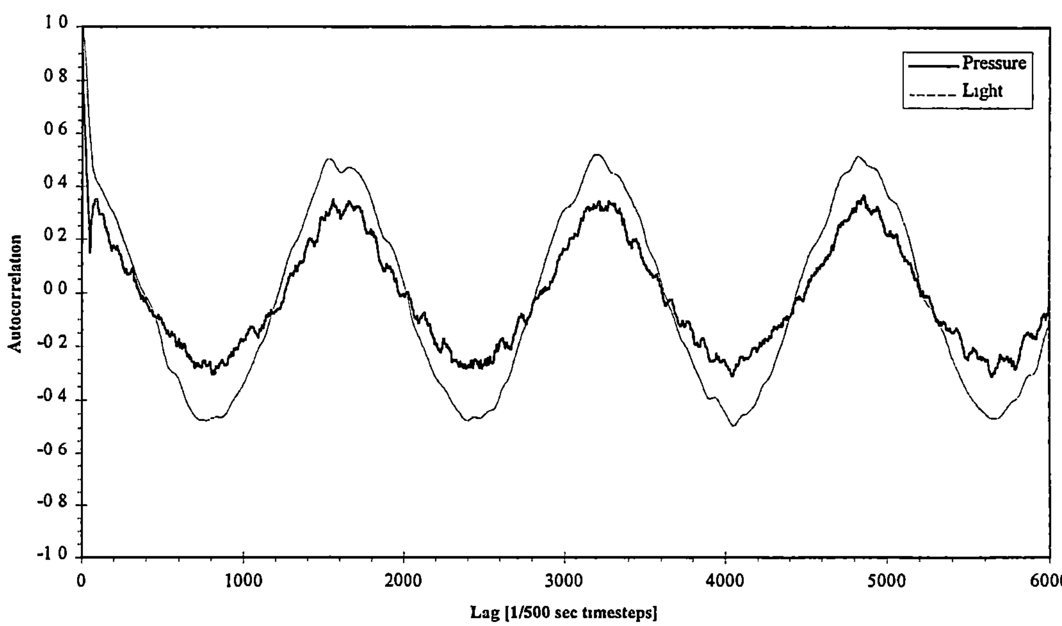

Figure 57: Autocorrelation Function for INJ-2 – AV = 18.9 Lpm and Φ = 1.72

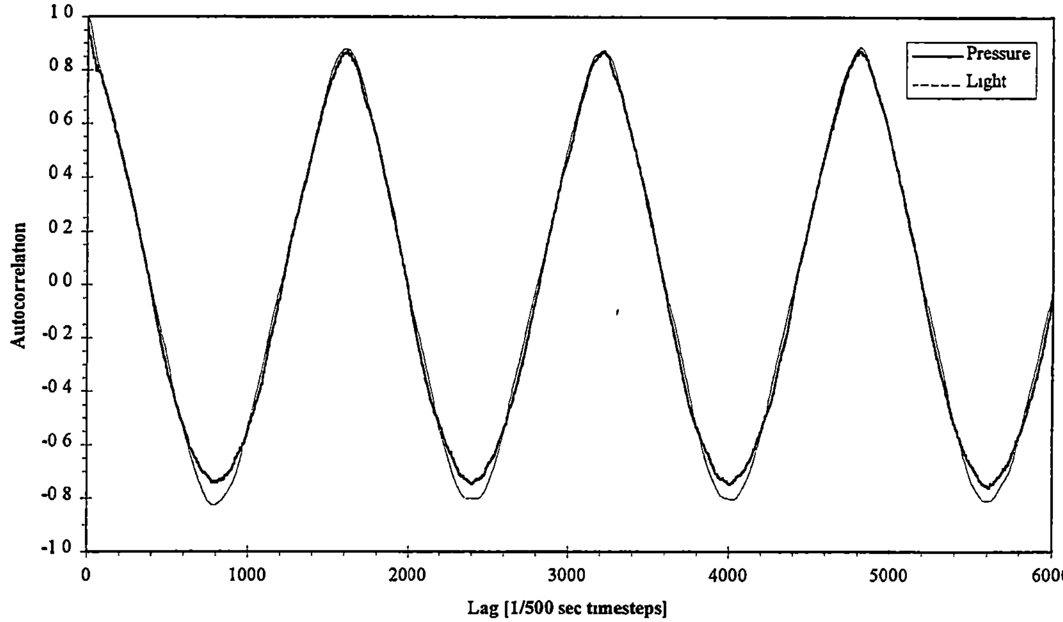

Figure 58: Autocorrelation Function for INJ-3 – AV = 18.9 Lpm and Φ = 1.63

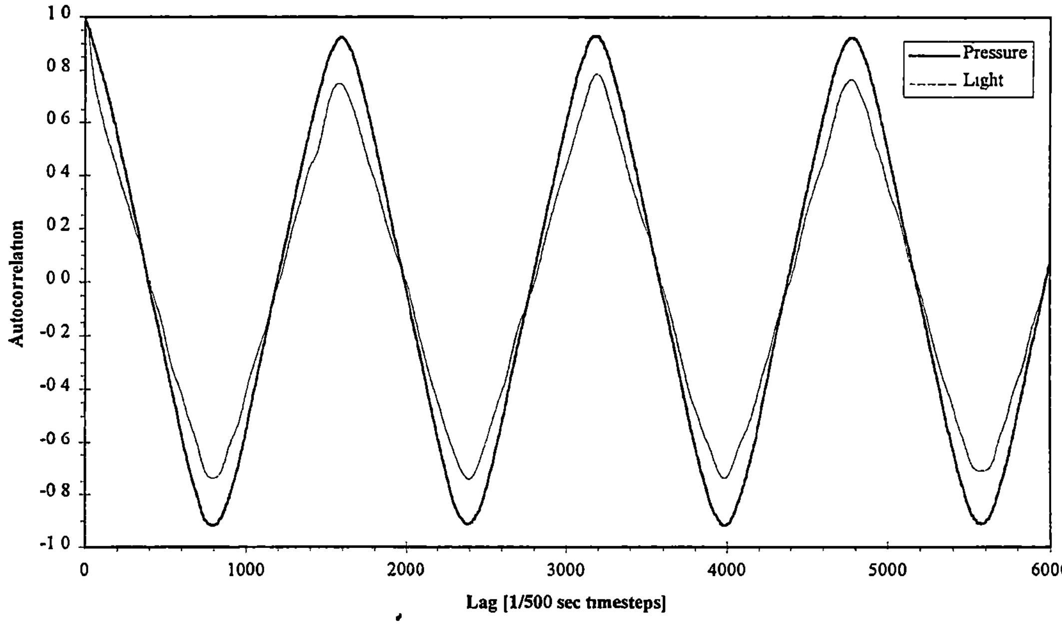

Figure 59: Autocorrelation Function for INJ-4 – AV = 18.9 Lpm and Φ = 1.57

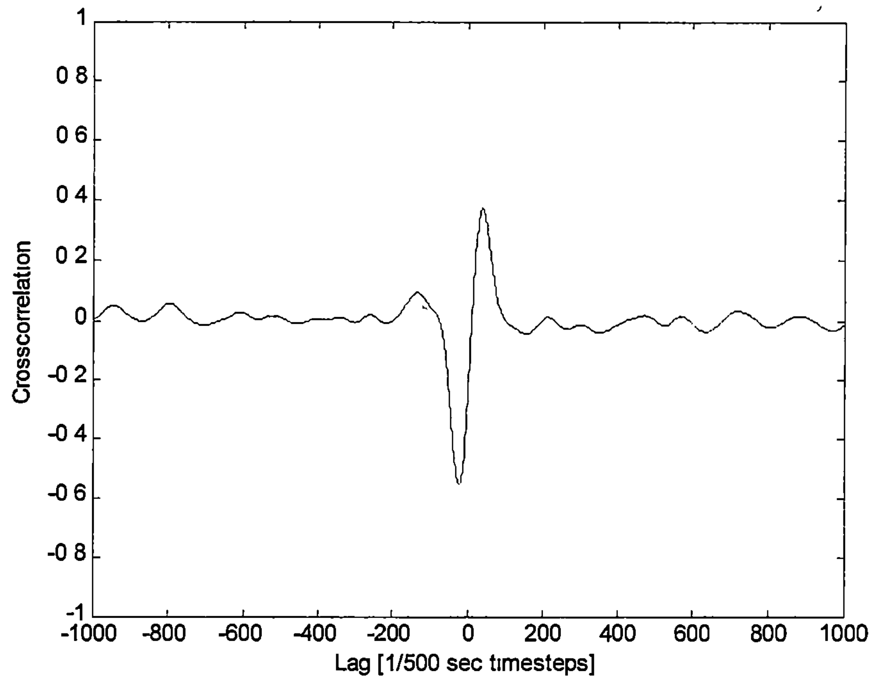

Figure 60: Crosscorrelation for INJ-1 – AV = 18.9 Lpm and Φ = 1.76

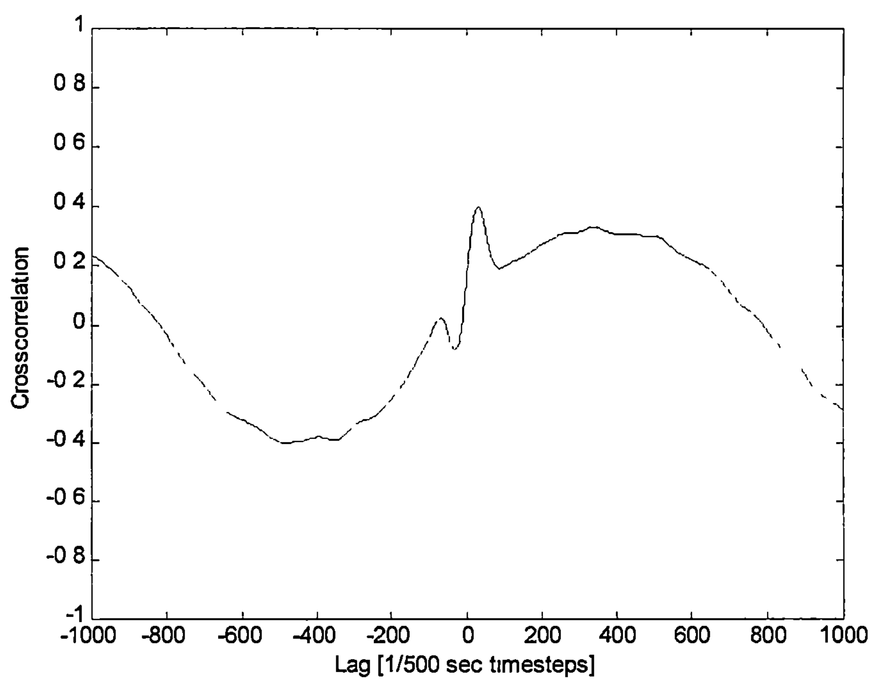

Figure 61: Crosscorrelation for INJ-2 – AV = 18.9 Lpm and Φ = 1.72

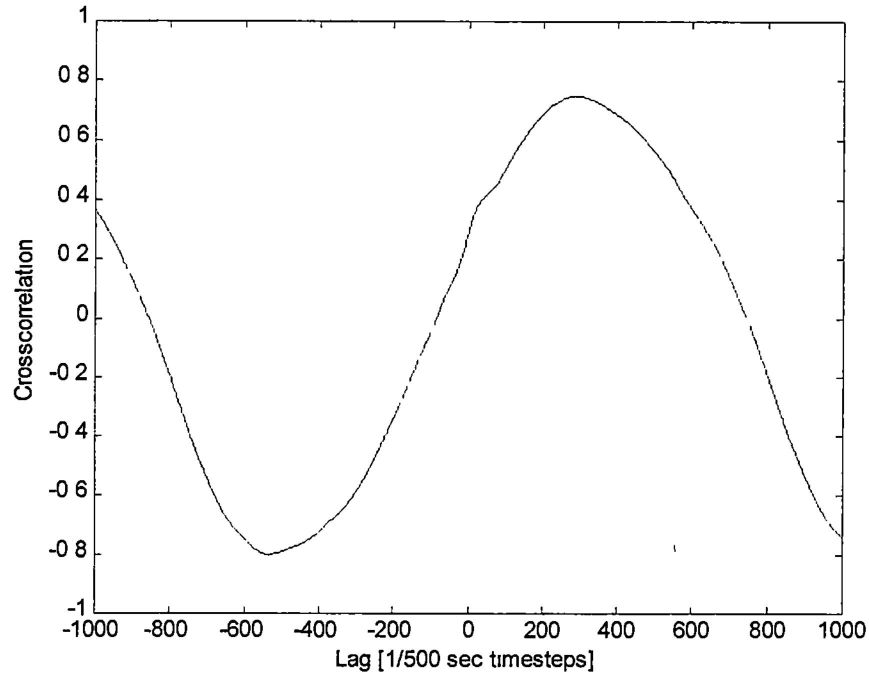

Figure 62: Crosscorrelation for INJ-3 – AV = 18.9 Lpm and Φ = 1.63

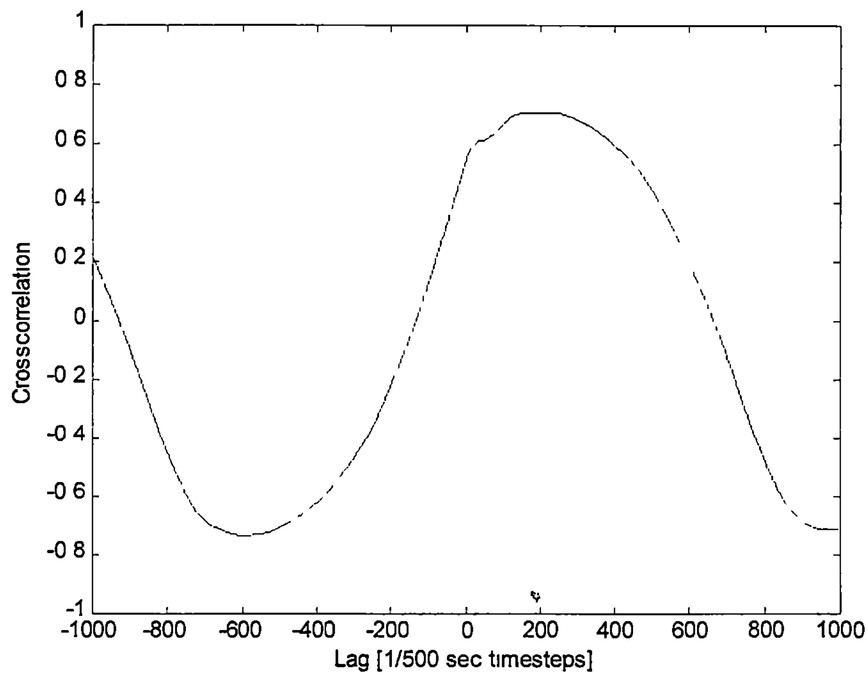

Figure 63: Crosscorrelation for INJ-4 – AV = 18.9 Lpm and Φ = 1.57

4.2.6 Kolmogorov Entropy

Figure 64 shows the Kolmogorov entropy for the frequency generator tests The results are exactly as expected based on the linear analysis techniques. The minimum value occurs at a Φ = 1 57 where the signal is the most periodic and a maximum at a Φ = 1.76 where the signal is most chaotic. The pressure is larger than the light except for the fourth test. Kolmogorov entropy provides reliable results as compared to the linear analysis methods.

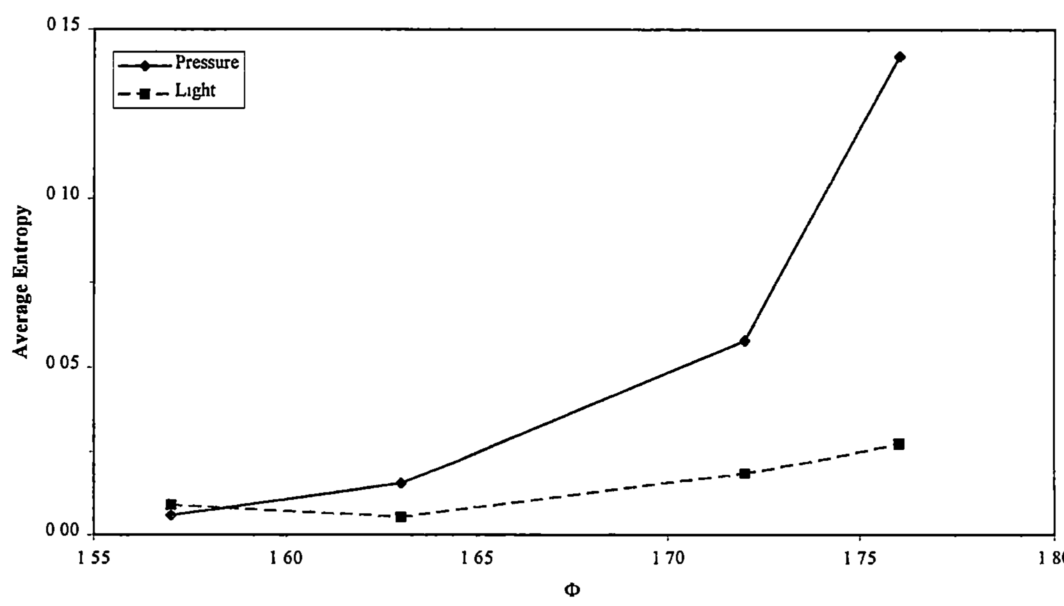

Figure 64: Kolmogorov Entropy for INJ – AV = 18.9 Lpm

Chapter 5

Conclusions and Recommendations

The results of this research demonstrate the unpredictability and inherent chaotic nature of flames. This was especially true around the rich-flammability limit of methane. As the burner became unable to support the flame, it had to find another place to anchor that was closer to stoichiometric conditions. This region of instability was explored with many interesting phenomena discovered, such as periodic flame propagation. Both linear and nonlinear time series analyses were found to be successful in characterizing the flame. This was found to be true for both pressure and light signals.

Due to the periodic nature of rich premixed-flame instabilities, linear time series analysis techniques were found to be adequate in monitoring the flame This was true for Fourier power spectrum, autocorrelation, and crosscorrelation. The period of the unstable flame could be found from all three techniques with reasonable accuracy and agreement The determination that pressure leads and in some cases prompts the light intensity of the flame was found using crosscorrelation

Kolmogorov entropy was also found to be a very useful and reliable method in monitoring and characterizing flame behavior. Both general trends and specific flame instabilities were indicated by entropy changes.

The equivalence ratio of the premixed gases was found to have a more pronounced effect on flame stability than the gas flowrate. Small perturbations in the fuel or air flowrate around the regions of instability were found to be very significant. This was proven by the frequency generator experiments in which flame stability was achieved by injecting small amounts of air into the primary combustion zone.

It is recommended that further investigations be conducted using a higher resolution pressure transducer in order to get more accurate pressure data. This would allow much better comparison between the pressure and light signals. Another item that would be useful to investigate would be analysis of the amount of oxygen present in the glass tube by using a high-speed O_2 sensor. This would provide another signal to be analyzed along with the pressure and light. It would also help quantify the reasons for the periodic behavior of the flame. The effect of varying the length (or diameter) of the glass tube above the burner on flame stability could also be studied. It is expected that the tube length will have a large effect on the flame oscillation period.

References

References

1. Baukel, Charles E., *Oxygen-Enhanced Combustion*, CRC Press, Boca Raton, FL, 1998.

2. U.S. Environmental Protection Agency, "Nitrogen Oxide Control for Stationary Combustion Sources", U.S. EPA report EPA/625/5-86/020, July 1986.

3. Ozone Transport Assessment Group, "OTAG Final Report, Chapter 5, Appendix C: Assessment of Control Technologies for Reducing Nitrogen Oxide Emissions From Non-Utility Point Sources and Major Area Sources", U.S. Environmental Protection Agency, 1997, http://www.epa.gov/ttnotag1/otag/finalrpt/chp5/appc htm.

4. Colburn, Ken, "Appendix A State's Report on Electric Utility Nitrogen Oxides Reduction Technology Options for Application by the Ozone Transport Assessment Group", Ozone Transport Assessment Group, April 11, 1996, http://www epa.gov/ttnotag/otag/finalrpt/appa.htm.

5. Federal Register Vol. 62, No. 131, July 9, 1997, http //www.epa.gov:80/ttnuatw1/combust/boiler/fr0797 pdf.

6. U.S. Environmental Protection Agency, "Feasibility of Installing NO_x Control Technologies by May 2003", U S EPA Office of Air and Radiation, September 1998.

7 Turns, Stephen R , *An Introduction to Combustion Concepts and Applications*, McGraw-Hill, Inc., New York, 1996.

8. "Fuel staging (burner out of services (boos), fuel biasing, reburning, or three-stage combustion)", http.//www iea-coal.org.uk/fuelstag.htm, IEA Coal Research, 1998.

9. "Fluidized-Bed Steam Generators", http //www.fwc.com/products/fluid.cfm, Foster Wheeler Corporation, 1999.

10. "Air staging for NO_x control (overfire Air (OFA) or two-stage combustion", http://www.iea-coal org.uk/airstag.htm, IEA Coal Research, 1998.

11. "Low-NO_X burners", http://www.iea-coal org uk/lownox htm, IEA Coal Research, 1998.

12. Finney, C.E.A., "Nonlinear Diagnostics of Low-NO_X Burners", 1998 (Unpublished).

13. Finney, C.E.A., "Identification and Characterization of Determinism in Spark-Ignition Internal Combustion Engines", M.S. Thesis, University of Tennessee, 1995.

14. Takens, F., "Detecting Strange Attractors in Turbulence," Lecture Notes in Mathematics, Rand, D.A. and Young, L.S., eds., Springer-Verlag, Berlin, Vol. 898, pp. 366-381, 1980.

15. Schouten, J.C , Takens, F. and Van der Bleek, C M , "Estimation of the dimension of a noisy attractor", *Physical Review E,* Vol. 50, Number 3, 1994.

16. Schouten, J.C., Takens, F. and Van der Bleek, C.M., "Maximum-likelihood estimation of the entropy of an attractor", *Physical Review E,* Volume 49, Number 1, 1994.

17. Kuan-yun Kuo, Kenneth, *Principles of Combustion*, John Wiley & Sons, Inc., New York, 1986.

18. Dodge, L.G., "Optical Absorption and Emissions", p. 156.

19. Chapter 4 Flame Phenomenon in Premixed Combustible Gases, pp. 141-159.

20. Hyun Kim, Jong and Stringer, John, *Applied Chaos*, John Wiley & Sons, Inc., New York, 1992.

Appendix

Table A-1: Parameters of Overfire Air Experiments

(AV) Air [SCFH]	(AV) Air [Lpm]	(AV) Fuel [SCFH]	(AV) Fuel [Lpm]	Flame Event ---	Phi ---	Pressure Fuel [psi]	Pressure P.A. [psi]	Velocity Air [m/s]	Velocity Fuel [m/s]
30	14 16	3.54	1 67	FE-1	0 99	11.5	20	0 985	0.136
30	14 16	5.32	2 51	FE-2	1 49	11 5	20	0 985	0 204
30	14.16	5 91	2.79	FE-3	1.65	11.5	20	0 985	0.227
30	14.16	6.02	2.84	FE-3	1.68	11.5	20	0 985	0.231
30	14.16	6.50	3.07	FE-4	1.82	11 5	20	0 985	0.250
30	14 16	8.26	3.90	FE-7	2 31	11 5	20	0 985	0.317
40	18.88	4 24	2.00	FE-1	1.35	20	20	1.319	0.188
40	18 88	5 30	2.50	FE-2	1.69	20	20	1 319	0.235
40	18.88	5 30^{+}	2.50^{+}	FE-3	1.73	20	20	1 319	0.237
40	18.88	5 83	2.75	FE-4	1 86	20	20	1.319	0.259
40	18.88	6 36	3.00	FE-7	2 03	20	20	1 319	0.282
40	18 88	7 42	3.50	FE-8	2.37	20	20	1 319	0 330
70	33.04	5.30	2.50	FE-1	0 97	20	20	2.308	0.235
70	33.04	7 42	3 50	FE-2	1.35	20	20	2 308	0 329
70	33 04	8 48	4 00	FE-5	1 55	20	20	2 308	0 376
70	33 04	9 53	4 50	FE-6	1.74	20	20	2.308	0.422
70	33.04	10 59	5.00	FE-7	1 94	20	20	2.308	0.469
70	33 04	12 71	6 00	FE-8	2 32	20	20	2.308	0 563
90	42 48	7 42	3 50	FE-1	1 05	20	20	2 948	0 326
90	42 48	9 53^{-}	4.50^{-}	FE-2	1.32	20	20	2 948	0.419
90	42.48	9 53^{+}	4 50^{+}	FE-4	1 39	20	20	2.948	0.421
90	42 48	11 12	5 25	FE-6	1.58	20	20	2 948	0.490
90	42.48	12 71	6 00	FE-6	1 81	20	20	2 948	0 560
90	42 48	13 77	6.50	FE-7	1.96	20	20	2 948	0 606
90	42 48	14 83	7 00	FE-8	2 11	20	20	2.948	0 653
110	51 91	9 53	4 50	FE-1	1.11	20	20	3.603	0.420
110	51.91	11 12	5 25	FE-2	1 29	20	20	3 603	0 490
110	51 91	11 65	5 50	FE-4	1.35	20	20	3 603	0 500
110	51 91	13 24	6.25	FE-5	1 54	20	20	3 603	0 583
110	51 91	13 77	6.50	FE-6	1 60	20	20	3 603	0 606
110	51 91	14 83	7 00	FE-6	1 72	20	20	3 603	0 653
110	51 91	16.42	7 75	FE-7	1.91	20	20	3 603	0 723
110	51 91	18 01	8 50	FE-8	2 09	20	20	3 603	0 793
130	61.35	10 59	5 00	FE-1	1.04	20	20	4 286	0 469
130	61.35	12.71	6 00	FE-3	1 25	20	20	4 286	0 563
130	61.35	13.77	6 50	FE-4	1 35	20	20	4.286	0 610
130	61 35	15 89	7 50	FE-5	1 56	20	20	4 286	0 704
130	61 35	18 01	8 50	FE-6	1 77	20	20	4 286	0 798
130	61 35	20.13	9 50	FE-7	1 98	20	20	4 286	0 892
130	61 35	21 19	10 00	FE-8	2 08	20	20	4 286	0 939

Table A-2: Parameters of Frequency Generator Experiments

(AV) Air	(AV) Air	(AV) Injected Air	(AV) Injected Air	(AV) Fuel	(AV) Fuel	Phi Global	Phi Local	Press. Fuel	Press Air	Press Injected Air	Vel. Fuel	Vel Air
[SCFH]	[Lpm]	[SCFH]	[Lpm]	[SCFH]	[Lpm]	---	---	[psi]	[psi]	[psi]	[m/s]	[m/s]
40	18.88	0.00	0.000	5.51	2.60	1.76	1.76	20	20	0	0.245	1.323
40	18.88	1.00	0.470	5.51	2.60	1.72	1.76	20	20	20	0.245	1.338
40	18.88	3.32	1.567	5.51	2.60	1.63	1.76	20	20	20	0.245	1.374
40	18.88	4.98	2.350	5.51	2.60	1.57	1.76	20	20	20	0.245	1.400

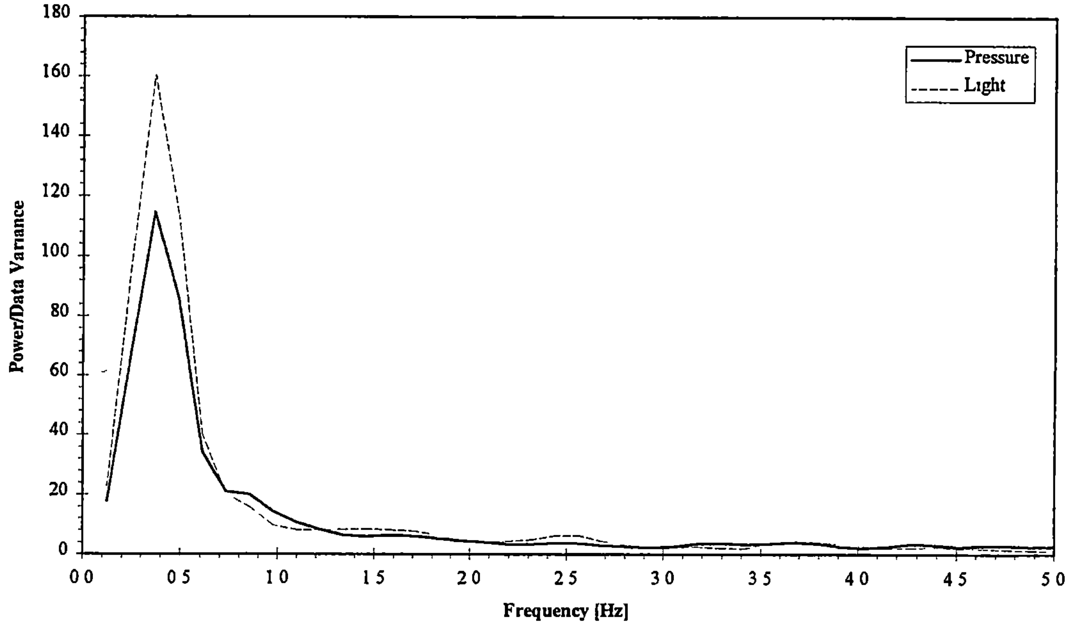

Figure A-1: Fourier Power Spectra for FE-5 – AV = 33.0 Lpm and Φ = 1.55

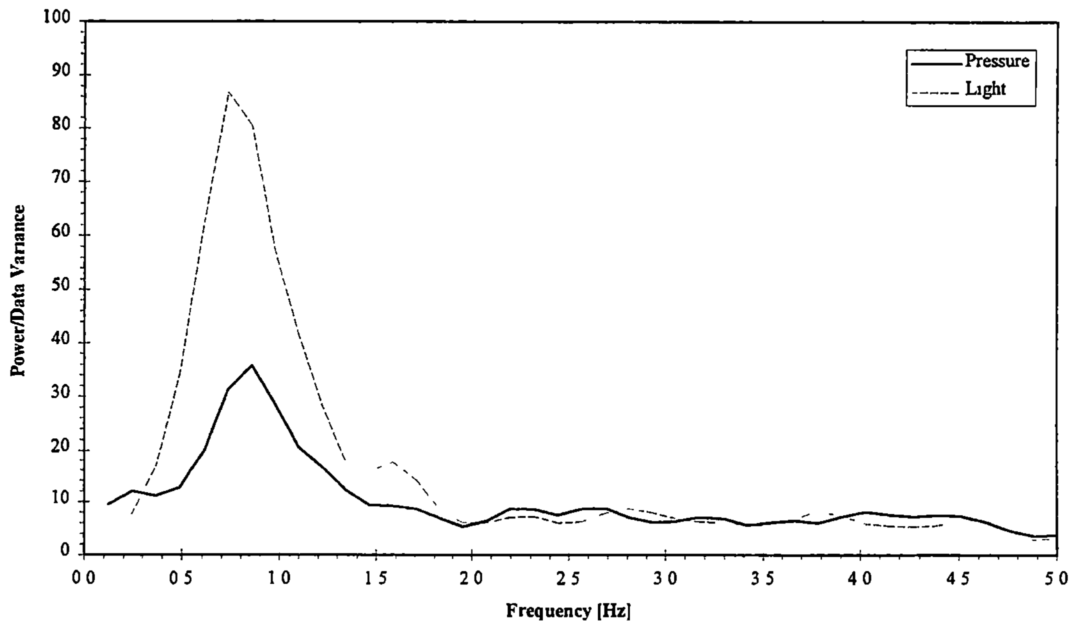

Figure A-2: Fourier Power Spectra for FE-5 – AV = 51.9 Lpm and Φ = 1.54

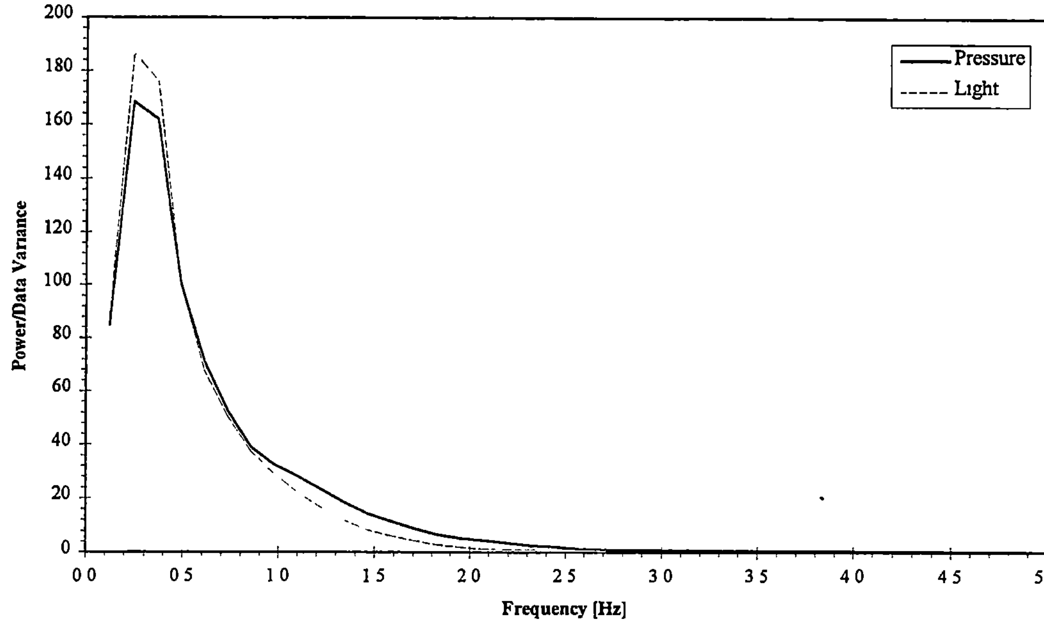

Figure A-3: Fourier Power Spectra for FE-6 – AV = 33.0 Lpm and Φ = 1.74

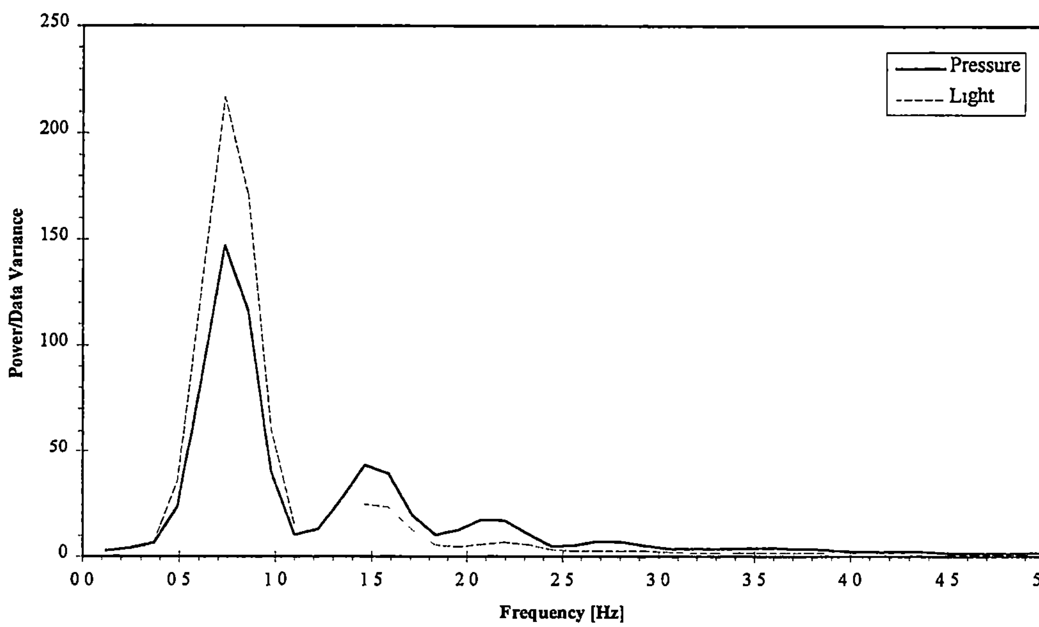

Figure A-4: Fourier Power Spectra for FE-6 – AV = 51.9 Lpm and Φ = 1.60

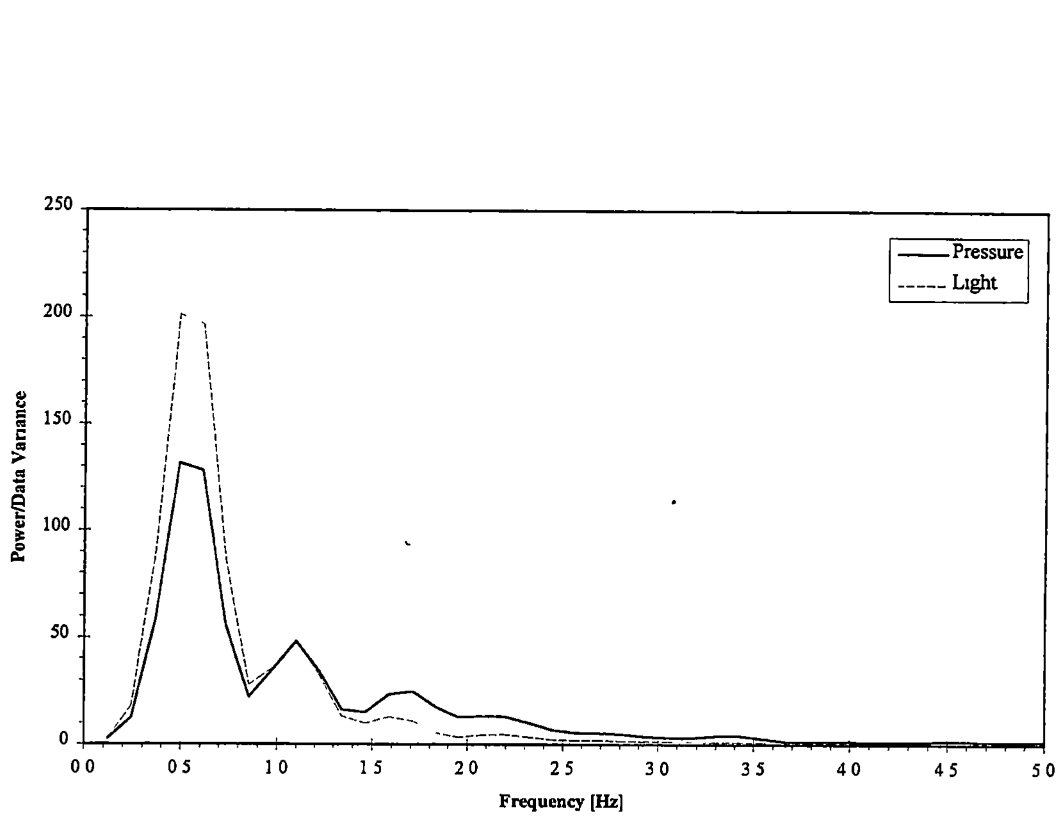

Figure A-5: Fourier Power Spectra for FE-6 – AV = 51.9 Lpm and Φ = 1.72

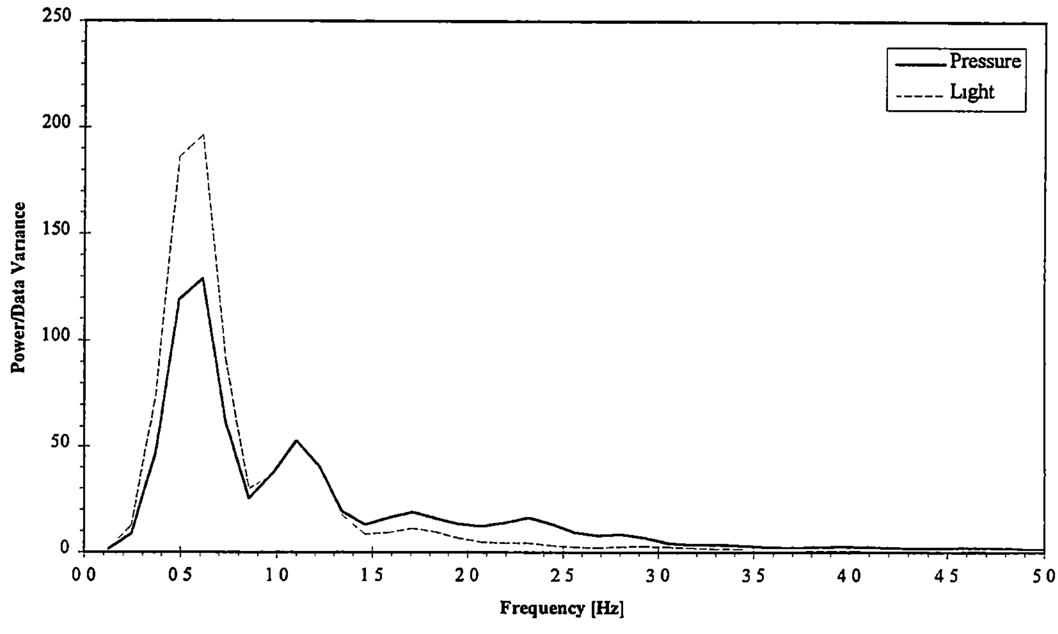

Figure A-6: Fourier Power Spectra for FE-6 – AV = 61.4 Lpm and Φ = 1.77

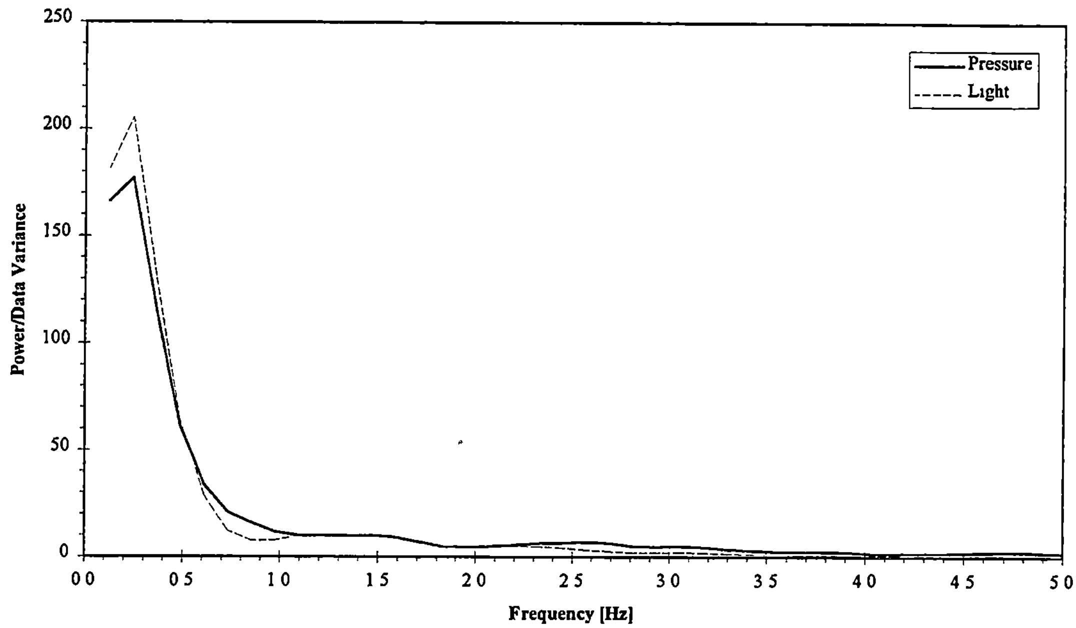

Figure A-7: Fourier Power Spectra for FE-7 – AV = 14.2 Lpm and Φ = 2.31

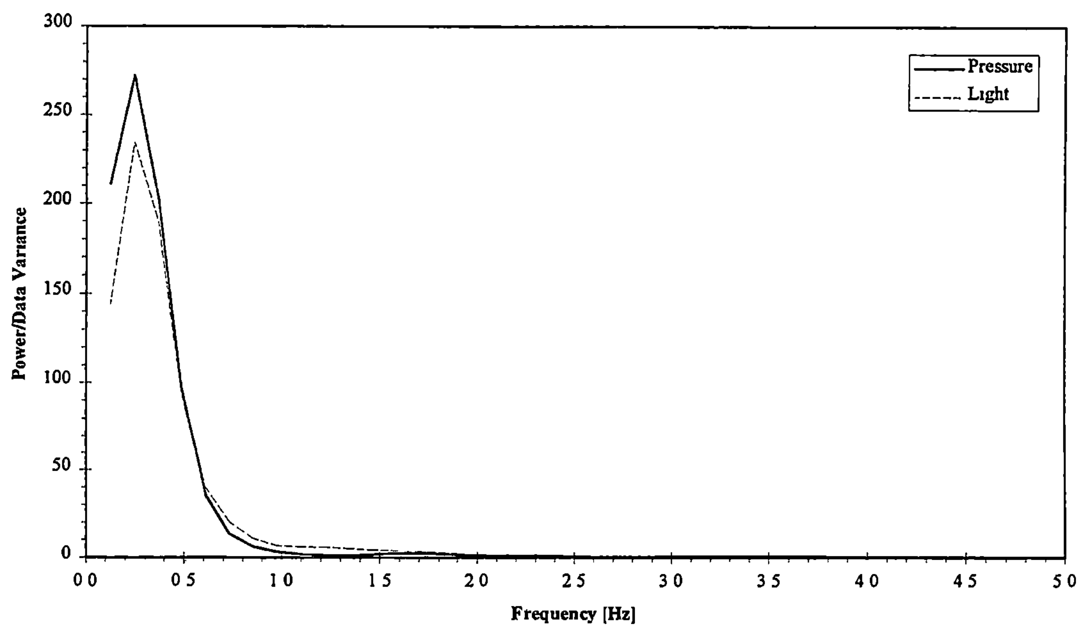

Figure A-8: Fourier Power Spectra for FE-7 – AV = 18.9 Lpm and Φ = 2.03

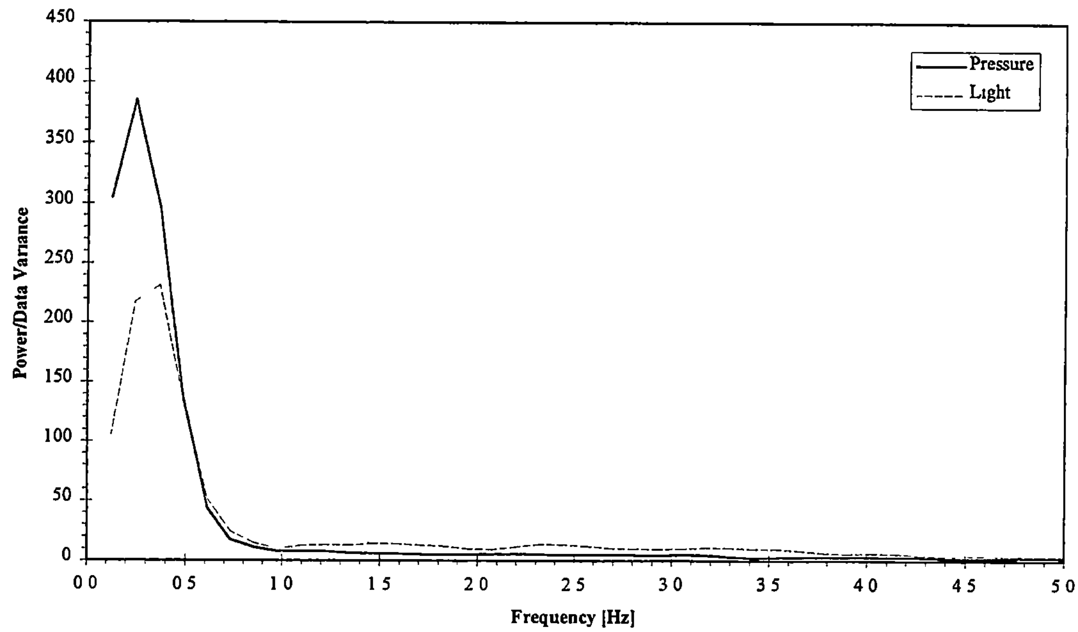

Figure A-9: Fourier Power Spectra for FE-7 – AV = 33.0 Lpm and Φ = 1.94

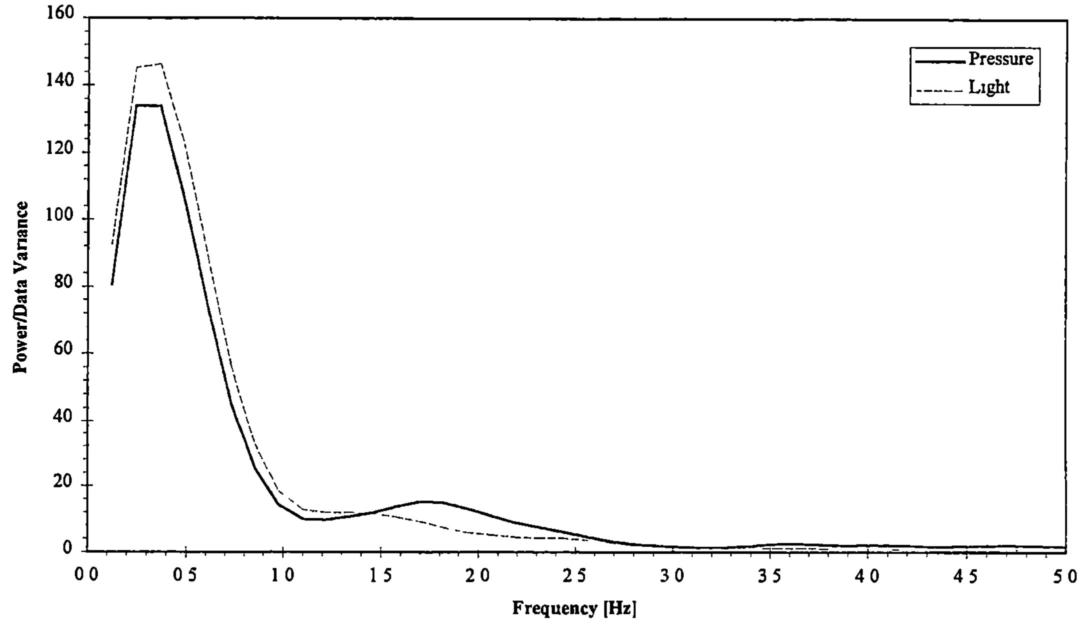

Figure A-10: Fourier Power Spectra for FE-7 – AV = 51.9 Lpm and Φ = 1.91

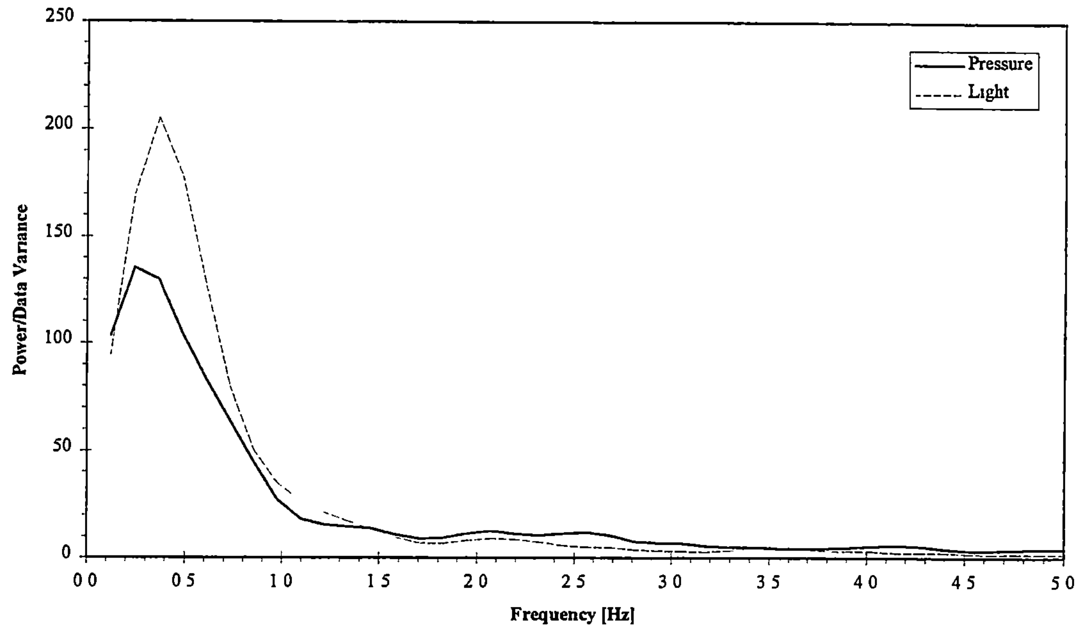

Figure A-11: Fourier Power Spectra for FE-7 – AV = 61.4 Lpm and Φ = 1.98

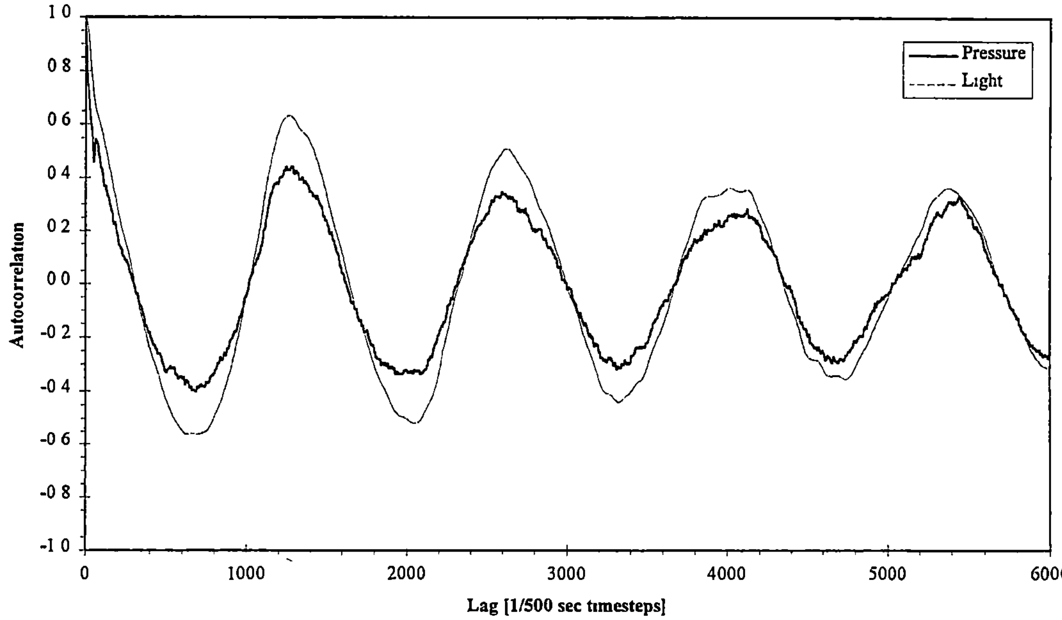

Figure A-12: Autocorrelation Function for FE-5 – AV = 33.0 Lpm and Φ = 1.55

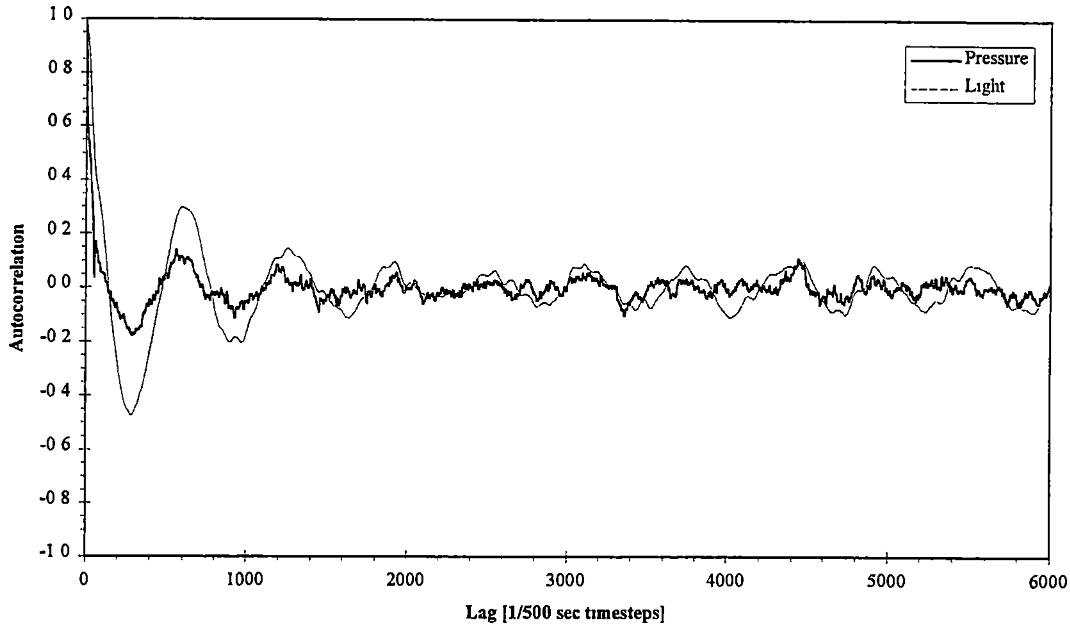

Figure A-13: Autocorrelation Function for FE-5 – AV = 51.9 Lpm and Φ = 1.54

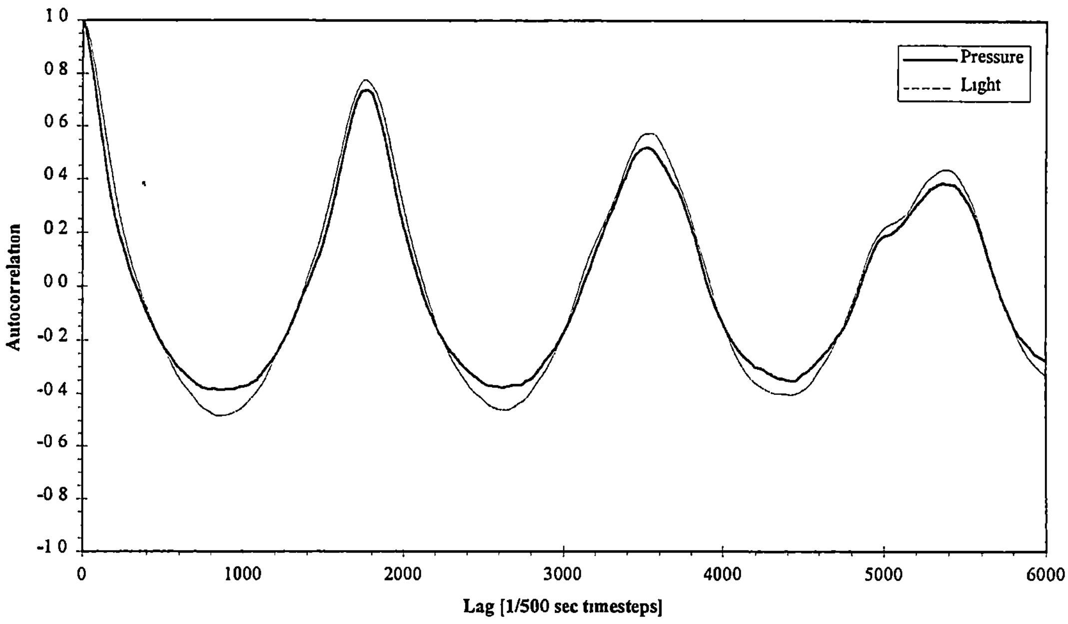

Figure A-14: Autocorrelation Function for FE-6 – AV = 33.0 Lpm and Φ = 1.74

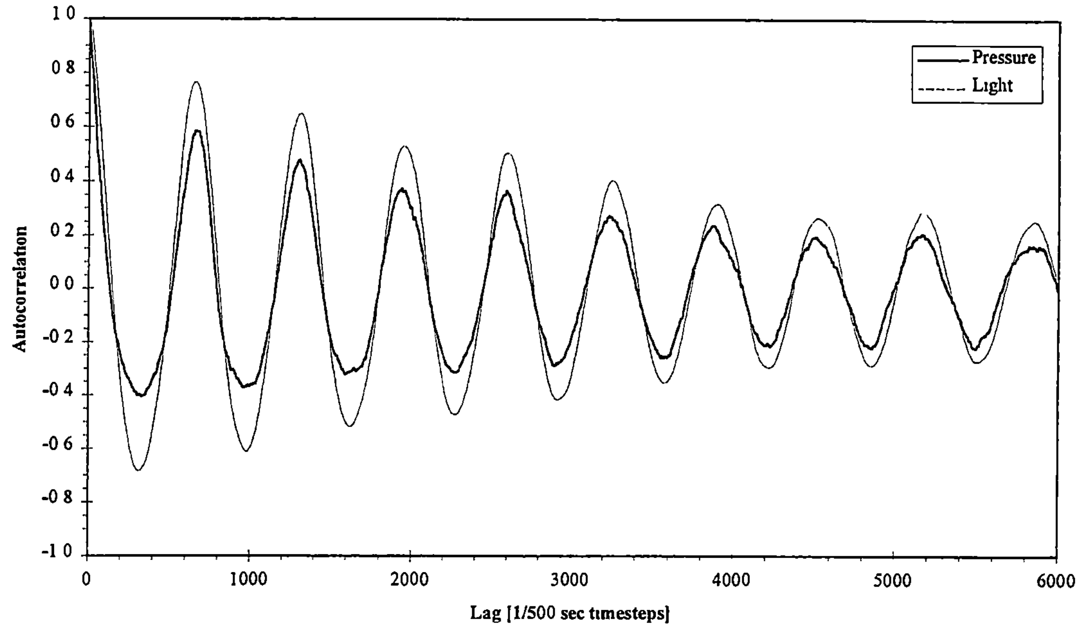

Figure A-15: Autocorrelation Function for FE-6 – AV = 51.9 Lpm and Φ = 1.60

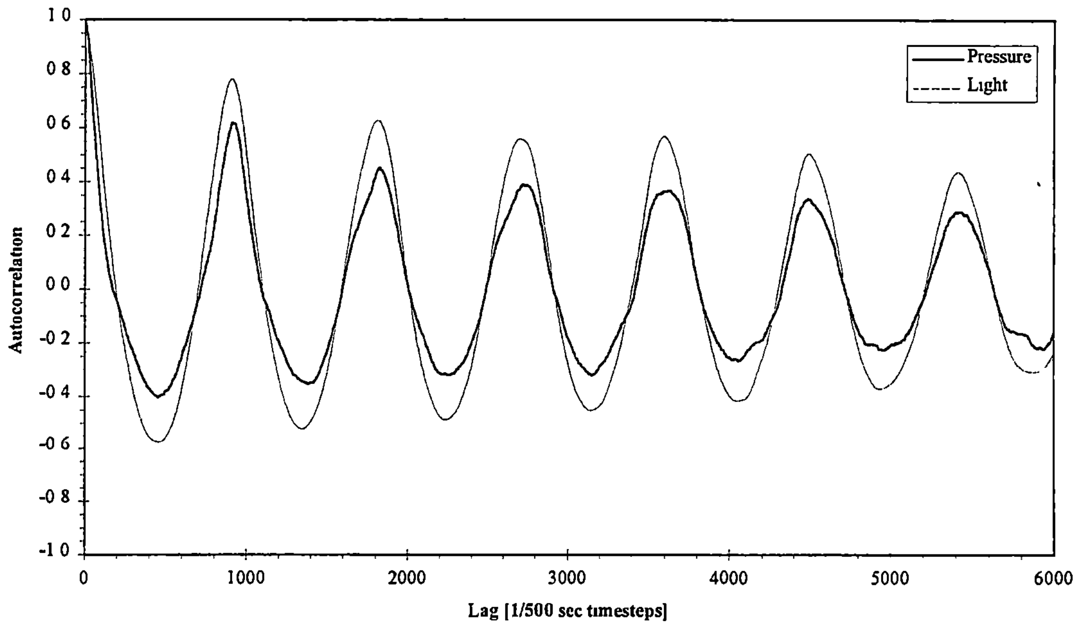

Figure A-16: Autocorrelation Function for FE-6 – AV = 51.9 Lpm and Φ = 1.72

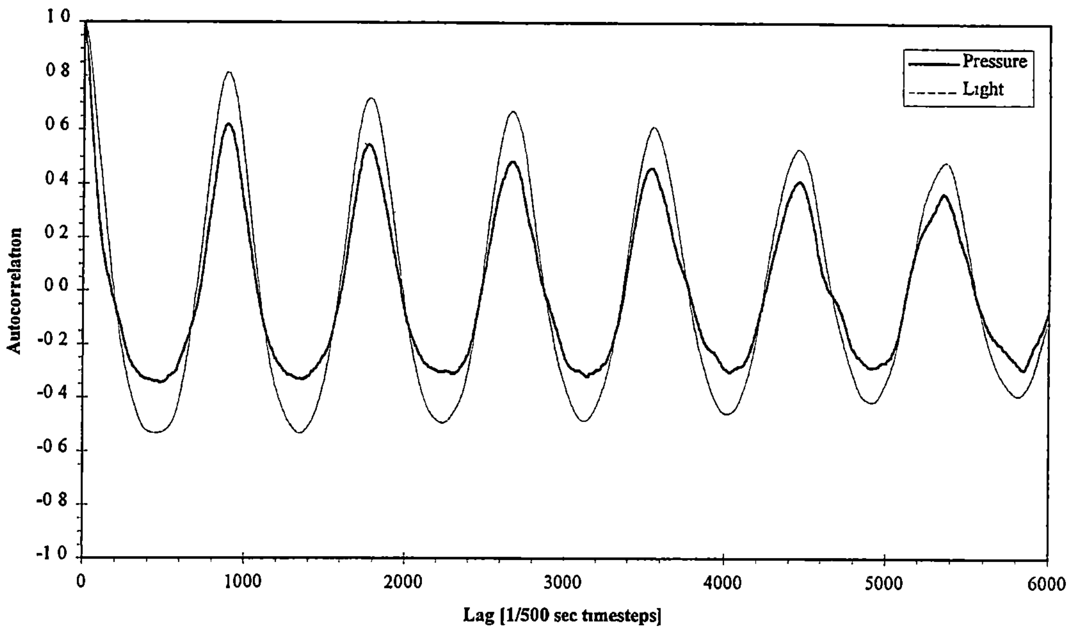

Figure A-17: Autocorrelation Function for FE-6 – AV = 61.4 Lpm and Φ = 1.77

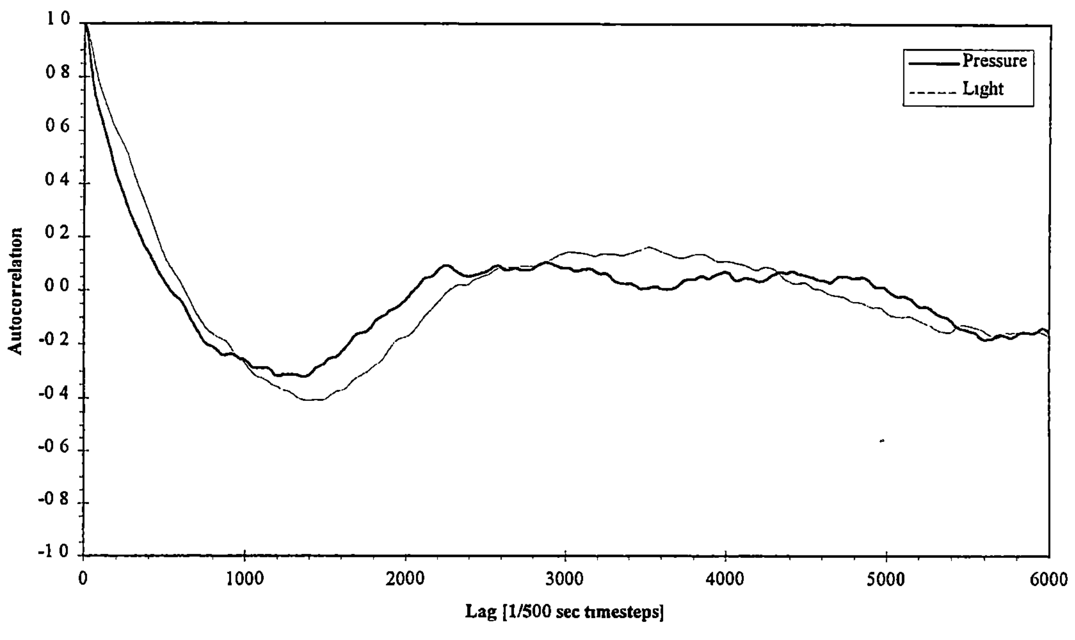

Figure A-18: Autocorrelation Function for FE-7 – AV = 14.2 Lpm and Φ = 2.31

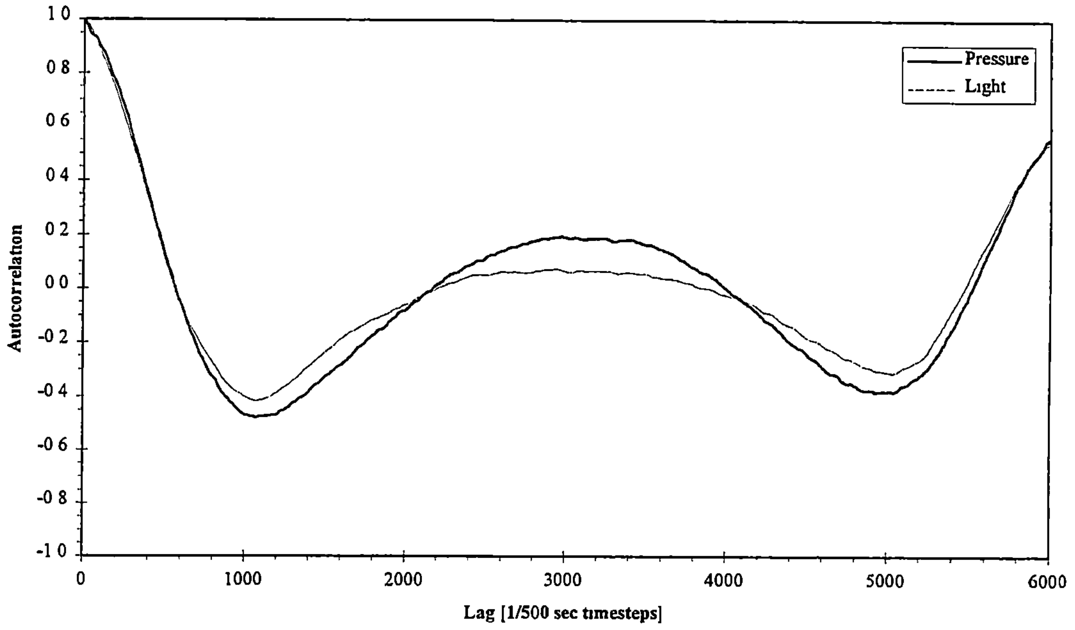

Figure A-19: Autocorrelation Function for FE-7 – AV = 18.9 Lpm and Φ = 2.03

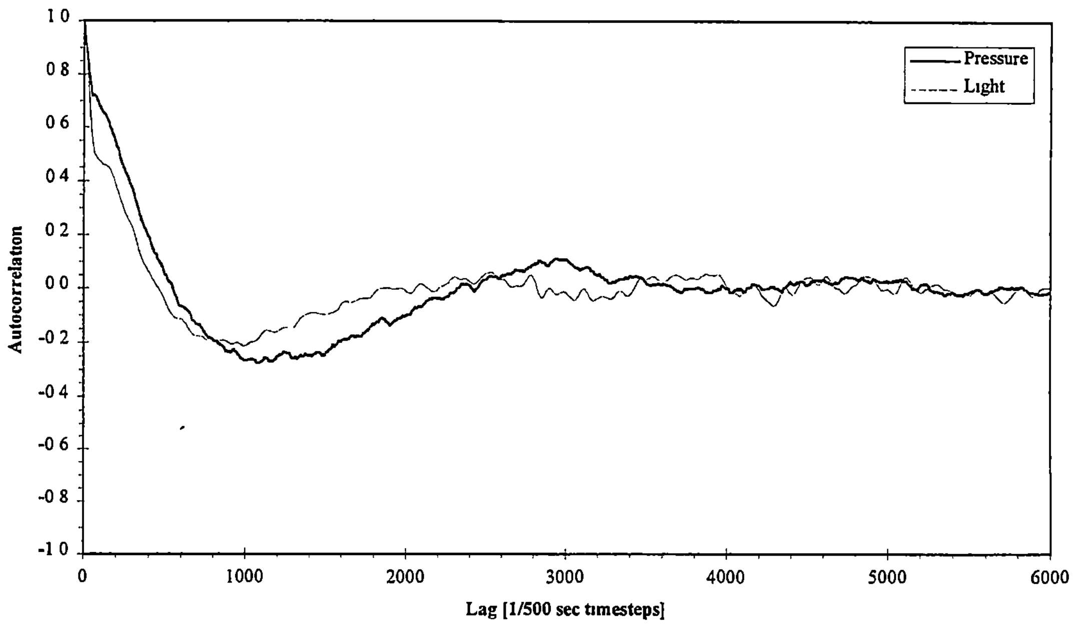

Figure A-20: Autocorrelation Function for FE-7 – AV = 33.0 Lpm and Φ = 1.94

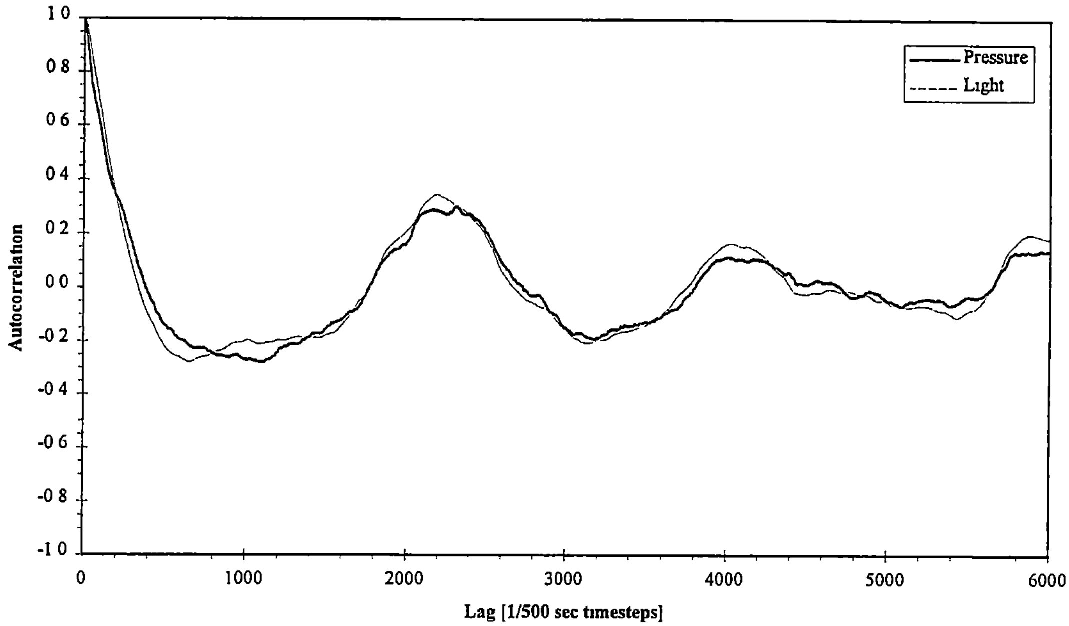

Figure A-21: Autocorrelation Function for FE-7 – AV = 51.9 Lpm and Φ = 1.91

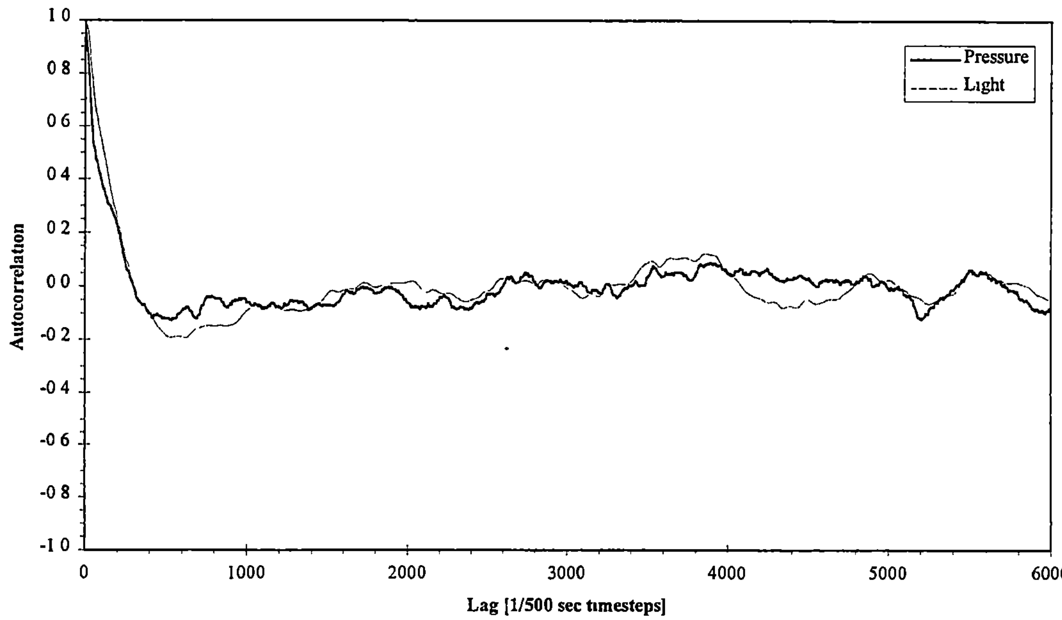

Figure A-22: Autocorrelation Function for FE-7 – AV = 61.4 Lpm and Φ = 1.98

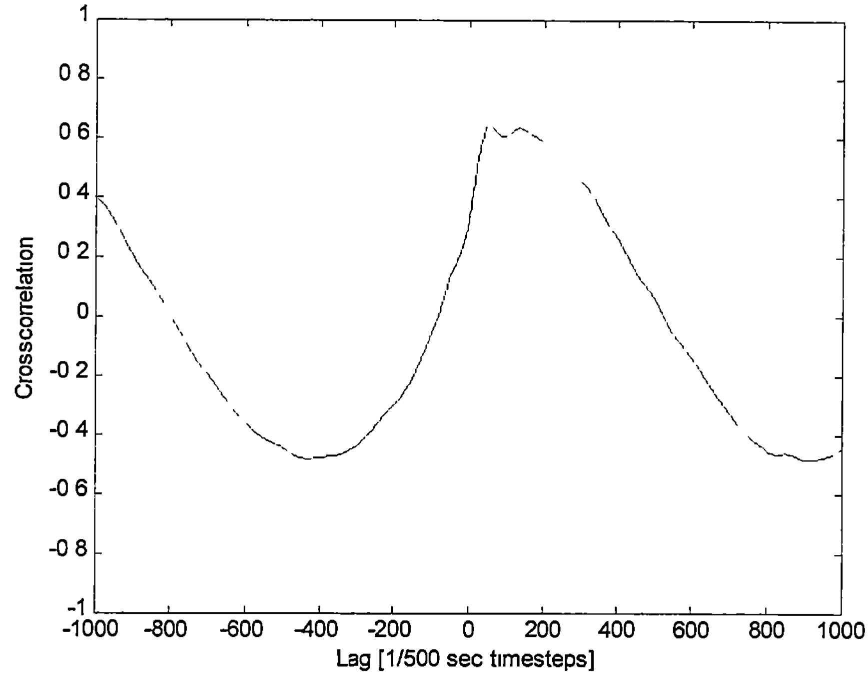

Figure A-23: Crosscorrelation for FE-5 – AV = 33.0 Lpm and Φ = 1.55

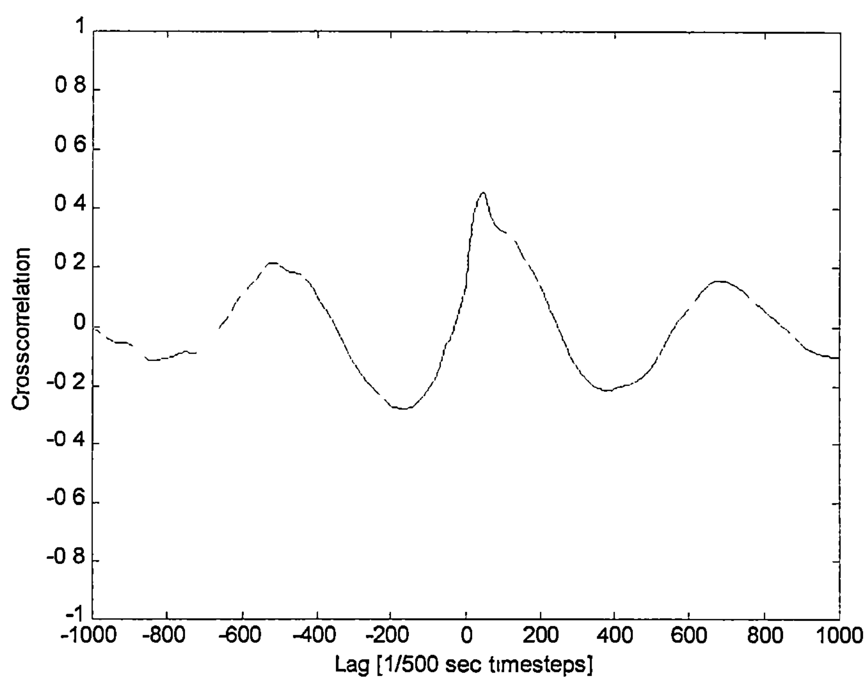

Figure A-24: Crosscorrelation for FE-5 – AV = 51.9 Lpm and Φ = 1.54

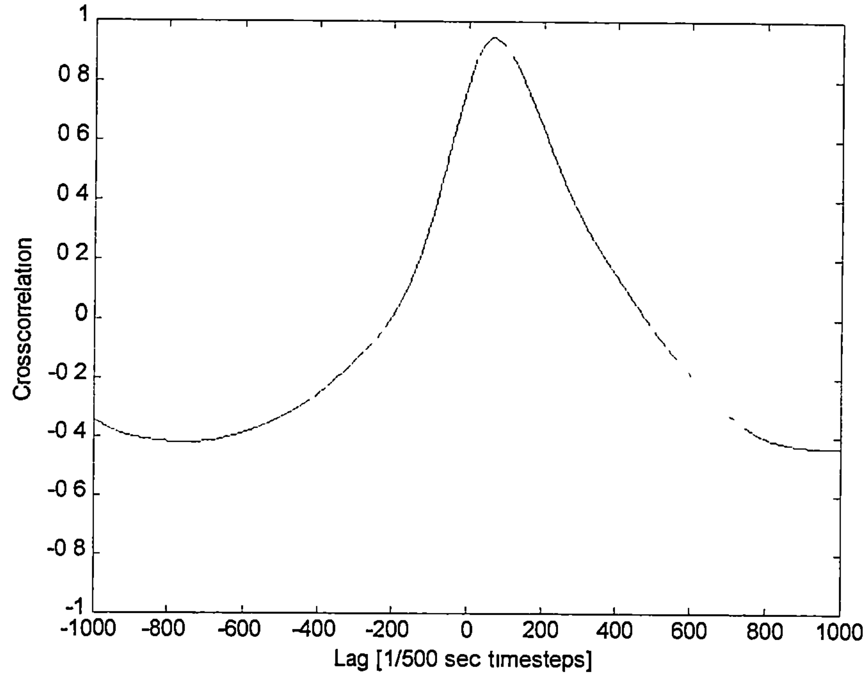

Figure A-25: Crosscorrelation for FE-6 – AV = 33.0 Lpm and Φ = 1.74

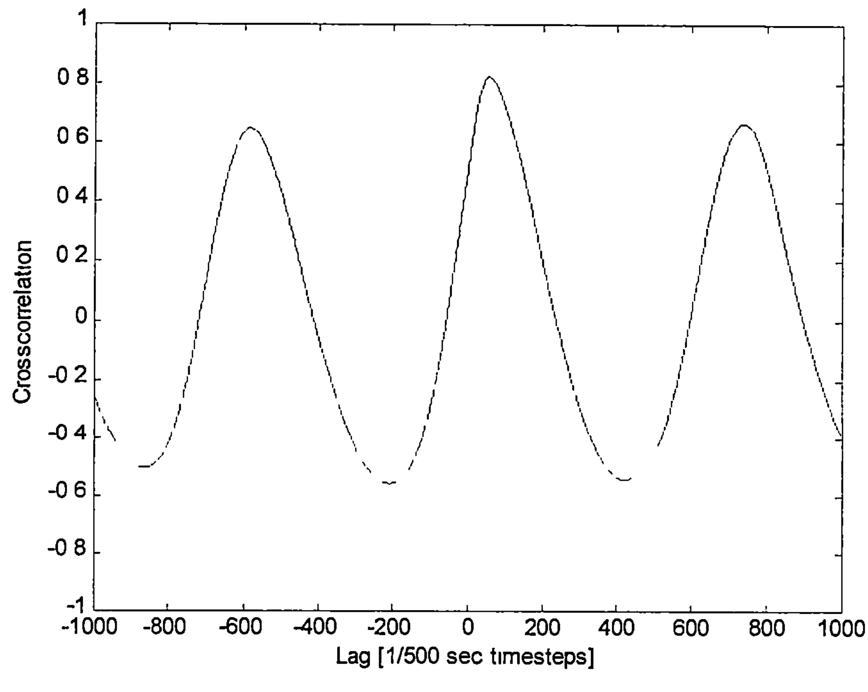

Figure A-26: Crosscorrelation for FE-6 – AV = 51.9 Lpm and Φ = 1.60

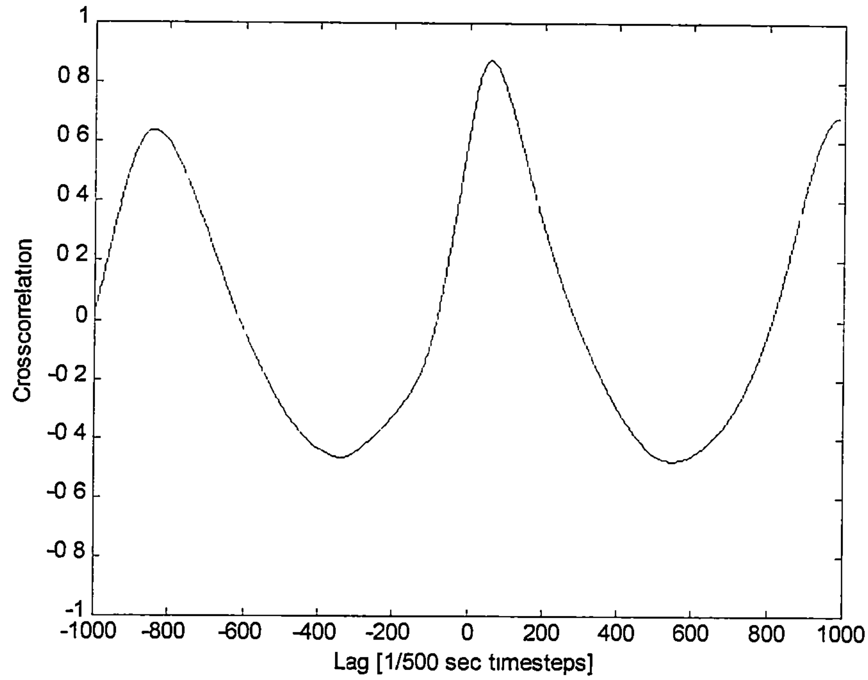

Figure A-27: Crosscorrelation for FE-6 – AV = 51.9 Lpm and Φ = 1.72

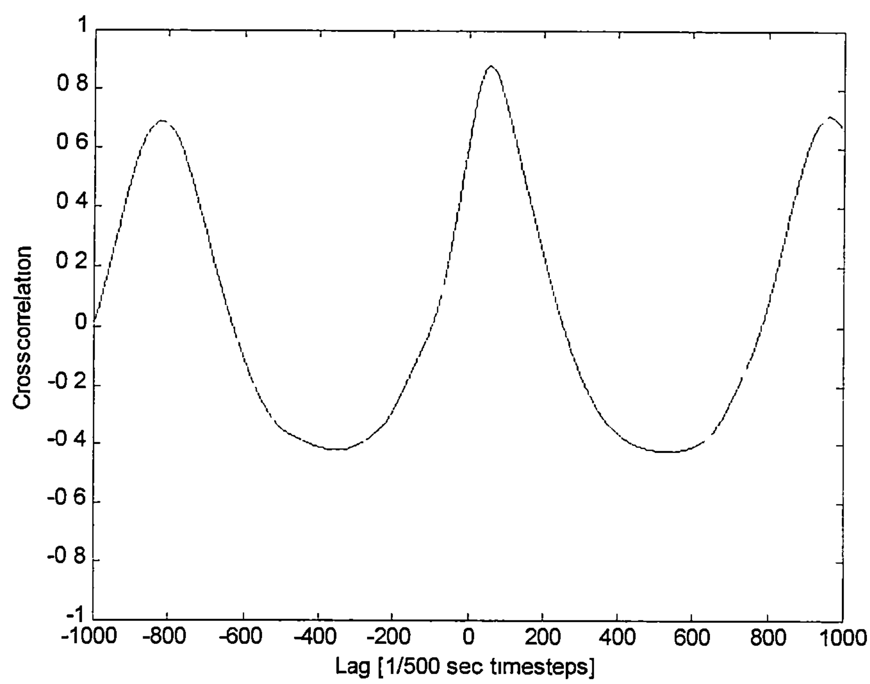

Figure A-28: Crosscorrelation for FE-6 – AV = 61.4 Lpm and Φ = 1.77

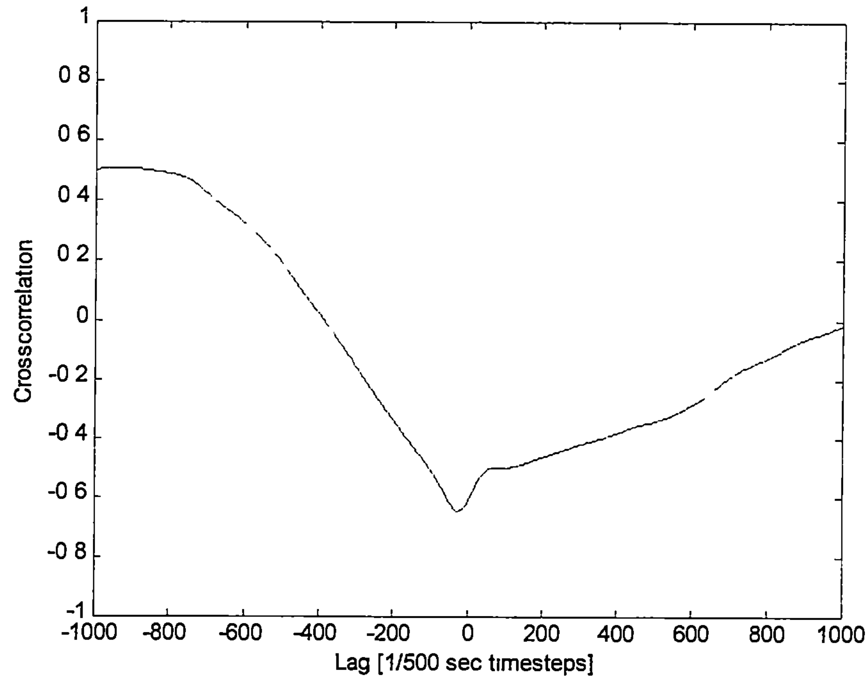

Figure A-29: Crosscorrelation for FE-7 – AV = 14.2 Lpm and Φ = 2.31

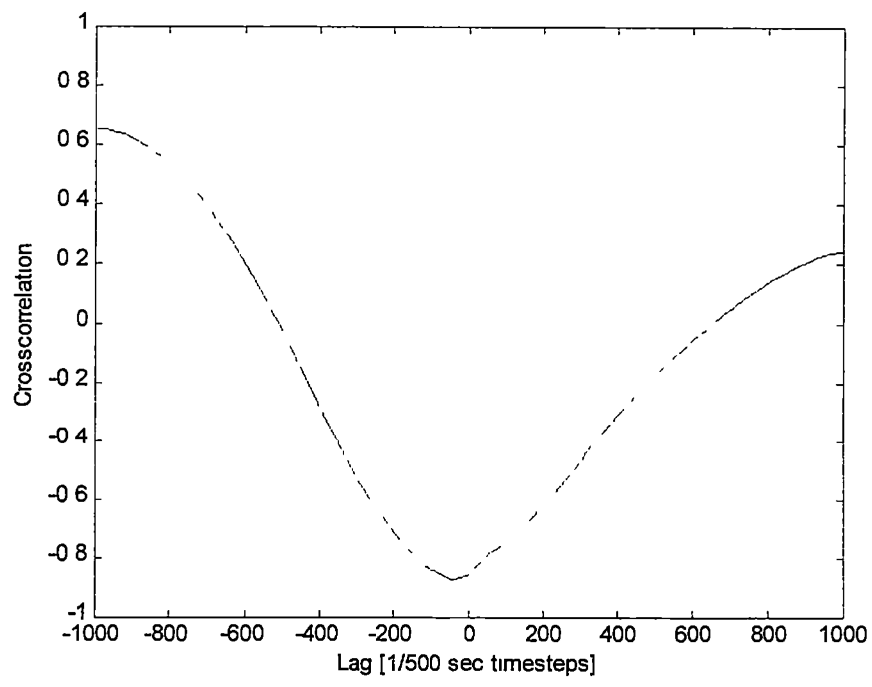

Figure A-30: Crosscorrelation for FE-7 – AV = 18.9 Lpm and Φ = 2.03

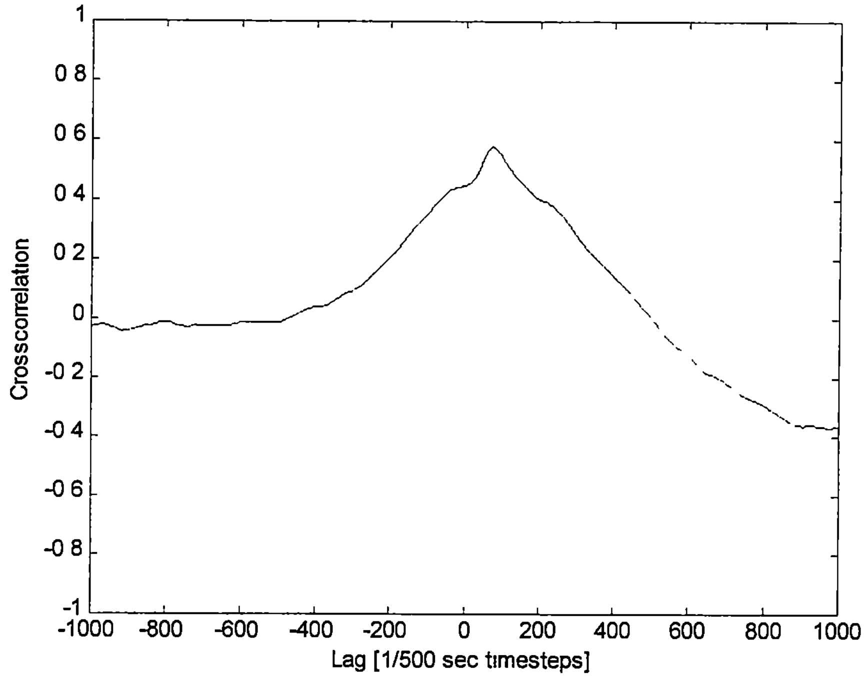

Figure A-31: Crosscorrelation for FE-7 – AV = 33.0 Lpm and Φ = 1.94

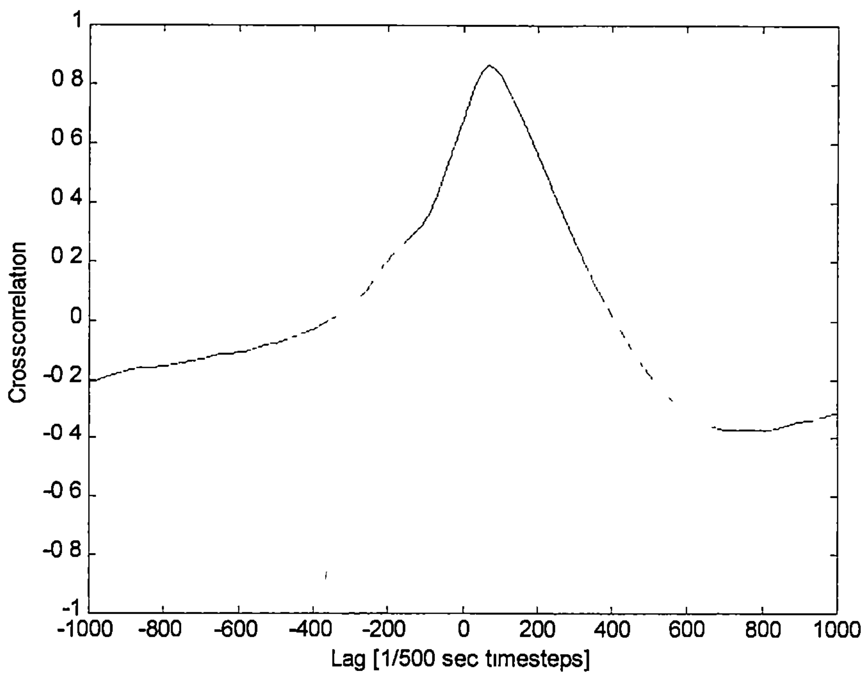

Figure A-32: Crosscorrelation for FE-7 – AV = 51.9 Lpm and Φ = 1.91

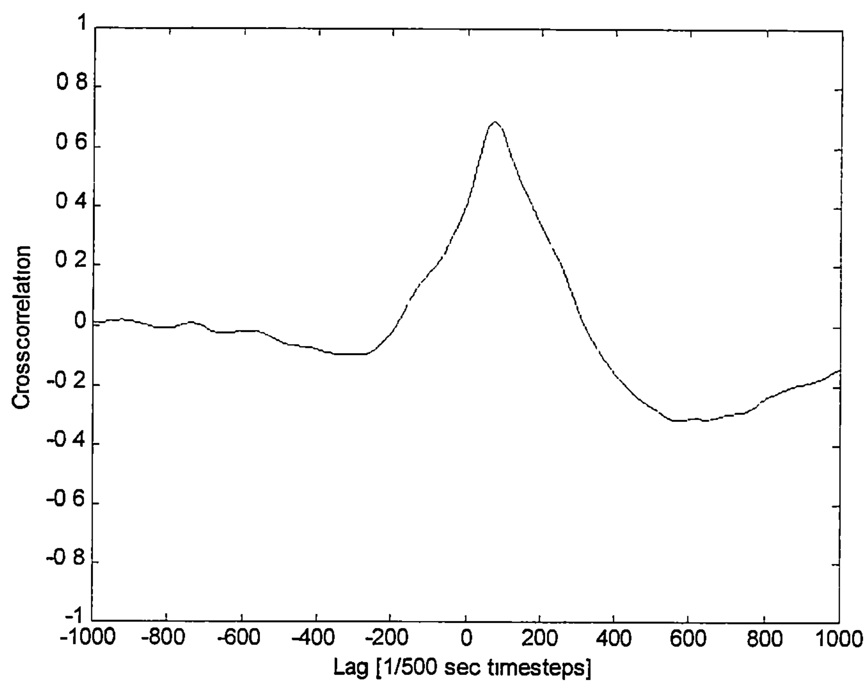

Figure A-33: Crosscorrelation for FE-7 – AV = 61.4 Lpm and Φ = 1.98

Uncertainty Analysis

$$\Phi = \frac{AF_{stoich}}{AF_{actual}} = AF_{stoich}\frac{m_{fuel}}{\dot{m}_{air}} = AF_{stoich}\frac{P_{o,f}R_aT_{o,a}(AV)_f}{P_{o,a}R_fT_{o,f}(AV)_a}$$

$$P_o = P_{o,a} = P_{o,f} \qquad T_o = T_{o,a} = T_{o,f}$$

$$\omega_\Phi = \pm\sqrt{2\left(\frac{\partial\Phi}{\partial P_o}\omega_{P_o}\right)^2 + 2\left(\frac{\partial\Phi}{\partial T_o}\omega_{T_o}\right)^2 + \left(\frac{\partial\Phi}{\partial(AV)_f}\omega_{(AV)_f}\right)^2 + \left(\frac{\partial\Phi}{\partial(AV)_a}\omega_{(AV)_a}\right)^2}$$

$$\frac{\omega_\Phi}{\Phi} = \pm\sqrt{2\left(\frac{\omega_{P_o}}{P_o}\right)^2 + 2\left(\frac{\omega_{T_o}}{T_o}\right)^2 + \left(\frac{\omega_{(AV)_f}}{(AV)_f}\right)^2 + \left(\frac{\omega_{(AV)_a}}{(AV)_a}\right)^2}$$

$$\omega_{P_o} = \pm\ 3\ 447\ \text{kPa} \qquad \omega_{T_o} = \pm\ 0.556\ ^\circ\text{C}$$

$$\omega_{(AV)_f} = \pm\ 0.5\ \text{Lpm} \qquad \omega_{(AV)_a} = \pm 2\ \text{Lpm}$$

Uncertainty Analysis Example

$$T_o = 23\ 33\ °C \qquad P_o = 137.9\ kPa \qquad \Phi = 2.08$$

$$(AV)_a = 61\ 4\ Lpm \qquad (AV)_f = 10.0\ Lpm$$

$$\frac{\omega_\Phi}{\Phi} = \pm\sqrt{2\left(\frac{3.447}{137.9}\right)^2 + 2\left(\frac{0.556}{23.33}\right)^2 + \left(\frac{0\ 5}{10\ 0}\right)^2 + \left(\frac{2}{61.4}\right)^2}$$

$$\frac{\omega_\Phi}{\Phi} = \pm\ 7.7\ \%$$

Vita

Jonathan Robert Vincent was born early in the morning on June 30, 1975 in Chattanooga, TN. Jon enrolled in the University of Tennessee, Knoxville for the fall semester of 1993 and graduated in the spring of 1997 with a B.S. degree in mechanical engineering. He decided to continue his education at UTK and attend graduate school in the fall of 1997 with the intent of taking the pure course option thinking that it was not required to write a thesis. A year later, after completing almost all of his courses, he was told by a professor that he did indeed have to do a thesis in order to graduate. He began working for Dr. Ke Nguyen in the fall of 1998 for no money on a staged combustor. He also became a graduate teaching assistant that semester tutoring *Statics* and *Dynamics* for 20 hours a week. In the spring and fall semesters of 1999, Jon received half of his support from Dr. Nguyen and half from grading papers. It was during this time that another professor told him that he did not really have to do a thesis after all. Jon decided to stick with the thesis even though there he wasn't getting any usable results using staged combustion. One day down in the lab while messing around with the staged combustor, he found out that when the combustor was operated at very high flowrates and with no secondary air, that the flame would propagate up and down through the glass tube above the burner. From this he was able to obtain some useful results which were used in this thesis. Jon graduated from UTK with a M.S. degree in mechanical engineering in the fall of 2000.